Microbial-derived Cellulose-reinforced Biocomposites

By Piao, Haiyuan

A thesis

submitted in partial fulfilment

of the requirements for the degree of

Master of Engineering

in the

Department of Mechanical Engineering

Engineering School, University of Canterbury

Christchurch, New Zealand

31st May 2006

Keywords: Bacterial cellulose, PLA, nanocomposite, biodegradable

Acknowledgements

This research was carried out in the Department of Mechanical Engineering, University of Canterbury, New Zealand. The researcher would like to thank the following people. Without their advice, encouragement and support, this thesis would not be completed.

I wish to express my heartfelt emotion to my supervisors, Dr. Mark Staiger and Dr. John Smail of the University of Canterbury and Dr. Johnason Harrington of the Forest Research for their inspiration, guidance and enthusiasm.

I am thankful to Dr. Peter Gostomski for his interest and advice.

Thanks are extended to Mr. Mike Flaws, Mr. Kevin Stobbs, Professor Robert Shank, Ms. Seema Dean, Mr. Thomas Hughes, Mr. Manfred Ingerfeld, Dr. Alexis Pietak, Mr. Sascha Schrecker and Ms. Liz Girvan for their help with the experimental program.

Thanks are also given to my friends Benoit Duchemin and Jerawala Huadmai for their friendship and discussions.

Last but foremost, to my wife, my parents and parents-in-law, for their unwavering support in spirit and livelihood.

Table of Contents

List of Figures

List of Tables

Microbial-derived Cellulose-reinforced Biocomposites

(Abstract)

The preparation and characterisation of novel nano-scale biodegradable biocomposite materials, consisting of bacterial cellulose (BC) in a poly(lactic acid) (PLA) matrix, are investigated. BC exhibits high purity, high mechanical strength and an ultra-fine fibrous 3D network structure, while PLA is low cost, biodegradable matrix material derived from natural resources. In this work, composites of BC reinforced PLA were prepared using a solution exchange process and compression molding.

The microstructure of the raw materials and composites was characterised using scanning electron microscopy (SEM), transmission electron microscopy (TEM) and atomic force microscopy (AFM). The thermal properties and crystallinity of PLA and composites were measured using differential scanning calorimetry (DSC). The mechanical properties of pure PLA and composite materials were evaluated using static and dynamic mechanical analysis (DMA).

In order to improve the interfacial adhesion between the BC and PLA matrix, BC was acetylated (ABC) or treated with 3-aminopropyltriethoxysilane (APS) coupling agent (SBC). The PLA was plasticized with glycerol (PLAG) in order to increase its ductility.

As compared to the Young's modulus of neat PLA (1.9 GPa), ABC generated the highest increase in Young's modulus (4.8 GPa) of the resulting composites followed

by BC (4.6 GPa) and SBC (4.5 GPa). The tensile strength of PLA (31 MPa) also was enhanced to 75 MPa with BC, 72 MPa with SBC or 38 MPa with ABC. The ductility of PLAG was degraded with the addition of glycerol. A large amount voids led to a reduction in the mechanical properties of PLAG and PLAG based composites. Every reinforcement led to an improvement in the storage modulus (E') of the neat PLA and PLAG, especially at temperatures above the glass transition temperature (T_g). The DMA results showed that the presence of BC based reinforcements significantly reduced the damping properties of PLA. The reinforcements also influenced the crystalline procedure of PLA. With the addition of BC or ABC to the PLA matrix, the melting points of the composites were increased ~ 4-7 °C with a slight change on crystallinity; the crystallinity of SBC-PLA composite decreased from 31.9 % to 26.9 % with only a change of ~ 1 °C in the melting point.

1 Introduction

1.1 Statement of Problems and Opportunities

Since the middle of the last century, there has been a continuously increasing requirement for stronger, stiffer, and lighter-weight engineering materials for industry. High demands on materials for better overall performance has led to extensive research and development efforts into polymer matrix composites. These materials have low specific gravity and high specific strength and modulus. Polymer matrix composites are now extensively utilised in the aircraft, aerospace, automotive, marine, infrastructure, military and sporting goods industries [1-3].

Most composites currently available on the market are designed with long-term durability in mind and are made using non-degradable polymeric resins, such as epoxies and polyurethane, and high-strength fibres, such as graphite, aramids and glass. Many of the polymers and fibres used in composite materials are derived from the petroleum industry. Advanced technology in the field of petrochemical-based materials has brought many benefits to humankind. However, it is becoming evident that impacts on our ecosystems are increasing due to the use of the non-degradable materials for disposable items. The environmental impact of persistent plastic-based wastes is increasing global concerns, and disposal methods are limited. In addition, the petroleum resources are finite and becoming increasingly costly. Fortunately, various biodegradable polymers are being developed to replace non-degradable plastics [4-7].

Plant-based fibres have a number of advantages over glass fibres, such as being renewable, abundant, cheap, lightweight and biodegradable while also providing competitive mechanical properties, *etc*. Plenty of examples can be found of plant-based fibres being used for reinforcing of non-degradable thermoplastic polymers such as polypropylene (PP), polyethylenes (PE), nylons and polyvinylchloride (PVC). Plant fibres have also been used in biodegradable polymers such as cellulose esters, polyhydroxybutyrates (PHB), polyesteramides (BAK), poly(lactic acid) (PLA) and starch derivatives and blends [4, 8].

Unfortunately, both the Young's modulus and strength of natural fibre composites with a thermoplastic matrix are significantly lower than that of glass mat thermoplastics [9]. It is well known that cellulose provides plant fibres with high mechanical properties. However, natural fibres are composed of only ~55-65% cellulose where the levels depend on plant species and a number of other environmental factors. The Young's modulus of bulk wood is ~10 GPa while the Young's modulus of the separated wood fibre by chemical pulping processes can be as high as 40 GPa. Wood fibres can be further separated by hydrolysis and then mechanical disintegration into microfibrils with a Young's modulus of 70 GPa. Theoretical calculations of the Young's modulus of the individual cellulose chains that form the microfibrils predict values of up to 250 GPa [10]. Therefore, it is presumed that the hollow structure of natural fibres reduces the strength of the fibre which further reduces the strength of plant fibre composites.

Some bacterial genera also naturally produce cellulose. Microbial or bacterial cellulose (BC) has found applications in the food industry, wound care products and

tissue engineering. However, the potential for bacterial cellulose in reinforcing polymers is not widely known. Compared with plant-based cellulosic fibres, bacterial cellulose is characterised by high purity (*i.e.* no lignin, hemicellulose or pectin as found in plant cellulose), high mechanical strength and an ultra-fine nano-sized 3D fibrous network structure. Due to these characteristics, bacterial cellulose would appear to be an interesting potential candidate for the development of high-strength nanocomposites.

1.2 Objective and Outcomes

The main objective of this work was to develop a new, type of nanocomposite consisting of PLA acting as a biopolymer matrix and bacterial cellulose as the reinforcement. The surface of the bacterial cellulose was treated with acetylation and a coupling agent to enhance the adhesion with the PLA matrix. Glycerol was trialled as a plasticizer to increase the ductility of PLA. The processing-microstructure-property relationship of the resulting BC-PLA nanocomposites was investigated. The static mechanical properties, viscoelastic behaviour and crystallinity of BC-PLA nanocomposites were measured and analysed.

2 Literature Review

2.1 Green composites

2.1.1 Introduction

Composite make up a very broad and important class of engineering materials. World annual production is over 10 million tones and the market has in recent years been growing at 5 – 10% per annum [1]. These composites show high mechanical and thermal properties. However, these advantages, on the other hand, cause environmental problems [11]. Because of increasing environmental consciousness and demands of legislative authorities, the manufacture, use and removal of traditional composite structures, usually made of glass, carbon or aramid fibres embedded in epoxy, phenolic, polyurethane or unsaturated polyester resins, are considered more critically [12]. On these backgrounds, there is an urgent need for the development of green polymeric materials that would not involve the use of toxic or noxious component in their manufacture and could be degrade in the natural environmental products. Further more, preparation of blends or composites using inorganic or natural fillers, respectively are among the routes to improve some of the properties of biodegradable polymers [13].

2.1.2 Degradable polymers

The synthetic polymers that are used in traditional composite materials are generally designed to be resistant to degradation. However, the cost of disposing of non-

degradable polymers is helping to push the development of biodegradable polymers for use in composite materials. Biodegradable polymers can be divided to two groups according to the raw materials used to make them. Natural biodegradable polymers are based primarily on renewable resources and can be either naturally produced or synthesised from renewable resources. Non-renewable synthetic biodegradable polymers are petroleum-based polymers [14]. Natural biodegradable polymers are derived from four main sources including animal (e.g. collagen and gelatine), marine (e.g. chitin), agricultural (e.g. starch) and microbial (e.g. PLA and PHA) [7]. Polylictide (or poly(lactic acid)) (PLA) is a kind of the most promising of the natural biopolymers. PLA is linear aliphatic polyester produced by poly-condensation of naturally produced lactic acid or by the catalytic ring opening of the lactide (polycondensated lactic acid into lactide) group [15]. Lactic acid is produced (*via* starch fermentation) as a co-product of corn wet milling. PLAs are authentic biopolymers because they are usually derived from agricultural products and their monomers can be produced by microbial fermentation. These melt-processable thermoplastics are completely nontoxic and fully compostable, reverting through biological action to their basic constituents - carbon dioxide and water [6].

2.1.3 Reinforcements of the bio-composites

In recent years, several biodegradable polymers have been reinforced with nature fibre and non-environmental impact inorganic. Hydroxyapatite and bioglass reinforced bio-composite have been used in the tissue engineering [16, 17]. The most heavily researched type of biodegradable composite uses layered silicate clay mineral

as the reinforcing phase due to its easy availability, low cost and more importantly environmentally friendly [13, 18].

Advantages of natural fibres over traditional reinforcing fibres such as glass and carbon fibres are low cost, low density, high toughness, acceptable specific strength, enhanced energy recovery, recyclability, and biodegradability. Therefore, natural fibres can serve as reinforcement by improving the strength and stiffness and also by reducing the weight of the resulting biocomposite materials although the properties of natural fibres vary with their sources and treatments [19]. Natural fibres are largely divided into two categories depending on their origin: plant-based and animal-based. The use of animal-based natural fibres like silk in a biodegradable composite material has been researched [20]. The idea of using plant-based fibre as reinforcement in composite materials is not a new or recent one. Man had used this idea for a long time, since the beginning of human civilisation when grass and straw were used to reinforce mud bricks [21]. Over the last 20 years, plant-based natural fibres like flax [19], jute [22], sisal[23] and kenaf [11] have been more frequently utilized and studied so far, due to their natural abundance, cost effectiveness, world annual production and a wide range of properties depending on the plant source. A large number of literatures have been reported on biocomposites based upon these plant-based natural fibres. Besides plant fibers, manufactured cellulose fibers, such as high-tenacity viscose rayon also has been used as reinforcement in biodegradable composites [24].

While these natural fibers may not be as strong as graphite or aramids (such as Kevlar® fibers used in traditional polymeric composites) fibres, on a ‘per weight’ basis, many plant fibers have closer or higher mechanical properties than E-glass

fibers as shown in Table 2.1 [1, 4]. Compared to glass fibre, the hollow tubular (cellular) structure of these lignocellulosic fibers also provides better insulation against noise and heat in applications such as automotive door/ceiling panels and panels separating the engine and passenger compartments. Panels made from such fibers and PP or other thermoplastics are already in use in many automobiles. All major automobile manufacturers are exploring their use in other interior applications as well [4].

Table 2.1 Mechanical properties of traditional reinforcement and plant fibres [1, 4].

Fibre	Density (g/cm^3)	Tensile strength (GPa)	Young's modulus (GPa)	Specific strength ($GPa/g \cdot cm^{-3}$)	Specific modulus ($GPa/g \cdot cm^{-3}$)
Jute	1.3	0.39–0.77	26.5	0.3-0.59	20.4
Flax	1.5	0.35-1.0	27.6	0.23-0.67	18.4
Sisal	1.5	0.51-0.64	9.4-22	0.34-0.43	6.3-14.7
Ramie	1.5	0.4-0.94	61.4-128	0.27-0.63	40.9-85.3
HM carbon	1.95	2.4	380	1.23	195
HS carbon	1.75	3.4	230	1.94	131
E-glass	2.56	2	76	0.78	29.7
Kevlar® 49	1.45	3	130	2.07	89.7

Within the walls of plant cells there are fine cellulosic structures at the nano scale known as cellulose microfibrils. Cellulose microfibrils normally have a diameter of 5–

50 nm and lengths of thousands of nanometers. The presence of cellulose microfibrils result in plant fibres having a greater energy absorbing capability than synthetic fibres. For example, Kevlar 149 fibres which have Young's modulus of 180 GPa and tensile strength of 3400 MPa. The highest Young's modulus and tensile strength measured for whole phloem fibre cells of flax are 80 GPa and 2000 MPa. However, these are composed of only 65% cellulose. Theoretical and experimental research has shown that cellulose microfibrils have a Young's modulus and strengths of up to 130 GPa and 7 GPa, respectively [25]. The Young's modulus of bulk wood is ~10 GPa while the Young's modulus of the separated wood fibre by chemical pulping processes can be as high as 40 GPa. Wood fibres can be further separated by hydrolysis and then mechanical disintegration into microfibrils with a Young's modulus of 70 GPa. Theoretical calculations of the Young's modulus of the individual cellulose chains that form the microfibrils predict values of up to 250 GPa [10]. However, the challenge of separating microfibrils into individual cellulose molecules remains to be solved [10]. All of above indicate that, as the backbone of plant-based fibre, Cellulose is of course the main contributor to the strength properties of the wood fibre with its highly arranged crystalline structure.

2.1.4 Problem with using plant-based cellulosic fibres

The components of plant-based fibres are cellulose, hemi-cellulose, lignin, pectin, waxes and water soluble substances, with cellulose, hemi-cellulose and lignin as the basic components with regard to the physical properties of the fibres [10]. Under dry conditions, values of Young's modulus for an extracted isotropic lignin has been reported to between 4 to 7 GPa, and the Young's modulus of hemicellulose was

described to between 2 to 8 GPa [26]. Most of plant-based cellulosic fibre contain 60-70% cellulose [10]. Combine this point with the hollow structure, plant fibres have a lower stiffness even the stiffness of cellulose is higher. Further more, the mechanical properties of plant fibre/polymer composite has been reduced.

It is possible to remove those amorphous substrates from plant fibre. In the paper-making industry, the chemical treatment of paper pulp is to separate fibres by dissolving the lignin. The lignin can then be washed away. However, the main purpose of chemical process is to produce papers that are whiter, brighter, stronger and more stable to light and ageing [27]. Exactly, the products of papermaking industry, such as pulp fibre [28] and waste paper [29], have been researched to study their potential as the reinforcement of polymeric composites. However, the pulp fibre still keeps the hollow structure, Especially, the mechanical properties of pulp fibre were reduced by mechanical treatment, bleaching and refining [27].

Plant-based cellulosic fibre not has only lower mechanical properties, but also others limitations, including: (i) Limited thermal stability at typical melt processing temperatures of about 200^{o}C. This limits the type of thermoplastic that can be used with the fibres. (ii) Poor dispersion characteristics in the melt non-polar thermoplastic due to strong hydrogen forces between the fibres. (iii) Limited compatibility with many thermoplastic matrix due to their highly hydrophilic character. (iv) High moisture absorption of the fibres that can affect the dimensional stability of the composites and the interfacial bond strength [21].

2.2 Cellulose-based nanocomposite

2.2.1 Plant-based cellulosic reinforcement for the nanocomposites

The walls of primary plant cells are natural nanocomposites, consisting of a framework of cellulose microfibrils embedded in a cementing matrix of other, mostly hemicelluloses and lignin, polymers. In the microfibrils, cellulose chains are aligned parallel to the microfibril axis. This perfect organisation confers to the microfibrils mechanical properties that are close to the theoretical limit for cellulose [30].

As described in section 2.1.3, these cellulose microfibrils have stiffness of 130 GPa and their strength may be as high as 7 GPa. They are 3~5 times as stiff and a lot stronger than secondary plant cells such as flax fibre cells and even better when compared to flax fibres in bundles, the normal form in which plant fibre is used in industrial composites [31]. Therefore, theoretically, cellulose nanocomposites should exhibit higher performances than conventional plant fibre composites.

As expected, the separation of cellulosic fibres into individual microfibrils has been observed to offer significant improvements in the reinforcement of composites. Some researchers have been able to isolate cellulose microfibrils from plant cell walls (*e.g.* potato [32, 33], sugar beet [34], swede [31], pulp fibre [35] and *Opuntia ficus-indica* [30]) Purified cellulose has been extracted from plant fibre pulp using chemical treatments. A homogeneous suspension of microfibrils can be obtained by a mechanical treatment. The homogeneous treatment is that the pulp suspension requires numerous passes through a special homogenizer that operates at high

pressures (500 bar) and temperatures (90-95°C). The effect of the homogenisation treatment is well displayed in Figure 2.1.

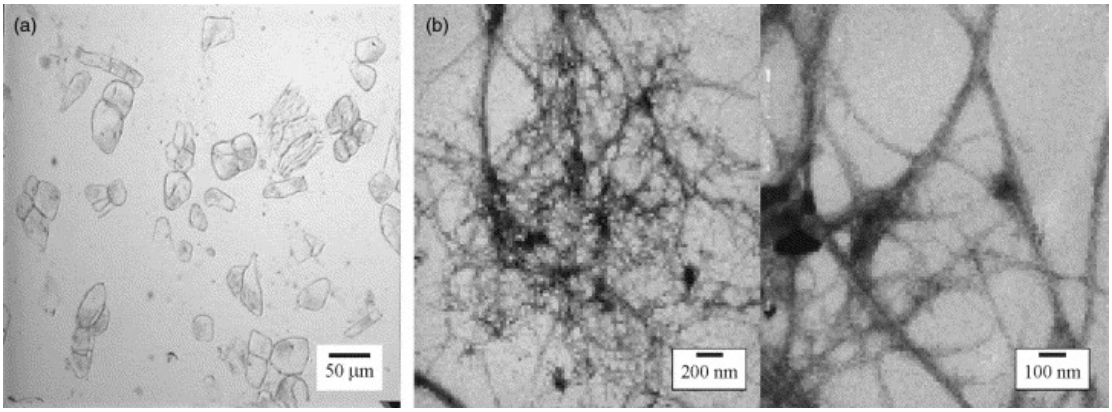

Figure 2.1 Effect of the homogenisation treatment on cell wall fragment of swede. a) Light micrograph showing cellular material after the first pass of treatment, b) and c) Electron micrographs showing a network of partially separated cellulose microfibrils, produced by completion of the full processing [31].

Based on an extensive study of the correlation between defibrillation and ultrasonic treatments, homogenization treatments of wood fibre suspensions by ultrasonic was found to produce fibrillated materials. The ultrasound treatment has a beating-like effect on the fibres. This effect has been ascribed to cavitations occurring in the solvent when sound waves pass through water. These cavitations will produce strong chock waves able to disrupt the fibre wall and separate microfibriles from the fibre surface. Figure 2.2 shows the development and disintegration of peracetic acid delignified spruce fibres with 7.5W/ml power output sort by time sequence [36].

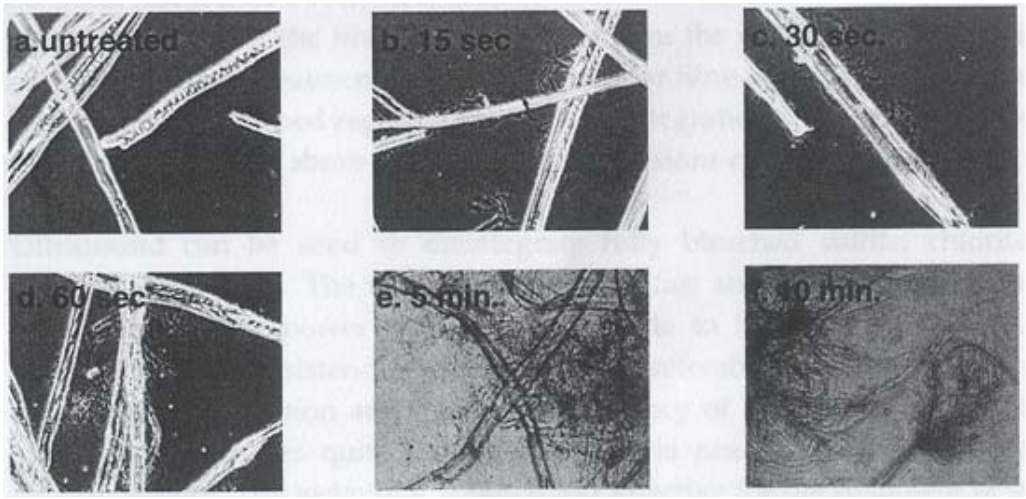

Figure 2.2 Development and disintegration of peracetic acid delignified spruce fibres with 7.5W/ml power output sort by time sequencen [36] .

Cellulose microfibrils bring a great reinforcing effect and improve the mechanical or thermal properties of the composite materials. For example, the Young's modulus of pure polyvinylacetate (PVA) was 0.46 GPa and its tensile strength was 30 MPa. The composite which reinforced by fibrillated cell wall of swede was significantly stiffer and stronger than pure PVA. The Young's modulus of composite with 50% filler was 8.49 GPa and its tensile strength was 145.1 MPa [31]. *Opuntia ficus-indica* cellulose microfibrils filled poly(styrene-co-butyl acrylate) (poly(S-co-BuA)) had higher glass transition temperature (Tg) than the pure poly(S-co-BuA) [30].

2.2.2 Animal-based cellulosic reinforcement for the nanocomposites

Tunicin is a type of cellulose from animals. Generally, tunicin is the form of a cellulose whisker (Figure 2.3). Tunicin whisker can be used as a reinforcement in synthetic polymers [37-39] or biopolymers [40-43] to produce nanocomposites. The

whiskers' main characteristics are a high average aspect ratio (about 70) with a diameter of 15 nm and an important interface area on the order of 150 m^2/g [37]. The isolation of this type of cellulose whiskers from the shell of sea animals had similar homogenisation process with fibrillation of plant cell wall.

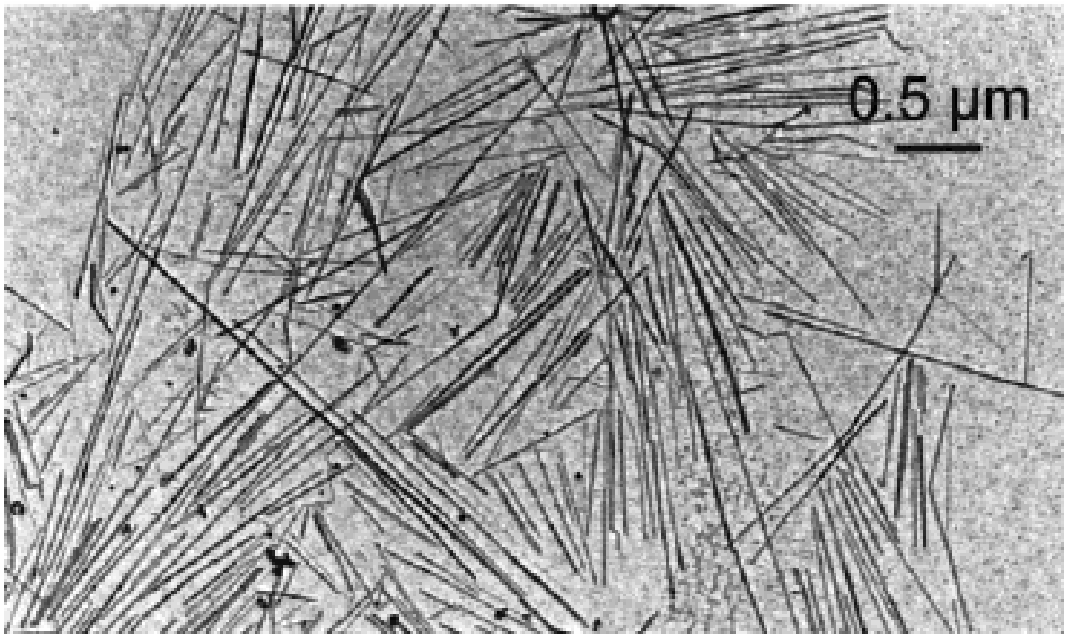

Figure 2.3 Tunicin whisker [41] .

The cellulose also can increase the mechanical properties of polymeric matrix. The Young's modulus of unfilled poly(oxyethylene) (POE) was 25 MPa at 22 °C. While the Young's modulus of composite with 13.3 wt.% cellulose whiskers was 60 MPa, respectively. It was ascribed to the formation of a rigid percolating cellulose whiskers network. This network, assumed to be formed through whisker/whisker hydrogen bonds interactions [39].

2.2.3 Disadvantage of cellulose microfibrils/whiskers isolation

It has been shown that it is possible to extract microfibrils from cell wall material (or whiskers from shell of sea animal) by homogenous treatment, but these extraction procedures involve harsh chemical and mechanical treatments that may significantly reduce the strength of the microfibrils/whiskers.

2.3 Bacterial cellulose

2.3.1 Introduction

Apart from plants and some lower animals (*e.g. Tunicata sp.*), cellulose is also produced by bacteria genera (*e.g. Rhizobium sp.*, *Agrobacterium sp.*, *Alcaligenes sp.*) [44]. Bacterial cellulose (BC) is a straight chain polysaccharide with the same chemical structure as cellulose that is derived from plants. However, bacterial cellulose has the advantage of being devoid of lignin, pectin, hemicellulose and other biogenic products that are normally associated with plant cell walls [45]. Due to the high purity and special physicochemical characteristics, bacterial cellulose has applications in a wide range of areas including food, biomedical (*e.g.* wound care [46]and tissue engineering [47, 48]) and engineering (*e.g.* nanocomposites [49-51]).

2.3.2 Cellulose

2.3.2.1 Structure of cellulose

Cellulose is the most abundant biopolymer on earth and is the major structural component of plant biomass. Cellulose is a straight chain polysaccharide consisting of

D-glucose molecules (Figure 2.4a) connected by β-1,4 bonding (Figure 2.4b) [52]. The basic chemical formula of cellulose is shown below.

$$C_{6P}H_{10P}+2O_{5P+1} \approx (C_6H_{10}O_5)_P \text{ or } (C_6H_{10}O_5)_n$$

where P = the degree of polymerisation; n = the number of units in the chain.

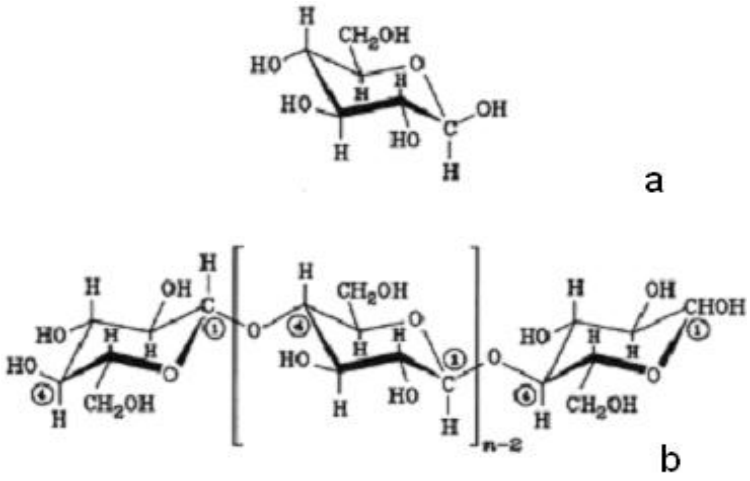

Figure 2.4 Chemical structure diagram of D-glucose molecules and cellulose. (a) D-glucose molecules and (b) cellulose [52].

The elemental composition of cellulose consists of 44.4 % C, 6.2 % H and 49.4 % O. The molecular mass (m_0) of the glucose base unit is 162 and the molecular mass of the cellulose polymer is $M_r = m_0P + 18 \approx 162P$ [52]. Table 2.2 lists the number average degree of polymerisation of a number of celluloses from various origins.

Table 2.2 Degree of polymerisation of celluloses of different origin [52]

Type of cellulose	Average degree of polymerisation
Cotton (raw)	7 000
Flax	8 000
Ramie	6 500
Spruce (pulped)	3 300
Beech (pulped)	3 050
Fir	2 500
Bacterial cellulose	2 700

Cellulose is known in at least four different crystalline modifications. X-ray spectrographs of native cellulose have shown that the microstructure components are invariably. Native cellulose is referred to as Cellulose I. After mercerisation, the translation lattice of native cellulose is found have undergone some slight changes and a different crystalline modification appears which is referred to as hydrated cellulose or Cellulose II. A third lattice modification, Cellulose III, is obtained by the decomposition of an addition compound of cellulose with ammonia. Cellulose II can be transformed to a fourth modification, Cellulose IV, by thermal treatment in a polar liquid such as formamide or glycol [53]. Cellulose I consists of two crystallographic phases — dominant I_α and minor I_β components [54].

2.3.2.2 Physical properties of cellulose

Cellulose absorbs around 8-14 % water under normal atmospheric conditions (20°C and 60% relative humidity). However, cellulose is insoluble in water or diluted acids.

In concentrated acids, dissolution can be achieved by severe degradation. Cellulose is a non-melting substance with thermal decomposition starting at 180 °C; the ignition point is >290 °C. The density of cellulose is 1.52-1.59 g/cm^3 [52].

2.3.3 Production of bacterial cellulose

As described in the section 2.3.1, some bacterial genera can produce the cellulose. However, only a few bacterial species related to *Acetobacter xylinum* (acetic acid bacteria) secrete cellulose in the form of fibres [44].

Bacterial cellulose has long been used as the raw material of *Nata-de-coco*, an indigenous dessert food of the Philippines. *Nata-de-coco* consists of cellulose cubes that are cut from a ~1 cm thick gel sheet fermented with coconut water. *Nata-de-coco* is also a popular diet food in Japan. *Teekvass* (or *tea-fungus*), grown in tea and served in some parts of Russia and Middle-Asia is said to be a similar ferment. A substance known as "vinegar plant" and of use for vinegar brewery in old days in Europe was cultured in pure condition and identified to be the same as cell-wall cellulose [55].

The *Acetobacter xylinum* strain is able to produce cellulose at a temperature of 25–30°C and pH of 4.5–7.5 within the carbon source [56]. Many substrates have been analysed for their potential to work as a carbon source in the production of bacterial cellulose including monosaccharides (*e.g.* D-Glucose), disaccharides (*e.g.* Lactose), polysaccharides (*e.g.* Starch), organic acid (*e.g.* Gluconate) and alcohols (*e.g.* Ethylene glycol) [45]. The cost of the carbon source contributes significantly to the overall production cost of bacterial cellulose, particularly fermentations at an

industrial scale. The current price of bacterial cellulose remains too high to make its use commercially feasible in a wide range of applications [57]. Waste water from some food industries contain saccharide and could provide a suitable medium for production of bacterial cellulose. Some researchers have also tried to grow bacterial cellulose using dairy waste [58]. Therefore, it is possible to produce bacterial cellulose on a larger scale.

Bacterial cellulose as synthesised by Gluconacetobacter xylinus consists of elementary protofibrils. Typically such elementary protofibrils make up a flat, ribbon like microfibril [51]. The mechanism of formation as well as the structure of microfibril is believed as illustrated in Figure 2.5 that cellulose molecules synthesized in the interior of bacterial cell are spun out of 'cellulose export components' or nozzles to form a protofibril of around 2–4 nm diameter and the protofibrils are bundled in the form of a microfibril of around 80×4 nm [59].

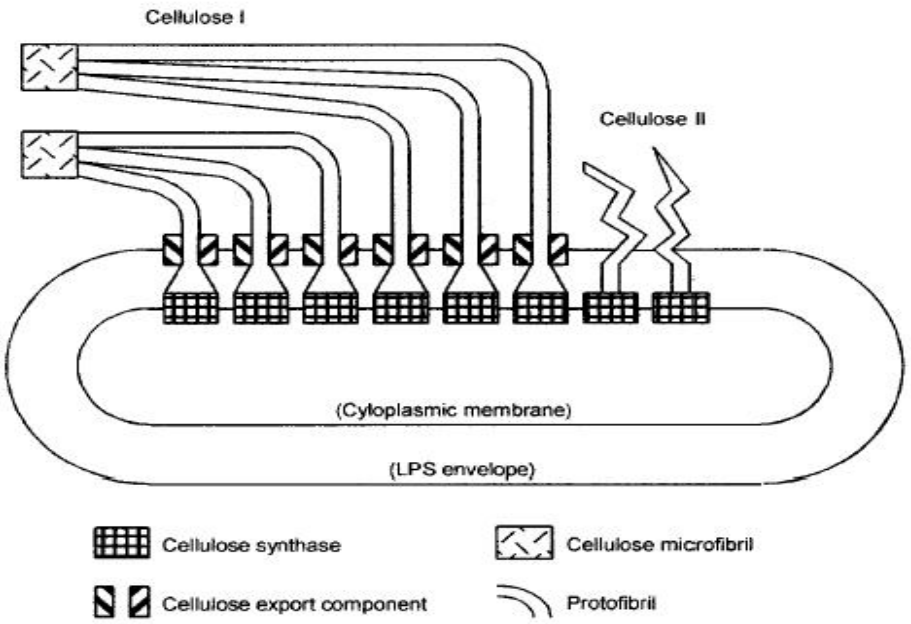

Figure 2.5 Schematic illustration of the biogenesis of bacterial cellulose and microfibril formation [59].

The macroscopic morphology of bacterial cellulose depends on the conditions of culturing. In static conditions (Figure 2.6), bacteria accumulate a cellulose "pellicle" on the surface of a nutrient broth at the oxygen-rich air/liquid interface. Protofibrils of cellulose are continuously extruded from linearly ordered pores at the surface of the bacterial cell, crystallized into microfibrils and forced deeper into the growth medium. The leather-like pellicle, supporting the population of *Acetobacter xylinum* cells, consists of overlapping and inter-twisted ribbon like cellulose microfibrils, forming parallel but disorganized planes. Under agitated culture conditions (Figure 2.7) bacterial cellulose is produced as a well-dispersed slurry of irregular masses including granules, stellate and fibrous strands [60]

Figure 2.6 Bacterial cellulose pellicle formed in a static culture [60].

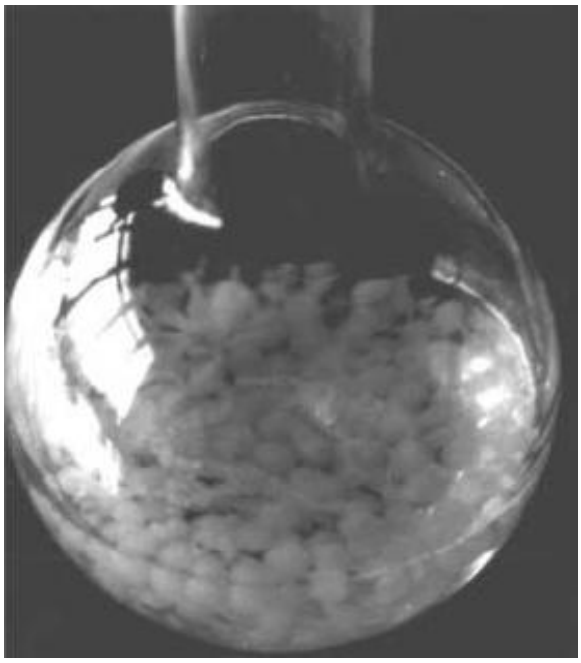

Figure 2.7 Bacterial cellulose pellets formed in an agitated culture [60].

The microfibrils of bacterial cellulose produced statically are more highly extended (Figure 2.8). In contrast, the microfibrils of bacterial cellulose produced under agitated conditions are curved and entangled resulting in a denser reticulated structure than static bacterial cellulose (Figure 2.9) [61]

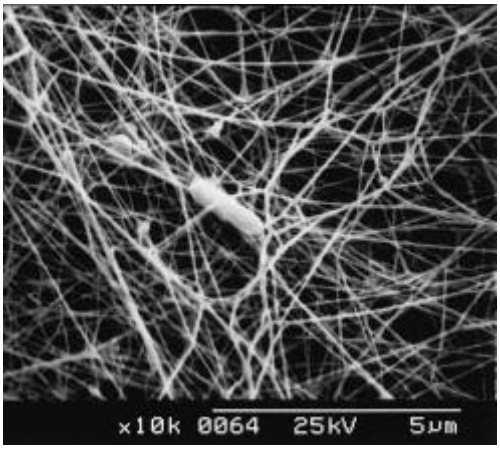

Figure 2.8 Scanning electron micrographs of the morphology of bacterial cellulose produced in static cultures [61].

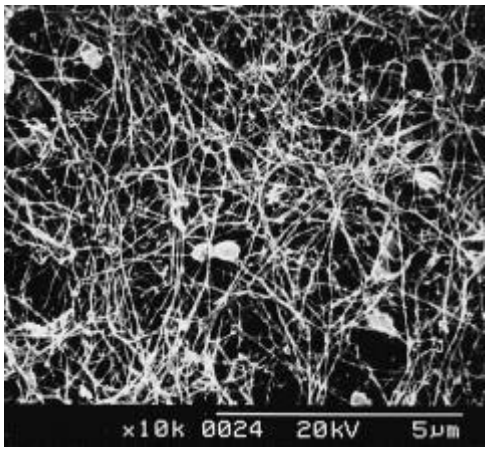

Figure 2.9 Scanning electron micrographs of the morphology of bacterial cellulose produced in agitated cultures [61].

The culturing of the bacteria under static conditions normally takes place at 28–30°C by adding an aliquot of activated seed broth to the culture medium in a vessel such as beaker. Initially, the system becomes turbid. After a period, a white pellicle begins to form on the surface, increasing in thickness with time [55]. After harvesting the bacterial cellulose is purified by boiling it in 1% NaOH for 2 hr, treating with 5% acetic acid and then thoroughly washing in distilled water until the pellicle becomes transparent [62].

2.3.4 Structure and properties of bacterial cellulose

Bacterial cellulose protofibrils bond together into ribbon like microfibrils, as shown in the Figure 2.10. The ribbons are ~3-4 nm in thickness, ~80 nm in width and 1-9 μm in length. The ultra fine ribbons of bacterial cellulose form a dense network structure, stabilized by extensive hydrogen bonding [60].

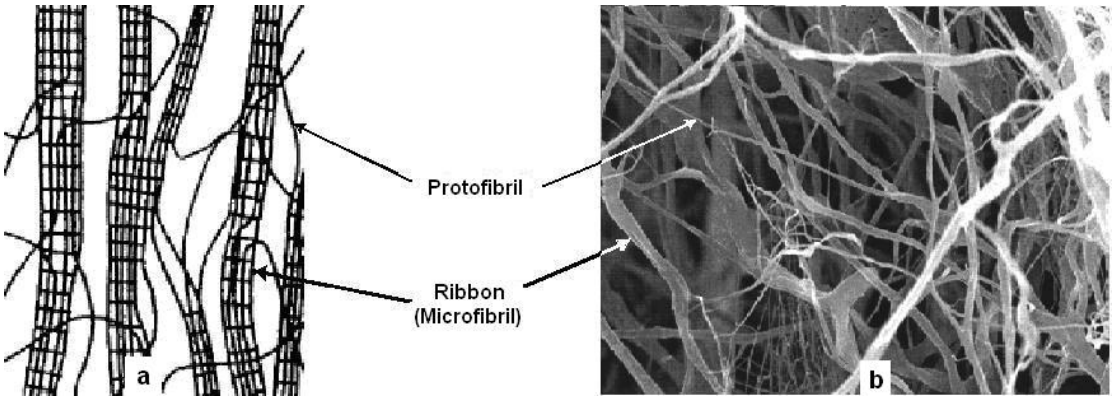

Figure 2.10 Structure of bacterial cellulose. (a) Schematic model of bacterial cellulose microfibrils and ribbons [60], (b) the network structure of bacterial cellulose in an aqueous solution [63].

Investigations of the texture of bacterial cellulose have shown that a surface layer built on the interface between the culture broth and the air delimitates the pellicle surface clearly. A gelatinous lower layer is adjacent to the broad middle layer (Figure 2.11) [48].

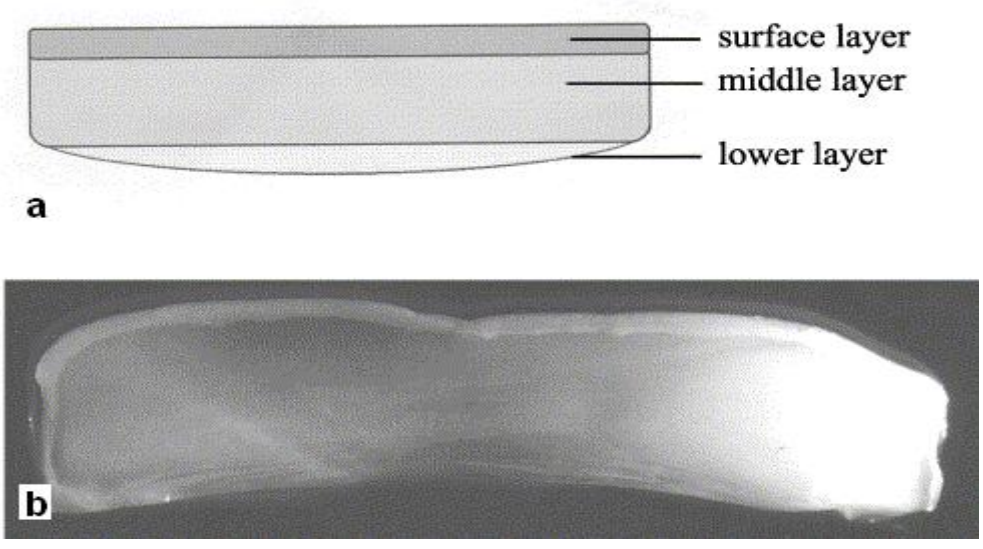

Figure 2.11 Representation of cellulose layers inside the pellicle (a) Schematic representation and (b) Cross-section of a purified bacterial cellulose pellicle [48].

By SEM investigations of bacterial cellulose pellicles washed only with water, the thickness of a surface layer was 6 µm. The layer is characterized by a compact cellulose network structure and an intensified presence of bacterial cells (Figure 2.12) [48].

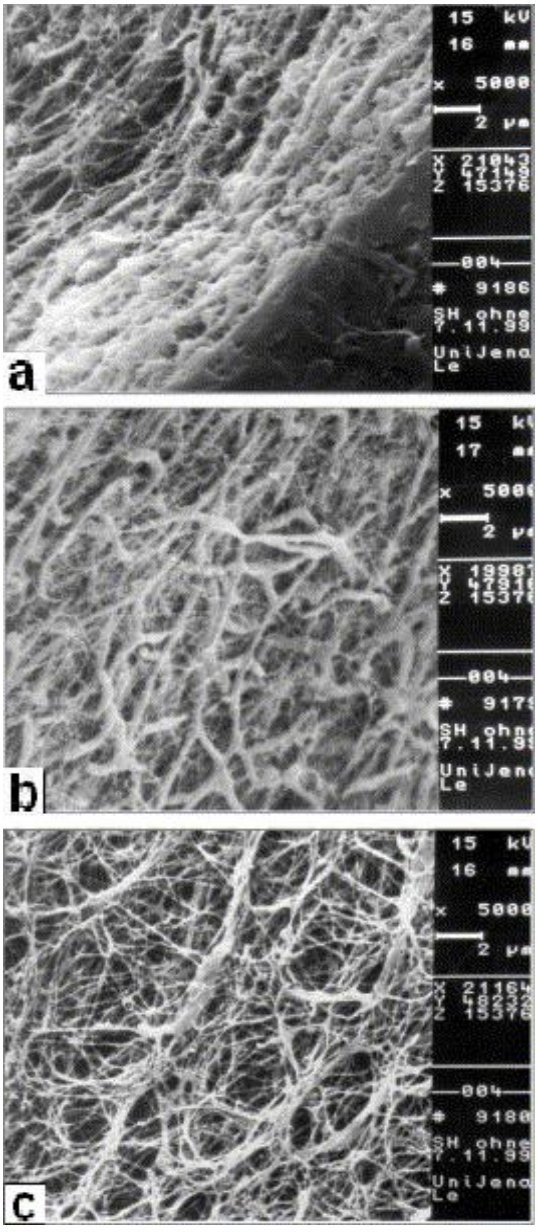

Figure 2.12 Scanning electron micrographs of surface and middle layer in the cross-section of a cellulose pellicle washed with water. (a) Frontier area between surface and middle layer, (b) section of the surface layer and (c) section of the middle layer (sample preparation: freeze drying) [48] .

Bacterial cellulose microfibrils in the sheets appear to constitute a pile of thin layers, as seen in Figure 2.13 [55].

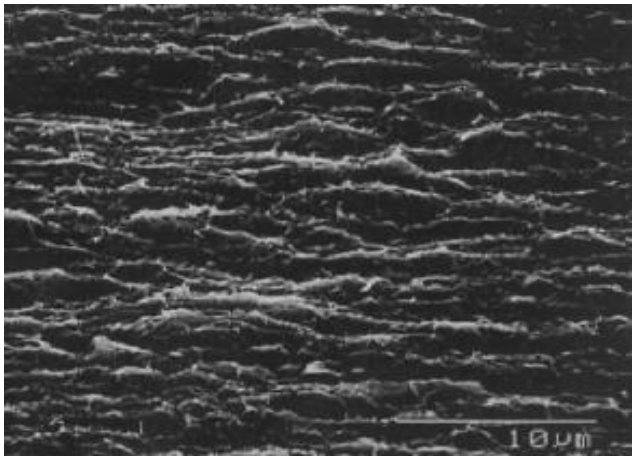

Figure 2.13 Scanning electron micrograph of the fracture edge of a bacterial cellulose film [55].

The structure of bacterial cellulose is a highly swollen fibre network. The hydrophilicity of the cellulose pellicle is explained by the presence of pore structures and 'tunnels' within the wet pellicle and depends on the extensive interior surface area of the interstitial spaces of the never dried pellicle. Water retention of never dried bacterial cellulose leads to values in the range of 1000%. As a comparison, air dried bacterial cellulose can hold 106 % water; freeze dried bacterial cellulose can hold 629% water and the cotton linters can hold 60% water [48].

Films can be prepared by drying a bacterial cellulose pellicle in air on a flat surface such as a glass plate. The mechanical properties of bacterial cellulose are greater. The Young's modulus and tensile strength are 16.9 GPa and 256 MPa, respectively [55]. In comparison, the Young's modulus and tensile strength of cotton linter paper is 0.085 GPa and 0.83 MPa, respectively [64].The higher mechanical properties of

bacterial cellulose film are ascribed to its microstructure. The microfibrils are bound through interfibrillar hydrogen bonds, as in pulp-paper. However, the density of the interfibrillar hydrogen bonds is higher since the microfibrils are much finer leading to a greater contact area [64]. Films also can be prepared under conditions of heat and pressure. However, the mechanical properties are not dramatically improved. For example, the Young's modulus and tensile strength under optimised conditions of heat and pressure (150 °C; 49 MPa) are 16.9 GPa and 260 MPa, respectively [55].]

The mechanical properties of single fibers of bacterial cellulose was measured by Atomic Force Microscopy, and a Young's modulus was determined as 78±17 GPa [65].

2.3.5 Applications of bacterial cellulose

2.3.5.1 Bacterial cellulose reinforced nanocomposite (review)

2.3.5.1.1 Introduction

The development of new composite materials is based upon both industrial and techno-economical criteria and therefore is dominated by the search for adequate mechanical performance at lowest cost. There is a demand for new composites that are recyclable or disposable by incineration without noxious/toxic gas emissions or residual matter at the end of their lifecycle. Bacterial cellulose has the potential for excellent mechanical performance due to low density in combination with high Young's modulus and tensile strength. The fact that it is biodegradable makes it very attractive for the future industrial purposes [49]. Therefore, some researchers have done investigations on bacterial cellulose reinforced polymer composites.

2.3.5.1.2 Source of the raw materials

Generally, most of researchers cultured (or were supplied) bacterial cellulose pellicles. Only Grunert *et al*. processed their nanocomposites by Primacel^{TM}, a powder-like commercial product (a kind of thickener in the food industry), consisting of bacterial cellulose nanocrystals [49, 50].

2.3.5.1.3 Investigative purposes

Not all of researchers focused on the mechanical properties of the novel composite in their investigation. Because of the very thin primary cell wall of plant, an alternative method is to construct *in vitro* composites which consisted bacterial cellulose and other compounds (e.g. xylan and pectin) in the primary wall as a simulation [66-68]. As a hydrophilic polymers, bacterial cellulose shows a stronger affinity to water, hence bacterial cellulose composite (with other hydrophilic polymers) membranes have been investigated for pervaporative separation of ethanol/water mixtures [69, 70]. Yano *et al.* studied the transparency of bacterial cellulose reinforced acrylic resin [71].

2.3.5.1.4 Fabrication

Those researchers processed their composite by different methods. Grunert *et al*. mixed cellulose nanocrystals in the polymer solution, and then cast composite film [49, 50]. Dammstrom *et al.* also processed their composite by film casting. However, the raw material was cellulose microfibril suspension - defibrillated bacterial cellulose by homogenous treatment [68].

Aqueous solution of some hydrosoluble polymers (e.g. PVA [72] and xyloglucan [66]) were added in the culture solution, bacterial cellulose could grow combine these polymers.

However, bacterial cellulose (wet pellicles or dried sheet) were immersed in the polymers' solution in more cases. If the solvent of polymer materials was water or water compatible, wet pellicle could be impregnated in the solution straightly [69, 73, 74]. Alternatively, if the polymer was not hydrosoluble, the water in the wet pellicle need to be exchanged by solvent, and then, the pellicles were impegneated in the polymer solution [51]. In the nature of things, dried BC sheets, whatever to dry the pellicles directly or to make paper from disintegrated BA pellicle, could be immersed in the polymer solution [51, 71, 75]. Nakagaito and Yano *et al*. also hot pressed their composite in the final step [71, 75]

2.3.5.1.5 Results

Grunert *et al*. processed nanocomposites by polydimethylsiloxane [49] and cellulose acetate butyrate [50] as the matrix materials. The storage modulus of pure polydimethylsiloxane was doubled by the addition of bacterial cellulose (without surface treatment). The reinforced cellulose acetate butyrate composites also exhibited higher dynamic mechanical properties. The storage modulus of pure cellulose acetate butyrate varied from 900 to 4 MPa with temperatures of 81°C and 124°C, respectively. The storage modulus of composite, reinforced by 10 wt.% native bacterial cellulose (without surface treatment) was found to be 1750 and 104 MPa at

temperatures of 81°C and 124°C, respectively. While the storage modulus of the composite reinforced with silylated bacterial cellulose crystal was 1509 and 73 MPa at temperatures of 81°C and 124°C, respectively [50].

Gindl *et al*. also produced cellulose acetate butyrate composites which were reinforced by bacterial cellulose. The Young's modulus and tensile strength of the pure cellulose acetate butyrate was 1.2 GPa and 25.9 MPa, respectively. The Young's modulus and tensile strength of a composite containing 10.3 vol.% bacterial cellulose was 3.2 GPa and 52.6 MPa, respectively. While the Young's modulus and tensile strength of composite with 32 vol.% bacterial cellulose was 5.8 GPa and 128.9 MPa, respectively [51].

Nakagaito *et al*. perpared phenol formaldehyde (PF) composites with bacterial cellulose reinforcement. From another literature, the Young's modulus and tensile strength of the pure phenol formaldehyde was 375 MPa and 10 MPa, respectively [76]. The Young's modulus and tensile strength of a composite containing 87.6 wt.% bacterial cellulose (without disintegrated treatment) was 28 GPa and 420 MPa, respectively. While the Young's modulus and tensile strength of composite with 87.5 wt.% bacterial cellulose (with disintegrated treatment) was 19 GPa and 350 MPa, respectively [75].

Yano *et al*. processed bacterial cellulose reinforced acrylic resin and epoxy resin composites. A web-like network of bacterial cellulose microfibrils had demonstrated very promising characteristics a reinforcement material for optically functional composite. Due to the size effect, the nanofibre network in variety of resins led to a

very low loss of transparency of the original resin, even at high fibre content as shown in the Figure 2.14. The significant reinforcement effect can also been seen in the mechanical properties of the BC/epoxy resin composite. The Young's modulus and tensile strength of composite with 65 wt.% bacterial cellulose was 20 GPa and 325 MPa, respectively [71]. While the Young's modulus and tensile strength of epoxy resin was 3-6 GPa and 35-100 MPa, respectively [1].

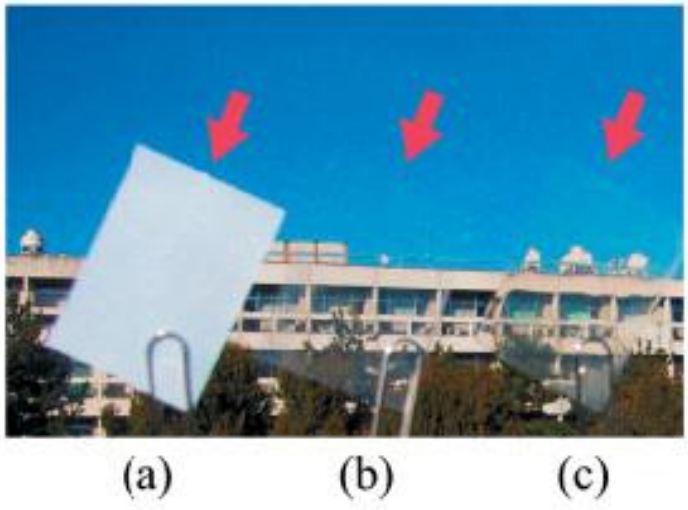

Figure 2.14 Transparency of bacterial cellulose reinforced polymeric composite. (a) Drid BC sheet, (b) BC/acrylic resin composite, (c) BC/epoxy resin composite [71].

2.3.5.2 Medical and tissue engineering applications of bacterial cellulose

The use of scaffolds in the tissue engineering of cartilage is essential in order to support cell proliferation and maintain their differentiated function in addition to definition of the shape of the new growing tissue [77]. Bacterial cellulose has potential to be used as a substrate for tissue engineering of cartilage due to its high

strength in the wet state, high moldability *in situ*, biocompatibility and relatively simple, cost-efficient production [47].

Svensson *et al*. used bacterial cellulose as scaffold for tissue engineering of cartilage. After several days of cultivation, the cells on bacterial cellulose had grown to or near confluence. The viability of chondrocytes growing on bacterial cellulose was significantly higher than on tissue culture plastic (Contrapositive material, a frequently used substrate for cultivation of cells, as well as on alginate, which is a well-known, biocompatible material commonly used in cartilage-related biomaterials) [47].

Commercial products (e.g. Biofill®, Xcell® and Bioprocess®) of bacterial cellulose had wide applications in surgery, especially, in the wounds healing. Cases of second and third degree burns, ulcers and others could be treated successfully with bacterial cellulose membrane as temporary substitute for human skin. Bacterial cellulose has the following advantages: immediate pain relief, close adhesion to the wound bed, diminished post-surgery discomfort, reduced infection rate, easiness of wound inspection (transparency), faster healing, improved exudates retention, and spontaneous detachment following reepithelization, and reduced treatment time and costs [46, 78, 79].

BASYC®, a patented bacterial cellulose product, has been developed as microvessel for the microsurgery. Using a patented matrix technique *Acetobacter xylinum* is able to build up the previously described cellulosic network as very regularly formed tubes of different length, wall thickness and inner diameter. The application of BASYC®

tube was investigated, in case of a typical end-to-end anastomosis using the carotid artery of the white rat. The BASYC® interposition is completely incorporated in the body without any rejection reaction [48].

2.3.5.3 Others applications of bacterial cellulose

The addition of bacterial cellulose in a very small amount will give foods good dispersion- and emulsion-stability, and also will give foods short mouthfeel based on a good shape-retainability. These functions are largely due to the three-dimensional network structure of cellulose fibres and are stable to physical and chemical treatments; they are also resistant to heat, acids and salts. These characteristics enable bacterial cellulose to be applied to foods for a wide range of purposes such as stabilisation of thickening, dispersion, suspension, and emulsion, replacement of fat, prevention of protein aggregation, etc [63].

Sony Corporation, in conjunction with Ajinomoto developed the first audio speaker diaphragms using bacterial cellulose. The unique dimensional stability of bacterial cellulose gives rise to a sound transducing membrane which maintains high sonic velocity over a wide frequency ranges, thus being the best material to meet the rigid requirements for optimal sound transduction [64].

Bacterial cellulose has been investigated as a binder in papers, and because of it consists of extremely small clusters of cellulose microfibrils, this property greatly adds to strength and durability of pulp when integrated into paper [80].

2.4 Poly(lactic acid) (PLA)

2.4.1 Production of PLA

Lactic acid (2-hydroxypropanoic acid) is one of the smallest optically active molecules, which can be either of (+) or (−) stereoisomer (Figure 2.15). Lactic acid is produced by animals, plants and micro-organisms in nature. Lactic acid can also be derived from intermediates with an origin in renewable materials (e.g. acetaldehyde, ethanol) or from chemicals derived from coal (e.g. acetylene) or oil (e.g. ethylene). The starting material for PLA is starches or sugars from corn, sugar beets, or other sources. The starch is converted into sugar, and then fermented to yield lactic acid. Fermentative production of lactic acid is preferably made by the group of lactic acid bacteria capable of converting hexoses into lactic acid. Lactic acid bacteria can produce either, or both of the stereoisomer as well as various by-products. The fermentation can be performed in batch or in continuous processes. Important parameters in the fermentation are pH-value, temperature, atmosphere, and in some cases also the agitation [15].

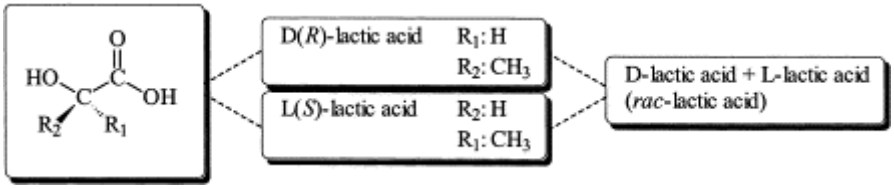

Figure 2.15 Stereoforms of lactic acid [15]

PLA can be synthesized by two different pathways: either the step polycondensation of lactic acid, or the ring opening polymerisation (ROP) of the cyclic diester lactide. In contrast to the more traditional polycondensation, that usually requires high temperatures, long reaction times and a continuous removal of water, to finally

recover quite low molecular weight polymers with poor mechanical properties, lactide ROP provides a direct and easy access to the corresponding high molecular weight polylactide [81].

PLA contains an asymmetrical carbon atom in its structural unit that enables it to become optically active. In this way, it is possible to obtain the isotactic L-PLA and D-PLA polymers. Consequently, D,L-PLA is a syndiotactically alternating D,L-copolymer or a copolymer having L-and D-units. Mostly, even no D- or L-designation can be found. The latter findings have been gathered under 'PLA' and are thought to be mostly non-syndiotactic D,L-PLA [82].

2.4.2 Properties of PLAs

PLAs are authentic biopolymers because they are usually derived from agricultural products and their monomers can be produced by microbial fermentation. These melt-processable thermoplastics are completely nontoxic and fully compostable, reverting through biological action to their basic constituents — carbon dioxide and water [6]. The properties of a series of PLAs are given in Table 2.3 [15].

Table 2.3 Physical properties of various PLAs [15].

Properties	Limits	Type of PLA		
		PLA	L-PLA	D,L-PLA
ρ (g/cm^3)	Upper	1.21	1.24	1.25
	Lower	1.25	1.30	1.27
σ (MPa)	Upper	21	15.5	27.6
	Lower	60	150	50
E (GPa)	Upper	0.35	2.7	1
	Lower	3.5	4.14	3.45
ε (%)	Upper	2.5	3	2
	Lower	6	10	10
T_g (°C)	Upper	45	55	50
	Lower	60	65	60
T_m (°C)	Upper	150	170	amorphous
	Lower	162	200	

2.4.3 Applications of PLA

2.4.3.1 Biodegradable composites

The use of natural fibres, to reinforce polymers as an alternative to synthetic or glass fibres has been and continues to be the subject of research and development. The potential advantages of using natural fibres have been well documented and are generally based on environmental friendliness as well as health and safety factors

[83]. Normally, researchers use long plant fibres (e.g. jute [22], kenaf [11] and flax [19]) as the reinforcement to process the PLAs based composite.

Plackett *et al*. describe composites prepared from L-PLA and jute fibres. Jute fibres were used in the form of a non-woven mat and L-PLA was used in the form of film. The processing method was hot-pressing. The fibre content is 40 wt.%. Final products had higher mechanical properties compare with the pure PLA sample. For example, the composite with highest properties was obtained under 210^{o}C. The Young's modulus and tensile strength of the composite was 9.4 GPa and 100.5 MPa, respectively. The Young's modulus and tensile strength of L-PLA was 3.5 GPa and 55 MPa, respectively [22].

T. Nishino *et al*. discussed the work in which composites were prepared from L-PLA reinforced by kenaf fibres. Kenaf fibres were used in the form of a sheet. But the processing method was impregnation, to immersed kenaf sheets into L-PLA dioxane solution. L-PLA film showed a low Young's modulus (1.3 GPa) and low tensile strength (21 MPa). Both properties increased with the increase of the fibre content, and showed the maximum values (Young's modulus; 6.4 GPa, and the tensile strength; 60 MPa) around the fibre content of 70% volume [11].

K. Oksmana *et al*. presented an investigation in which composites were prepared from PLA and flax fibres. Flax fibres were used in the form of hand made roving. The composite materials were manufactured using a twin-screw extruder. The fibres were fed into the side extruder and the fibre content in the composite was calculated according to feeding speed and the weight of the roving per meter. The pure PLA had

a tensile strength of 50 MPa and a Young's modulus of 3.4 GPa. When the fibre content was 40 wt%, the composite had the greatest properties: Young's modulus was 8.3 GPa and the tensile strength was 53 MPa [19].

Not only nature fibres but also some mineral [13, 18, 84, 85] and others polysaccharid (e.g. starch [86] and chitosan [87, 88]) can be used as the reinforcement of PLA based biodegradable composite to reduce the cost and improve the mechanical properties.

2.4.3.2 Medical and tissue engineering application of PLA

PLA is a biocompatible and biodegradable material with wide utility for many medical and tissue engineering applications, including drug-release systems [89], scaffold of tissue and organ regeneration [90], wound care [91] and implant [92] etc.

PLA is able to hydrolytic degrade through de-esterification. Once degraded, lactic acid can be cleared through the tricarboxylic acid cycle. Thus, the body already contains highly regulated mechanisms for completely removing residual traces of the polymers. Due to this property, PLA can be used as the scaffold of tissue engineering [90].

A biodegradable matrix can act as a temporary scaffold within which tissue can develop. Ultimately the biodegradable matrix is entirely replaced by cells and natural extracellular matrix. An ideal scaffold in tissue engineering should be three-dimensional, highly porous (high pore-to-volume ratio and surface area) and possess a permeable structure with a uniformly distributed and interconnected open pore

network. Adequate pores (size, shape, wall morphology) for cell seeding, attachment, growth and new tissue formation, for flowtrans port of nutrients and metabolic waste products to and from the are important considerations. Various methods can prepare the porous PLA scaffold, including: solvent casting/particulate leaching, textile technology, melt molding/particulate leaching, supercritical fluid-gassing process, solution casting (dissolution/precipitation) and thermal-induced phase separation methods [93]. To enhance the mechanical properties of scaffold, especially the application for bone regeneration, hydroxyapatite short fibres can be fill in to process reinforced polymer foam [94].

Another useful application of PLA namely the dressing of large wounds (above all burn wounds) was developed. The films consist of an amorphous D,L-PLA. Due to its transparency the physicians can observe and control the healing process without removal of the wound dressing. Furthermore, the D,L-PLA film will be resorbed by the wound in the course of 4~6 weeks (depending on the film thickness). If the resorption is too fast a second film can be fixed on top of the partially degraded first one. The films are fixed with a resorbable glue on the intact skin surrounding the wound [91].

2.4.3.3 Others application of PLA

The original purpose to develop PLA is to find out an alternative to synthetic plastic with low cost and degradability. Therefore, many applications of PLA around human's life: shopping bag, agricultural film, drinks bottle, paper coating and cloth etc [6].

3 Experimental Methods

3.1 Materials

The materials used in this research were bacterial cellulose (BC) and poly(lactic acid) (PLA). The BC pellicles were kindly supplied by Chemical and Process Engineering (CAPE) department, University of Canterbury, New Zealand. The PLA (Natureworks® 4046D and 4060D) was kindly supplied by Cargill Dow LLC in the form of film. 1,4-dioxane and yeast extract were supplied by Sigma Aldrich NZ; acetic acid, acetic anhydride, acetone, ammonium sulfate, citric acid, ethanol, glucose, glycerol, magnesium sulfate, sulphuric acid, sodium hydrate and sodium phosphate were supplied by Biolab Scientific NZ.

3.1.1 Production of bacterial cellulose

Acetobacter xylinum, ICMP 15569 was grown in a rotating (7 rpm) biological contactor for 192 hours, using a 120 mm diameter cylinder that was partly submerged in medium - a modified method after Serafica *et al*. [95]. A litre of medium contained 50 g glucose, 5 g ammonium sulfate, 2.7 g sodium phosphate (dibasic), 1 g magnesium sulfate, 0.5 g yeast extract, 1.5 g citric acid, 14 mL ethanol and 2 mL of a trace element solution. BC pellicles were harvested and boiled in 1 M NaOH solution for 15 minutes to remove cell debris and medium. Pellicles were rinsed twice and soaked in deionised water (DIW) for 48 hours. The thickness of the wet pellicle was ~2 mm.

3.1.2 Properties of PLA film (Naturework® 4046D and 4060D)

The film was biaxial oriented and produced as either an A/B or A/B/A co-extrusion where the A layer is PLLA (4060D) to give good heat seal properties and the B layer is a PLLA (4042D) to give development of the required physical properties during the post extrusion, biaxial orientation process. The L/D ratio of 4042D and 4060D is from 24:1 to 30:1.Therefore, 4042D and 4060D are different grades from same PLLA polymer by different processing. The PLLA film is simply designated as PLA here throughout this work. The properties of PLLA 4042D and PLLA 4060D are shown in Table 3.1 and Table 3.2, respectively, as taken from the manufacturer.

Table 3.1 Properties of PLLA 4042D

Property	Typical value
Density (g/cm^3)	1.25
T_g (^oC)	52
Tensile Strength (MPa) MD (machine direction) TD (transverse direction)	 110 145
Young's Modulus (GPa) MD TD	3.3 3.86
Tensile Elongation at Break (%) MD TD	160 100

Table 3.2 Properties of PLLA 4060D

Property	Typical value
Density (g/cm^3)	1.25
Tg (^oC)	58
Seal Initiation Temperature (^oC)	80

3.2 Preparation of composite materials

3.2.1 Preparation and treatment of bacterial cellulose

Excess water on the surface of BC pellicle was wiped with tissue paper. The pellicle was cut into ~15 × 50 mm^2 pieces in the followed experiments.

3.2.1.1 Drying

The purpose of drying was to obtain the weight of dried BC film for the calculation of the fabric ratio of the composites. Figure 3.1 shows a schematic of the drying. A flat aluminium plat was drilled many holes. A piece of filter paper was attached on the Al plate. The plastic film was pricked many tiny hole by needles. Water would easy to evaporate through the holes on the plastic film, the filter paper and the holes on the Al plate. A pressure of ~ 200 kPa was kept with the heavy block. The pellicles were dried at 70 ^oC for 6 hours. After that, the dried BC films were peeled off from the plate. Those cellulose films were placed in the vacuum oven at 50 ^oC for 12 hours to remove residual moisture. The final step was to measure the size and weight of those cellulose films.

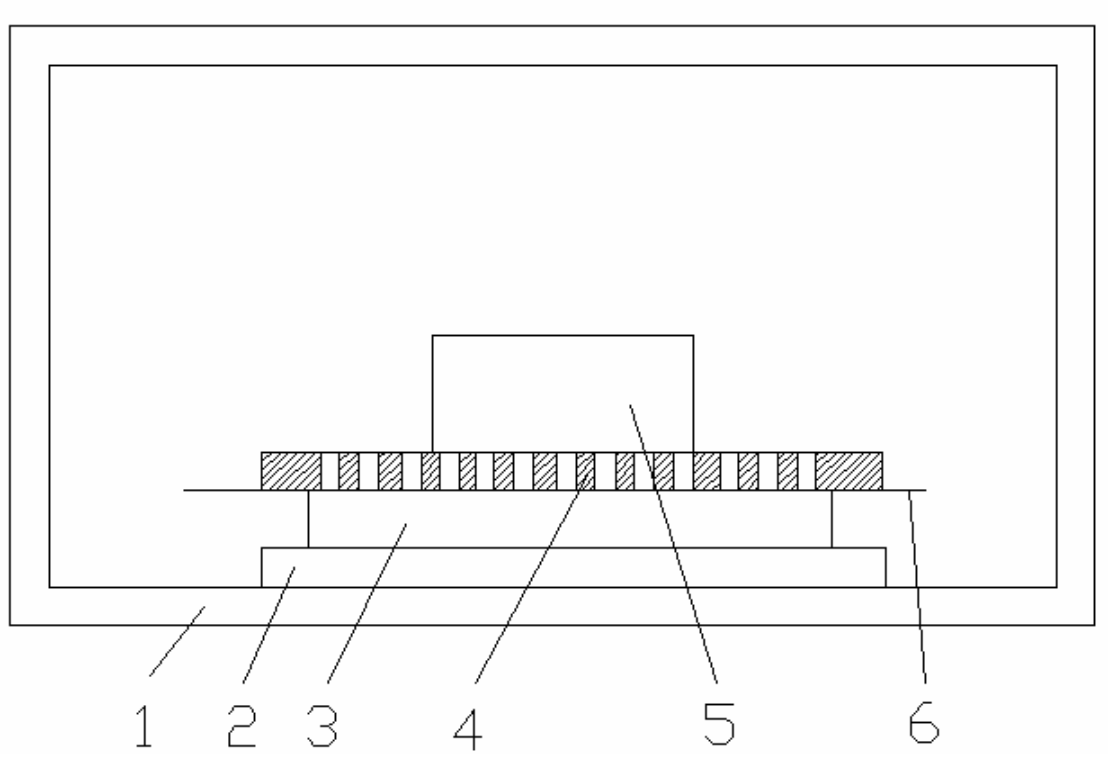

Figure 3.1 Schematic of the BC drying. 1) Oven, 2) glass plate, 3) wet BC pellicle, 4) Al plate, 5) heavy block and 6) plastic film and filter paper.

3.2.1.2 Solvent exchange route

As the BC pellicles contained over 99% water [48], the water can be removed by solvent exchange. Two different solvent exchange routes were utilised in this work. The first solvent exchange method was based on work by Gindl *et al* [51] and preparation methods for fresh biological specimen for the electron microscopy [96] and was carried out in the following sequence: immersing in 70% ethanol for 15 min, pure ethanol for 15 min, pure acetone for 15 min twice, and finally pure 1,4 dioxane for 15 min twice.

The second solvent exchange method was to immerse the BC pellicle in pure 1,4-dioxane for 15 min. The immersion of the pellicle was carried out three times to ensure exchange of the water with solvent.

Composites prepared from the first solvent exchange route had lower void content compared with the second route as determined from scanning electron microscopy (SEM) micrographs. The second route has the advantage of being shorter than the first route. The second route was selected in the followed experiment. The pellicles were not modified by surface treatments. Therefore, BC pellicles which were only exchanged for water by solvent are designated as *native* BC pellicles in this work.

3.2.1.3 Acetylation

Cellulose is a hydrophilic polymer. The unfavourable absorption of moisture in cellulose is due to the attraction of hydrogen in water molecules to the groups of hydroxyl along the cellulose chain. Moisture reduces the adhesion between cellulosic reinforcements and hydrophobic polymer matrices, lead to a loss of stress transfer and thus poor mechanical properties in the composite material. Acetylation can be used reduce the hydrophilicity of cellulosic fibres. During acetylation, acetyl groups are introduced into molecular combinations containing OH–, SN– or NH/2 groups [10]. Fibres of cotton [97], bamboo [98], flax, hemp and wood fibres [99] have been treated using this procedure.

The BC pellicles were immersed in pure acetic acid for 15 min. The immersion of the pellicle was carried out three times, followed by storage in a mixture of acetic acid,

acetic anhydride and 1 drop of sulphuric acid at room temperature for 1 hour. 0.1 mL of acetic anhydride was used for every gram of wet pellicle. This was based on the work of Kim *et al*. that used 10 mL acetic anhydride to treat 100 cm^3 of BC pellicle [100]. The density of the wet pellicle is essentially that of water since the BC pellicles contain over 99% water [48]. Thus, the weight of 100 cm^3 of BC pellicle is close to 100 g.

Following the above treatment, the BC pellicle was washed in acetone in ~ 7 passes. The pH of the acetone was tested by a water soaked indicator paper after washing to ensure all of reactants were washed out. Finally, the acetone in the pellicles was exchanged with 1,4 dioxane. BC with the acetylated surface treatment is designated as "acetylated BC" or "ABC" in this work.

3.2.1.4 Application of silane coupling agent

As described in last section, hydrophilic cellulose reinforcements are inherently incompatible with hydrophobic polymers. It is possible to bring about compatibility by introducing a third material that forms a bridge of chemical bonds between the reinforcement and polymeric matrix [10]. For example, organosilanes are the main group of coupling agents for glass-fibre reinforced polymers. Silane coupling agents have the ability to form a strong bond between organic and inorganic materials [101]

Analogous to glass-fibres, silanes have also been used as coupling agents for natural fibre reinforced polymer composites [102-105]. In addition, Silane treated kenaf or pineapple leaf fibre-reinforced composites offered superior physical and mechanical

properties of the PLA based composites over that of untreated fibres reinforced PLA [106]. 3-aminopropyltriethoxysilane (APS) has been used to treat the surface of cellulosic fibres in various studies [104, 105, 107]. APS has also been shown to be an effective coupling agent in calcium carbonate-PLLA composites [108]. Therefore, APS has the potential to increase the bonding between the cellulosic reinforcements and PLA.

In this work, 2 wt. % APS was dissolved by hydrolysis in a mixture of ethanol–water (80/20 v/v) at 25°C and stirred for 30 min. The pH of the solution was adjusted to 4 with the addition of acetic acid with continuous stirring for 10 min. The BC pellicles were then immersed in this solution for 1 hr with stirring.

After immersion the BC pellicle was washed with acetone in ~ 7 passes to remove residual reactants and dissociated silanol (i.e. the hydrolytic resultant of silane). After washing, the pH of the acetone was tested with a water soaked indicator paper to ensure all of reactants were washed out. Finally, the acetone in the pellicles was exchange with 1,4 dioxane. BC treated with APS is designated as “silane-treated BC” or “SBC” in this work.

3.2.2 Preparation of PLA matrix

3.2.2.1 Dissolution of PLA film

PLA film was washed with ethanol and dried at room temperature. The PLA film was then dried in a vacuum oven at 50 ºC for 12 hrs to remove residual moisture and

ethanol. The PLA was finally dissolved in 1,4-dioxane to obtain a 10 wt.% PLA solution.

3.2.2.2 Glycerol-plasticized PLA

PLLA is an isotactic polymer that is crystallizable, unlike the racemic form that remains amorphous. The L-enantiomorph is the form referred to in this research. PLLA is slow to crystallize and can form large spherulites [109]. However, one limitation of PLLA that restricts its range of applications is its brittleness despite its high modulus and tensile strength. To overcome the brittleness of PLLA, plasticizers such as citrate esters, 1, 2-propylene glycol, glycerol, poly (ethylene glycol), glucose monoesters, and partial fatty acids have been used with some success [109-112]. Plasticizers are actually low molecular weight (MW) resins or liquids, which form secondary bonds to polymer chains and spread them apart. Thus, plasticizers reduce polymer-polymer chain secondary bonding and provide more mobility for the macromolecules, resulting in a softer, more easily deformable mass [113].

Glycerol is a common and cheap plasticizer to obtain. It is normally added during the extrusion process In some cases, glycerol has also been combined with the polymer when it is in solution [114]. In this work, glycerol was first dissolved in 1,4-dioxane, followed by dissolving of PLA in the glycerol-1,4-dioxane solution. The solubility of glycerol in 1,4-dioxane is reported to be limited [115]. Thus, the solubility of glycerol in 1,4-dioxane was first measured to check its solubility.

1,4-dioxane and glycerol were mixed in a beaker and stirred for ~30 min to obtain a saturated solution. Any residual glycerol settled to the bottom of the solution in the

beaker. The solution was then placed in a vacuum oven at 40ºC to evaporate the solvent. The mass of the residual glycerol after evaporation was divided by the mass of the solution before evaporation to obtain the solubility limit of glycerol in 1,4-dioxane, yielding a solubility limit of 5.26 wt.%. The final plasticized PLA was then designed to contain 10 wt.% glycerol. Thus, the solution was made with 9 wt.% PLA and 1 wt.% glycerol. The glycerol-plasticized PLA is designated as PLAG in this work.

3.2.3 Combining of BC and PLA: Immersion and drying

The native BC, ABC or SBC pellicles were fully immersed in the PLA or PLAG solution for 24 hrs. The PLA or PLAG treated pellicles were placed on a glass plate and then dried at different vaporisation rates at room temperature for 24 hrs. PLA and PLAG solutions were cast directly onto a glass plate and vaporised at different rates at room temperature for 24 hrs to obtain PLA and PLAG films. And then, the as cast materials were dried with vacuum oven at 50 ºC for 12 hrs to remove residual moisture and solvent.

Three different vaporisation rates were trialled for preparing the PLA and PLA composite samples. The fastest rate involved placing the samples under a vacuum during drying. A lower (or normal) vaporisation rate was achieved by simply drying the samples in air. The lowest vaporisation rate was achieved by placing the sample in a covered Petri dish with only a small gap between the edge of the dish and cover. With the fastest vaporisation rate, the PLA and PLA composites produced were severely shrivelled after desiccation. At the normal vaporisation rate by air drying, the

cast PLA film contained some visible bubbles inside the sample. At the lowest vaporisation rate, the cast PLA film did not have any visible bubbles as observed by light microscopy, although SEM revealed very fine voids. From SEM of the composites under the normal and lowest vaporisation rates, statuses of voids were observed without much difference. Even though the lowest vaporisation rate yielded the best results, subsequent hot pressing would remove these voids and thus the normal vaporisation rate was used to shorten the sample preparation time.

3.2.4 Hot pressing of PLA and PLA composites

The purpose of hot pressing the samples following drying was to (i) reduce the voids in the composites/films; (ii) obtain flat surfaces on the samples; and (iii) release any residual stresses in the samples due to the drying process.

Dried PLA-treated pellicles (composite) were cut into samples of ~5-7 mm in width and 40~50 mm in length avoiding any shrivelled regions. A sample was then wrapped in smooth piece of Al foil that had been coated in a release wax. The foil wrapped sample was then placed in a mould for hot pressing. The samples were hot pressed at a temperature of 180ºC, pressure of 2.5~3 MPa and using a processing time of 3 min. Figure 3.1 shows a schematic of the hot pressing apparatus.

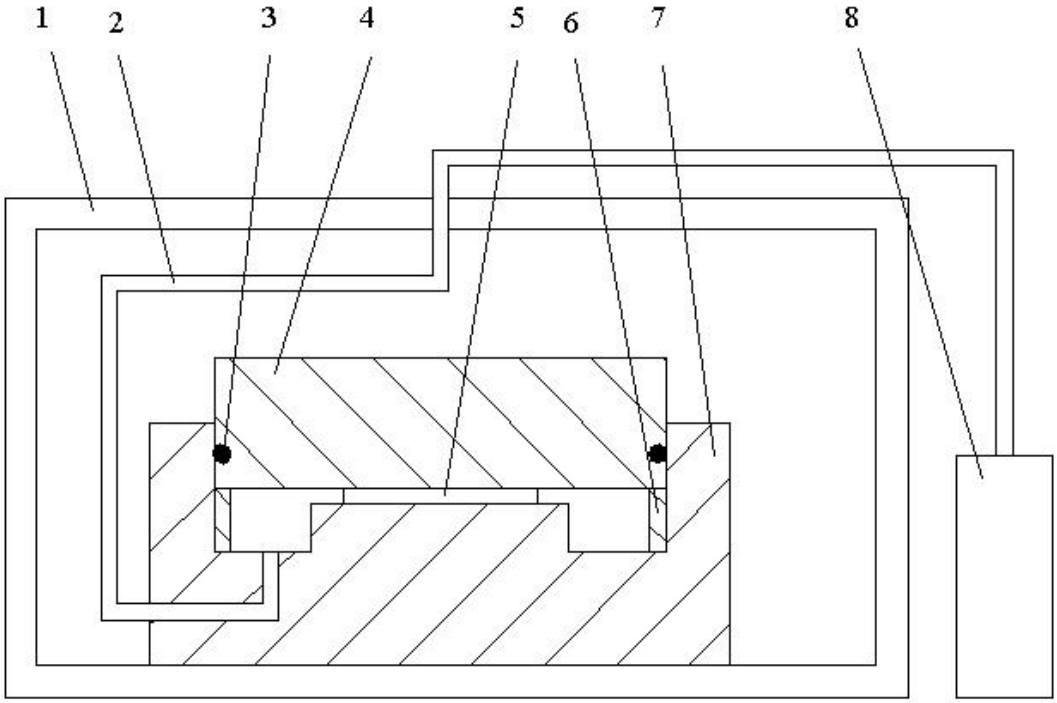

Figure 3.2 Schematic of the hot press used to prepare the PLA and PLA composites. 1) Vacuum oven, 2) Pipe, 3) O-ring, 4) Piston of mould, 5) Composite (wrapped with aluminium foil), 6) Spacer ring, 7) Housing of mould, 8) Vacuum pump.

The dried BC film and composites were measured the size and weight. The fibre content of various composites was calculated with the following equation:

$$W_f = M_{bc}/M_{com} \times 100\%$$

where W_f is the fibre content in weight percent; M_{bc} is the mass per unit area of dried BC film and M_{com} is the mass per unit area of composite. The designated names and fibre content of the various materials used in this work are summarised in Table 3.3.

Table 3.3 Designations and fibre contents of the PLA-based samples.

Material	Designated name	Fibre content (wt. %)
PLA	PLA	-
PLA-10 wt.% glycerol	PLAG	-
Native BC reinforced PLA	BC-PLA	11.39
Native BC reinforced PLAG	BC-PLAG	11.28
Acetylated BC reinforced PLA	ABC-PLA	10.24
Acetylated BC reinforced PLAG	ABC-PLAG	10.1
Silane treated BC reinforced PLA	SBC-PLA	10.62
Silane treated BC reinforced PLAG	SBC-PLAG	10.75

3.3 Materials characterization

3.3.1 Differential scanning calorimetry (DSC)

DSC is a commonly used thermal analysis technique for the measurement of the heat capacity and changes in heat capacity of polymers as a function of temperature. Thermally-driven processes such as crystal structure transitions, phase changes (*e.g.* melting and T_g) can be studied with DSC [116]. *Scanning* calorimeters are devices in which the sample temperature is deliberately changed during the course of an experiment according to a prescribed program. Typically, the heating or cooling of the sample is used to control the temperature linearly with time and the heat flow rate required to accomplish the desired temperature is determined and output as a function

of time or temperature [117]. A generalized DSC curve for a polymer is shown in Figure 3.3.

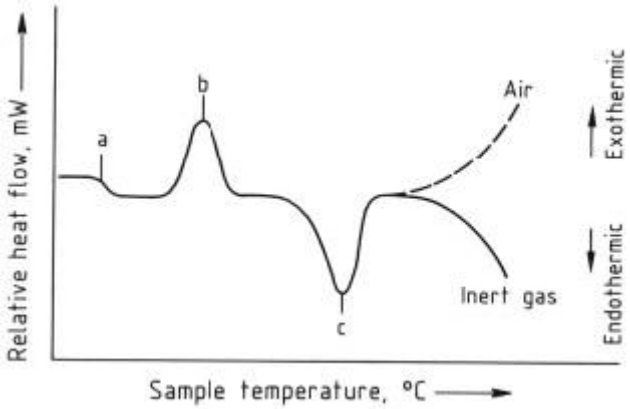

Figure 3.3 Generalized DSC curve for a polymer showing the a) glass transition; b) crystallisation peak and c) melting point [117].

With regard to the principle of measurement, two varieties of scanning calorimeters can be distinguished: (i) *differential-temperature* and (ii) *power-compensated calorimeters*. Power-compensated scanning calorimeters always feature duplex construction, with sample and reference holders heated in such a way that at every instant the temperature of each corresponds almost exactly to a programmed set temperature. Any temperature differences that arise between sample and reference by reason of thermal events in the sample are compensated immediately by appropriate changes in the electrical heating. The output signal is proportional to the instantaneous differential heat flow rate. Figure 3.4 shows the operating principle of a power-compensated differential scanning calorimeter.

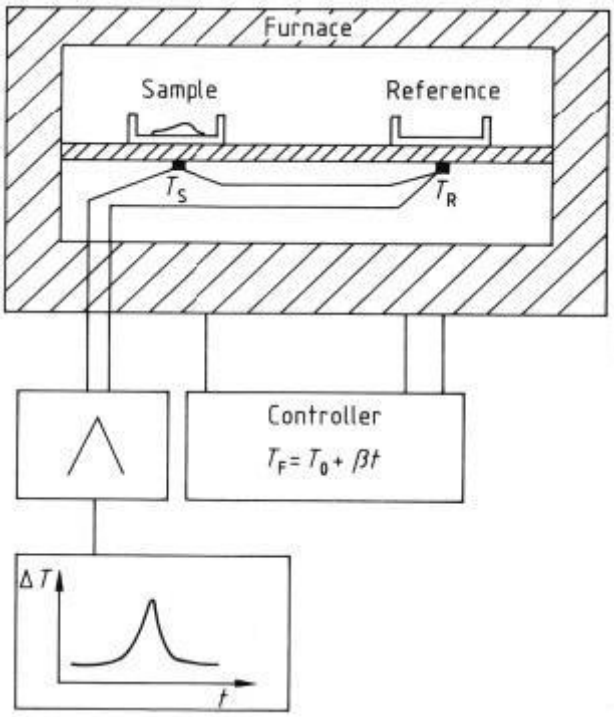

Figure 3.4 Operating principle of a power-compensated differential scanning calorimeter. T_0: initial temperature; T_S: sample temperature; T_R: reference temperature; <T>: temperature between sample and reference; ΔP: differential power; β: heating rate; t: time [117].

In this work an MS-DSC 4100 (Calorimetry Sciences Corp.) was used to measure the thermal properties of the polymers and composites. Firstly, the melting point of the PLA was determined with DSC for optimising the temperature used during hot pressing. The temperature scanning range was 20-200ºC and the scanning rates were 0.4 or 2.0ºC/min. Although a slower scanning rate provides greater accuracy, there is a chance that the PLA may degrade at higher temperatures (~160 ºC) if held for too long (~30 min) [118]. The faster scanning rate was used to identify whether the PLA in this work was degraded during slow scanning.

The melting points of the original PLA film, cast PLA film and cast PLAG film were determined by DSC. ~0.1 g of sample was used for the DSC measurements. Samples were wrapped in Al foil to avoid contamination of the ampoules with the PLA. The mass of Al foil was ~0.15 g. Baselines of empty ampoules and Al foil were also measured. The results of sample which subtracted the results from the empty ampoules and aluminium foil were used to obtain the final results. The scanning rate and mass of every material in the DSC experiments are shown in Appendix C.

DSC can also be used to determine the crystallinity of polymer. The crystalline fraction may be expressed as a percentage of a value representing complete crystallisation [119]. Thus, the crystallinity of a specimen may be calculated as:

$$X_c = \Delta H_m / \Delta H_m^0 \times 100\%$$

where, X_c is the percentage crystallinity of the sample, ΔH_m is the experimental heat of fusion and ΔH_m^0 is the literature value of heat of fusion for a 100% crystalline material [119]. ΔH_m^0 of 100% crystalline PLA is reported as 93.7 J/g [120].

The DSC experiments for measuring the crystallinity of materials were performed using a Perkin Elmer Pyris 1. DSC crystallinity studies were performed on neat PLA, BC-PLA, ABC-PLA and SBC-PLA using a sample mass between 2 and 5 mg. In order to remove prior thermal history, specimens were initially heated to 200ºC at 40ºC/min and then held for 5 minutes at 200ºC to ensure complete melting. The experimental data was collected for both a cooling scan at 5 ºC /min to 20ºC and a subsequent heating scan at 5ºC /min to 200 ºC.

3.3.2 Scanning electron microscopy (SEM)

In a scanning electron microscope, a small electron probe 1-10 nm in diameter scans in a raster across the surface of the specimen (Figure 3.5). The incident electrons are elastically and inelastically scattered by the specimen. Elastic scattering results in large scattering angles and zigzag electron trajectories. Therefore, a fraction of electrons can leave the specimen as *backscattered electrons* (BSE). The slowing down of electrons by inelastic scattering results in an electron range *R*. Electrons from the specimen atoms that are excited by inelastic scattering can leave the specimen as *secondary electrons* (SE) from a thin surface layer SE of ~1-10 nm. By convention, electrons in the energy spectrum with $E \leq 50$ eV are called SE. The secondary electrons consist of (1) SE1 excited by the primary electrons; (2) SE2 excited by BSE on their path through the surface; (3) SE3 are excited when BSE strike the lower pole piece; or flow (4) as SE4 through the pole piece bore. The ionization of inner atomic shells results in the emission either of characteristic X-ray quanta (X) or of Auger electrons (AE). The image is formed by the signal of emitted secondary electrons, backscattered electrons, Auger electrons, absorbed specimen current (SC), or X-ray quanta, which modulate the intensity of a cathode-ray tube rastered in synchronism [121].

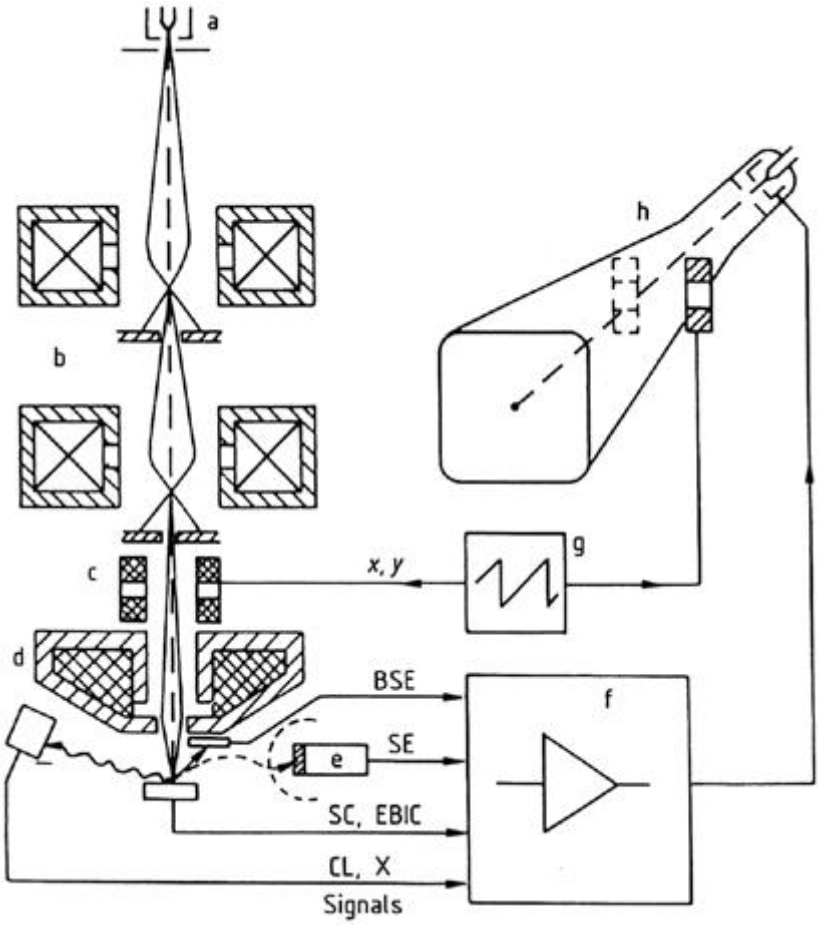

Figure 3.5 Schematic cross section of a scanning electron microscope showing the a) electron gun; b) condenser lenses; c) scan coils; d) objective; e) photomultiplier; f) amplifier; g) scan generator and h) cathode-ray tube. BSE = Backscattered electrons; SE = Secondary electrons; SC = Specimen current; EBIC = Electron-beam-induced current; CL = Cathodoluminescence; X = X-rays [121].

Composites and PLA films were studied using the JEOL JSM-6100 and JEOL JSM-7000F scanning electron microscopes in ultra high vacuum mode at an accelerating voltage of 2-5 kV. JEOL JSM-7000F can generate high resolution graphics due to it is a field emission SEM (FE-SEM). The morphologies of different cross section of composites and films were studied including the tensile fracture surface, freeze-

fractured surface (in liquid nitrogen) and polished surface. Specimens were prepared for SEM by sputter coating with gold (for JEOL JSM-6100 and JEOL JSM-7000F).

3.3.3 Transmission electron microscopy (TEM)

The images produced in transmission electron microscopy (TEM) are essentially due to local diffraction phenomena. The ray paths in an electron microscope are shown in Figure 3.6, according to the geometrical optics approximation. The microscope is essentially a three-lens system: an objective lens (c), an intermediate lens (e), and a projector lens (f). Each lens may be a composite lens. A movable selector aperture (b) is present in the image plane of the objective lens. With the first aperture a small area (≤1 μm) of the image (i.e., of the specimen) is selected, with the second aperture a single beam is selected or a number of the image-forming diffracted beams. In the imaging ray path the beam produced by a source and collimated by a condenser lens system, is scattered by the object, and an image is formed in the image plane of the objective lens. By means of the selector aperture, an area of the specimen is selected and magnified by the intermediate lens, which is focused on the image plane of the objective lens and provides a magnified image in the image plane of the intermediate lens. This image serves as the object for the projector lens, which forms the final image either on a fluorescent screen, on a photographic plate [121].

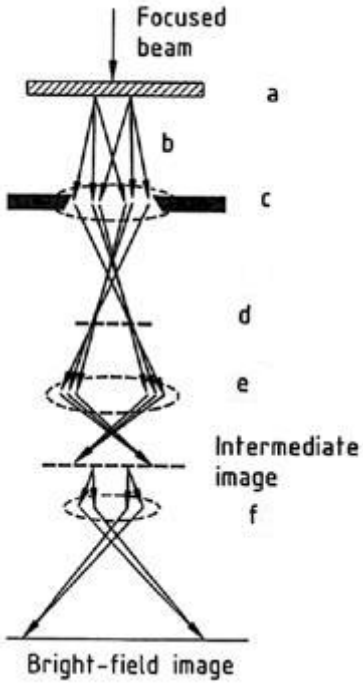

Figure 3.6 Schematic of the beam path in an electron microscope according to the geometrical optics approximation. a) specimen; b) objective aperture; c) objective lens; d) gaussian image plane; e) intermediate lens and f) projector lens [121].

The cross section of composites was studied using a Hitachi H600 transmission electron microscope. The BC-PLA composite (before and after hot pressing) and the BC-PLAG composite (before and after hot pressing) were examined by TEM. Composites were embedded in epoxy resin and cured for 24 hrs, followed by cutting with a microtome. The thickness of the microtomed specimens was ~100 nm. Finally, specimens were stained with uranyl acetate and lead to distinguish the cellulose and matrix.

3.3.4 Atomic force microscopy (AFM)

Atomic force microscopy (AFM) belongs to the group of scanning force microscopy (SFM) techniques that are based on the measurement of different forces (*e.g.* attractive, repulsive, magnetic or electrostatic) between a sharp tip and the sample surface. Imaging is accomplished by measuring the interaction force by means of the deflection of a soft cantilever while raster-scanning the tip across the surface (Figure 3.7). Although various types of forces are encountered when a tip approaches the sample surface, signal generation in AFM is essentially based on interatomic repulsive forces (Figure 3.8), which are of extreme short range nature [122].

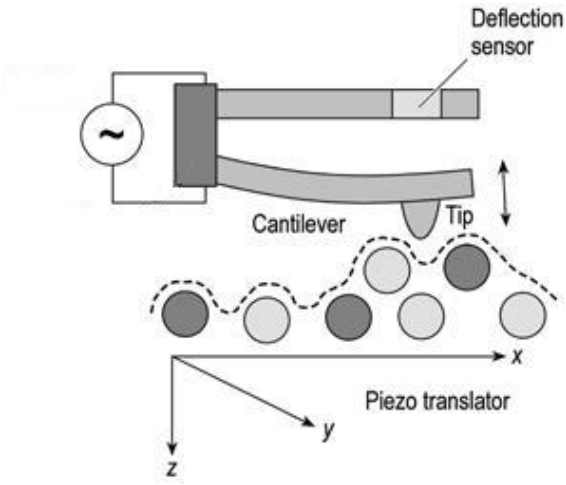

Figure 3.7 Principle of AFM [122].

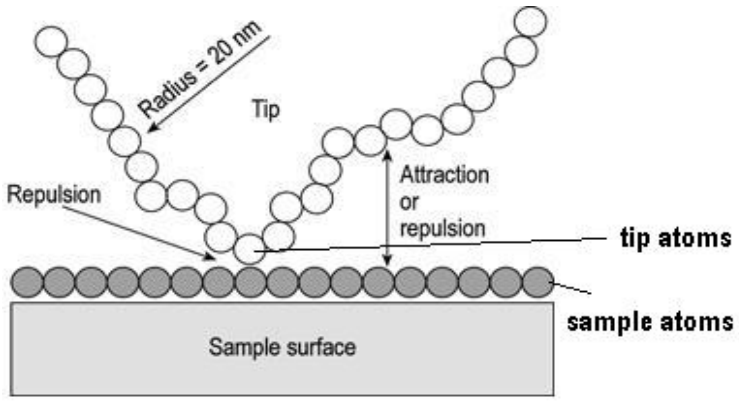

Figure 3.8 Schematic view of forces when the tip touches the sample surface [122].

Atomic force microscopy (AFM) was performed with a Digital Instruments 3100 with a Nanoscope IIIa controller to study the BC. Ambient atmosphere measurements were made in contact mode using oxide-sharpened silicon nitride tips on triangular cantilevers with soft spring constants of ~0.06 N/m (Veeco SPN-20). Load forces for the samples were on the order of 5 nN, and no image degradation was observed during scanning. Scan speeds ranged from 1 to 5 Hz. Contact mode was chosen above tapping mode as it demonstrated much higher lateral resolution of these samples.

3.3.5 Dynamic mechanical analysis (DMA)

Polymers exhibit both elastic and viscous behaviour under stress. The study of elastic and viscoelastic materials under conditions of cyclic stress or strain is called dynamic mechanical analysis (DMA) [123]. In DMA, a sinusoidal modulated stress, often flexural (though measurement is also possible under tensile, compressive, shear or torsional conditions) is applied to a specimen of material maintained under a specified temperature regime. Displacement transducers measure strain induced in-phase with the stress, as well as strain that lags behind. The former gives a measure of the sample's modulus, or stiffness, and the latter reflects damping characteristics [117].

If a constant load applied to a sample begins to oscillate sinusoidally (Figure 3.9a), the sample will deform sinusoidally. This will be reproducible if the material is deformed within its linear viscoelastic region. For any one point on the curve, the stress applied is described as:

$$\sigma = \sigma_o \sin \omega t$$

where σ is the stress at time t, σ_o is the maximum stress, ω is the frequency of oscillation, and t is the time. The resulting strain wave shape will depend on how much viscous behaviour the sample has as well as how much elastic behaviour. In addition, the rate of stress can be determined by taking the derivative of the above equation in terms of time:

$$d\sigma/dt = \omega\sigma_o \cos \omega t$$

The two extremes of the material's behaviour, elastic and viscous, provide the limiting extremes that will sum to give the strain wave. The behaviour can be understood by evaluating each of the two extremes. The material at the spring-like or Hookean limit will respond elastically with the oscillating stress. The strain at any time can be written as:

$$\varepsilon(t) = E\ \sigma_o \sin (\omega t)$$

where $\varepsilon(t)$ is the strain at anytime t, E is the modulus, σ_o is the maximum stress at the peak of the sine wave, and ω is the frequency. Since in the linear region σ and ε are linearly related by E, the relationship is:

$$\varepsilon(t) = \varepsilon_o \sin (\omega t)$$

where ε_o is the strain at the maximum stress. This curve shown in Figure 3.9b has no phase lag (or no time difference from the stress curve) and is called the in-phase portion of the curve.

The viscous limit was expressed as the stress being proportional to the strain rate, which is the first derivative of the strain. This is best modelled by a dashpot and for that element, the term for the viscous response in terms of strain rate is described as:

$$\varepsilon(t) = \eta d\sigma_o/dt = \eta\omega\sigma_o \cos(\omega t)$$

or

$$\varepsilon(t) = \eta\omega\sigma_o \sin(\omega t + \pi/2)$$

where the terms are as above and η is the viscosity. Substituting terms as above makes the equation:

$$\varepsilon(t) = \omega\sigma_o \cos(\omega t) = \omega\sigma_o \sin(\omega t + \pi/2)$$

This curve is shown in Figure 3.9c. Now, take the behaviour of the material that lies between these two limits. The difference between the applied stress and the resultant strain is an angle, δ, and this must be added to equations. So the elastic response at anytime can now be written as:

$$\varepsilon(t) = \varepsilon_o \sin(\omega t + \delta)$$

Using trigonometry this can be rewritten as:

$$\varepsilon(t) = \varepsilon_o [\sin(\omega t) \cos\delta + \cos(\omega t) \sin\delta]$$

This equation, corresponding to the curve in Figure 3.9d, can be separated into the in-phase and out-of-phase strains that correspond to curves like those in Figure 3.9b and c respectively.

These are the in and out phase modular and are:

$$\varepsilon' = \varepsilon_o \sin(\delta)$$

$$\varepsilon'' = \varepsilon_o \cos(\delta)$$

and the vector sum of these two components gives the overall or complex strain on the sample:

$$\varepsilon^* = \varepsilon' + i\varepsilon''$$

These terms are often written with E instead of the ε used here and referred to as E' (storage modulus) and E" (loss modulus).

The ratio of the loss modulus to the storage modulus is also the tan of the phase angle and is called damping:

$$\text{Damping} = \tan \delta = E''/E'$$

Damping is a dimensionless property and is a measure of how well the material can disperse energy. Damping lets us compare how well a material with absorb or loss energy [124].

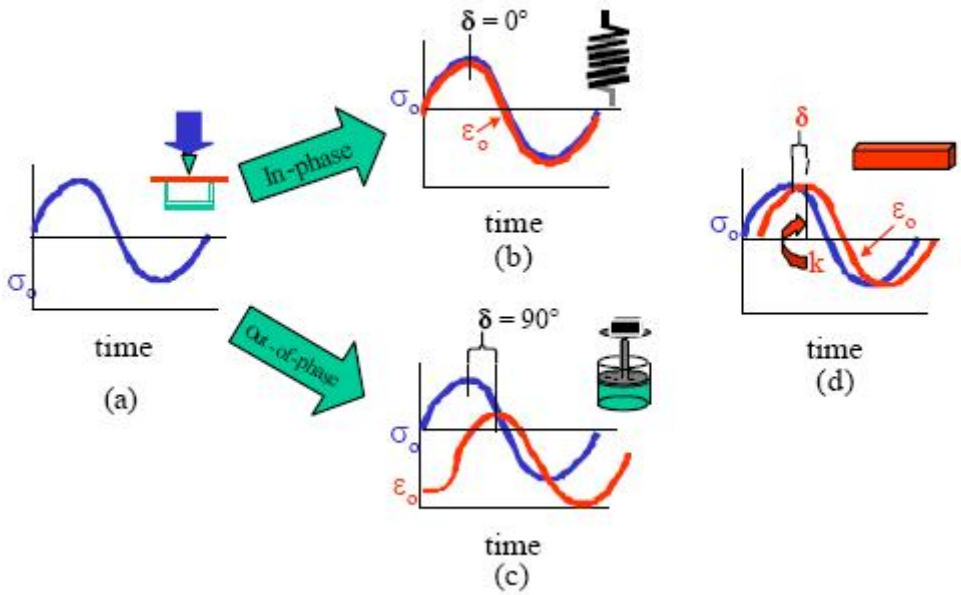

Figure 3.9 Relationship between stress and strain during a dynamic mechanical test [124].

The thermal transitions in polymers can be described in terms of either free volume changes or relaxation times. The molecules in polymer have some degree of free movement. As the free volume of the chain segment increases, its ability to move in various directions also increases. This increased mobility in either side chains or small groups of adjacent backbone atoms results in a greater compliance (lower modulus) of the molecule. Moving from very low temperature, where the molecule is tightly compressed, to higher temperature the first changes are the solid-state transitions. As the material warms and expands, the free volume increases so that localized bond movements (bending and stretching) and side chain movements can occur. As the temperature and the free volume continue to increase, the whole side chains and localized groups of backbone atoms begin to have enough space to move and the material starts to develop some toughness. As heating continues, the T_g or glass transition appears when the chains in the amorphous regions begin to coordinate large scale motions. One classical description of this region is that the amorphous regions have begun to melt. Finally the melt is reached where large-scale chain slippage occurs and the material flows. This is the melting temperature, T_m [119, 123, 125].

As the free volume continues to increase with increasing temperature, the glass transition, T_g, occurs where large segments of the chain start moving. The T_g represents a major transition for many polymers, as physical properties changes drastically as the material goes from a hard glassy to a rubbery state. It defines one end of the temperature range over which the polymer can be used, often called the operating range of the polymer. For where strength and stiffness are needed, it is normally the upper limit for use [119, 123, 125].

Dynamic mechanical analysis (DMA) of the hot pressed composites and PLA films was carried out on a Perkin Elmer Instruments Inc. Diamond DMA. Samples were dynamically tested in tension mode using frequencies of 1, 2, 4, 10 and 20 Hz, amplitude of 5 μm and a preload of 10 mN. Samples of ~0.1-0.2 mm in thickness were prepared with a gage length of 10 mm and width of 3-8 mm. The storage modulus (E'), loss modulus (E") and tan δ (E"/E') were measured over the range of -50 to 150°C using a heating rate of 5°C/min. The PLA or PLAG was softened rapidly with high heating rate around T_g. On the other hand, the force controlling system of DMA could not response with the change of specimens; the load still kept high level and stretched the softened specimens. Therefore, for some particularly soft samples, such as PLAG, the heating rate was reduced to 1°C/min, and the heating rate of PLA was reduced to 2 °C/min. All samples were conditioned in accordance with Procedure C of Test Method in ASTM D 5229/D 5229M and stored and tested at standard laboratory atmosphere (23 ± 3 °C and 50 ± 10 % relative humidity) [32-35].

Due to a breakdown on the PE Diamond DMA at the University of Canterbury (UC), the DMA samples of ABC-PLA, ABC-PLAG, SBC-PLA and SBC-PLAG were tested on the same model of DMA instrument at Applied Sciences, RMIT University (Melbourne, Australia). As a comparison, PLA and BC-PLA specimens also were measured at RMIT University. Due to some scaling errors in the viscoelastic calibration on the RMIT University DMA machine, data from each of the two machines could not be directly compared without some correction. For example, E' of PLA from UC was 1.3-4 times that obtained from RMIT and E" from RMIT University was 3.1-4 times that obtained from UC. T_g of PLA from UC was 6.57-8.26 °C more than that obtained from RMIT. In order to compare the results from UC and

RMIT, E' from RMIT is multiplied by a factor of 3.5, E" from RMIT will be divided by 3.5 and the temperature increased by 7.5 °C in the DMA results of Chapter 4. It must be noted that it is likely that some errors will occur after this normalization. Therefore, comparisons between different samples from the two different instruments will be cautiously stated in Chapter 4.

3.3.6 Tensile properties measurement

Static mechanical tests (tensile) were carried on an MTS858 Desktop tensile testing machine using a 2.5 kN load cell. Strain was calculated from the cross head displacement. Samples of ~0.1-0.2 mm thickness were prepared with a gage length of 20-25 mm and a width of 3-8 mm. Samples were conditioned using the same procedure as for the DMA.

4 Results and Discussion

4.1 Melting point of PLA

Measurements of melting point based on differential scanning calorimetry (DSC) were carried out on a MS-DSC 4100 (Calorimetry Sciences Corp.). To avoid the contamination of the ampoule by molten PLA, samples were wrapped in aluminium foil. The Al foil and containers will also absorb heat. Therefore, baseline scans of the empty ampoules were performed. These baseline scans were subtracted from the sample scans. Also the enthalpy is proportional to the mass of sample; thus, the mass of sample must be included in the calculation of the heat flow measured by DSC. MS-DSC 4100 has 3 channels for specimens; thus, it is possible to scan up to 3 samples within one scanning route. For example, Figure 4.1 shows the unmodified DSC curve of original PLA film at heating scan with 0.4 °C/min rate. “Unmodified” means the results were not subtracted the baselines of empty ampoules and Al foil. After calculation, the melting point (Tm) was 159.44°C from this curve. Figure 4.2 shows the baseline of empty ampoule in channel 1 at 0.4 °C/min temperature ramp. Figure 4.2 shows the baseline of empty ampoule in channel 1 at heating scan with 0.4 °C/min rate. Figure 4.3 shows the DSC curve of 0.15048 g Al foil at same scanning rate. They suggested that not only ampoules but also Al foil involved in heat exchange.

There was a little difference between the mass of wrapping Al foil for the PLA and the Al foil without PLA for the baseline scan. In order to avoid the error from this difference, the calculation would as follows:

$$\Delta H_{Al}=H_{Al}-H_{Baseline}$$

$$\Delta H_{PLA}=H_{PLA}-H_{Baseline}-\Delta H_{Al}\cdot M_{PLA\text{-}Al}/M_{Al}$$

where ΔH_{Al} is the heat flux of Al foil only; H_{Al} is the heat flux of Al foil in ampoule; $H_{Baseline}$ is the heat flux of empty ampoule; $M_{PLA\text{-}Al}$ is the mass of wrapping Al foil for the PLA; M_{Al} is the mass of Al foil in the scanning for Al only; H_{PLA} is the unmodified heat flux of PLA; ΔH_{PLA} is the modified heat flux of PLA, "modified" means the results were subtracted the baseline of empty ampoules and aluminium foil.

The modified DSC results of original PLA film is shown in the Figure 4.4. T_m of original PLA film was 159.71 °C. The difference of melting points between modified and unmodified curves was 0.37 °C. The modified curve also was shifted up because the heat flux of ampoule and Al were removed. This method could obtain more accurate results on enthalpy of polymer during the phase transition; however, this point would be not discussed in this thesis. Therefore, all of DSC results have been processed by same modifying method, following discussion and figures (Figure 4.5, Figure 4.6, Figure 4.7 and Figure 4.8) in this section will base on the modified results unless those with indications.

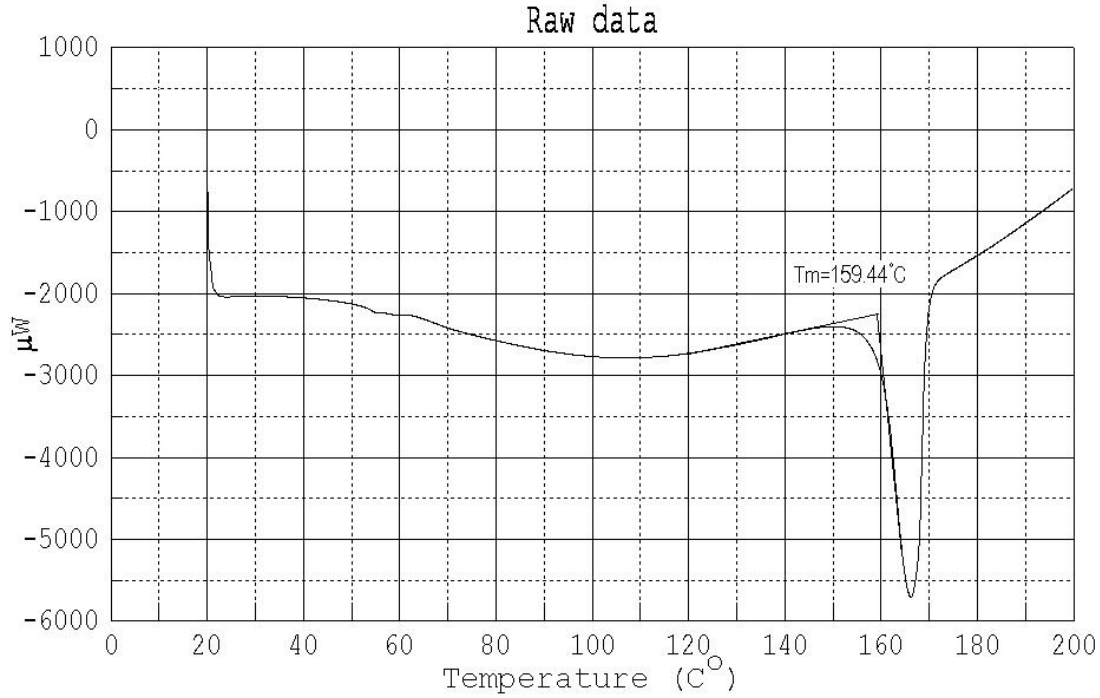

Figure 4.1 Unmodified DSC curve of 0.10079g original PLA film wrapped with 0.14879g aluminium foil at 0.4 °C/min heating rate (in channel 1 of MS-DSC 4100).

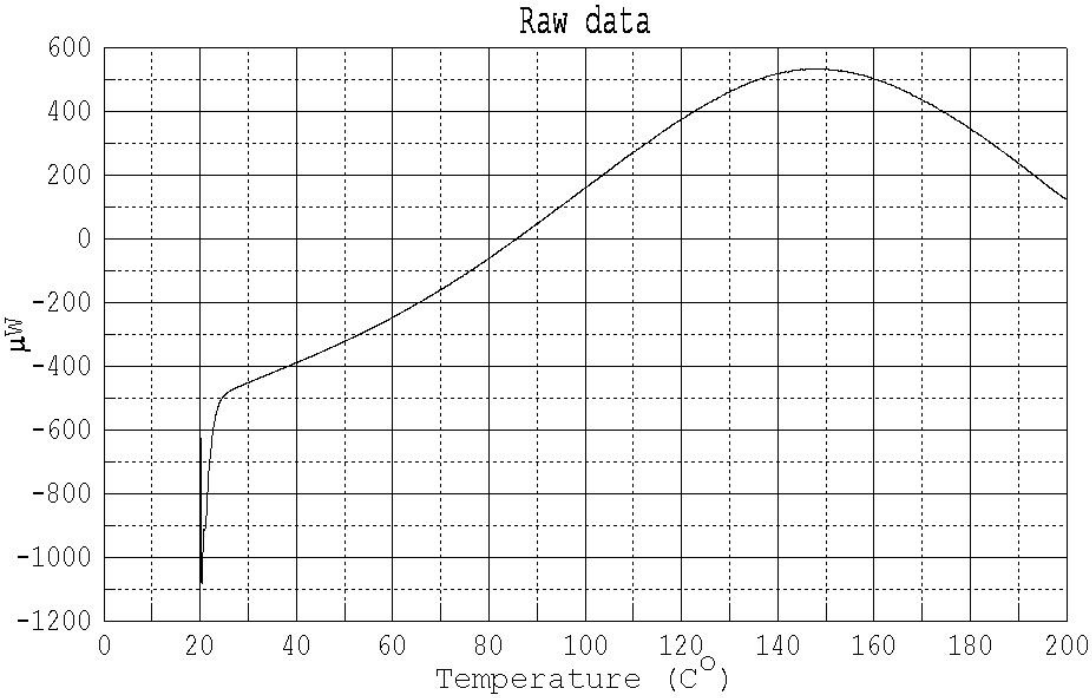

Figure 4.2 Baseline of empty ampoule at 0.4 °C/min heating rate (in channel 1 of MS-DSC 4100).

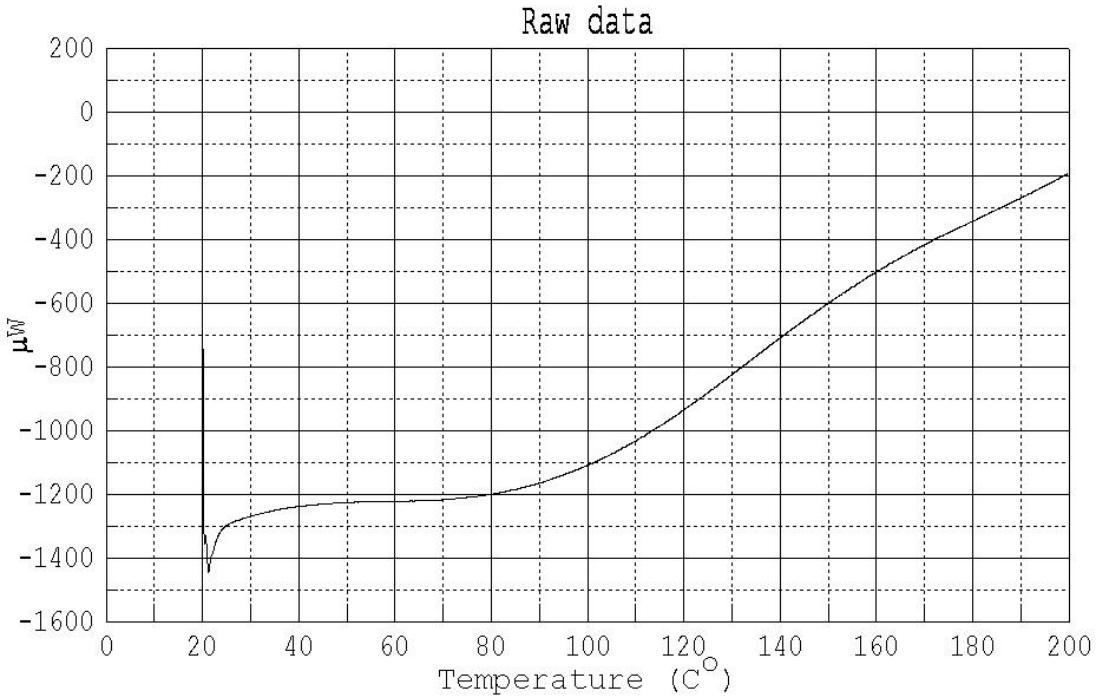

Figure 4.3 DSC curve of 0.15048g aluminium foil at 0.4 °C/min heating rate (in channel 1 of MS-DSC 4100).

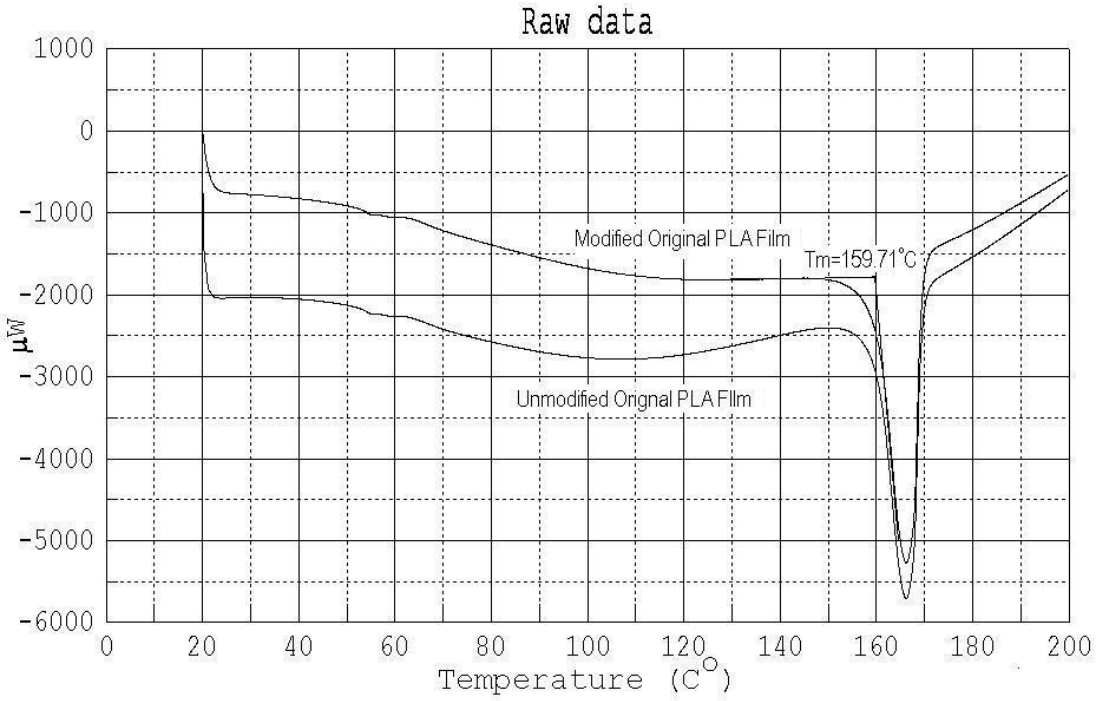

Figure 4.4 Comparison of modified/unmodified DSC curves of original PLA film at 0.4 °C/min heating rate (in channel 1 of MS-DSC 4100).

Figure 4.5 shows whole scanning (includes heating up and cooling down) DSC results of original PLA film at 0.4 °C/min temperature ramp. The crystalline peak on the cooling curve was shifted to lower temperature compare with the melting peak on the heating curve. It suggested that the original PLA film was degrade after being held over high temperature (160 °C) for long time as expect. The holding time is:

$$(200 - 160) / 0.4 \times 2 + 20 = 220 \text{ min} \approx 3.67 \text{ hrs.}$$

More than the holding time condition (~ 30 min [118]) at high temperature. However, PLA could degrade over 60 °C under special environment [126]. The Figure 4.6 shows DSC results of original PLA film at 2.0 °C/min heating rate. The melting point was 159.57 °C. It was quite close to the result with the scanning at 0.4 °C/min heating rate. It is difficult to prove the PLA would not degrade during the heating up progress under 160 °C. At lease it could prove that there was not much difference between the results of higher and lower heating rate.

Figure 4.7 shows the DSC results of cast PLA film at 0.4 °C/min heating rate. The melting point of cast PLA film was 159.1 °C, indicating that no much difference between the cast and original PLA films. It suggested that the solvent does not change the chain structure of PLA. Figure 4.8 shows the DSC results of cast PLAG film at 0.4 °C/min heating rate. The melting point of cast PLAG film was 147.64 °C. It suggested that the melting point was reduced due to the addition of plasticizer (glycerol).

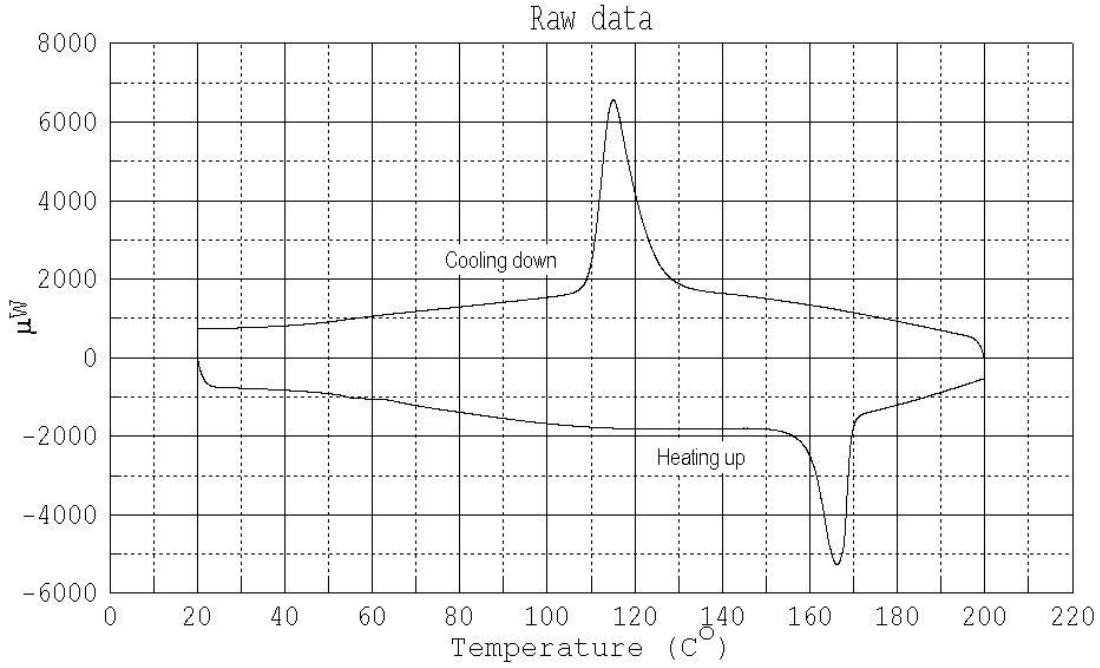

Figure 4.5 Whole DSC results of original PLA film at 0.4 °C/min temperature ramp (in channel 1 of MS-DSC 4100).

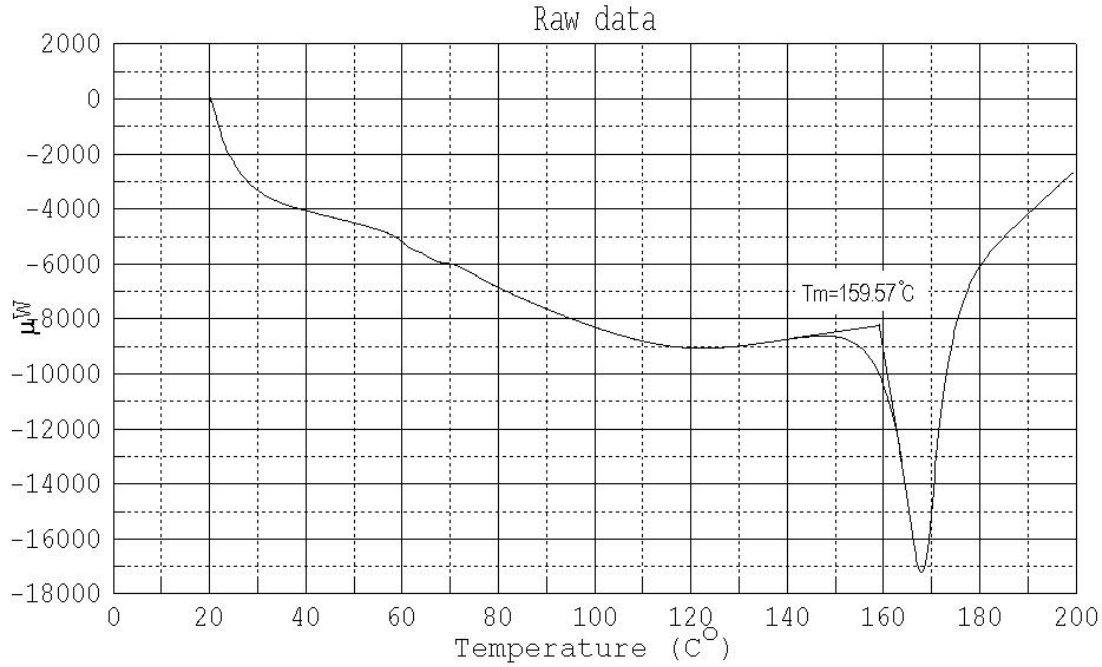

Figure 4.6 DSC results of original PLA film at 2.0 °C/min heating rate (in channel 1 of MS-DSC 4100).

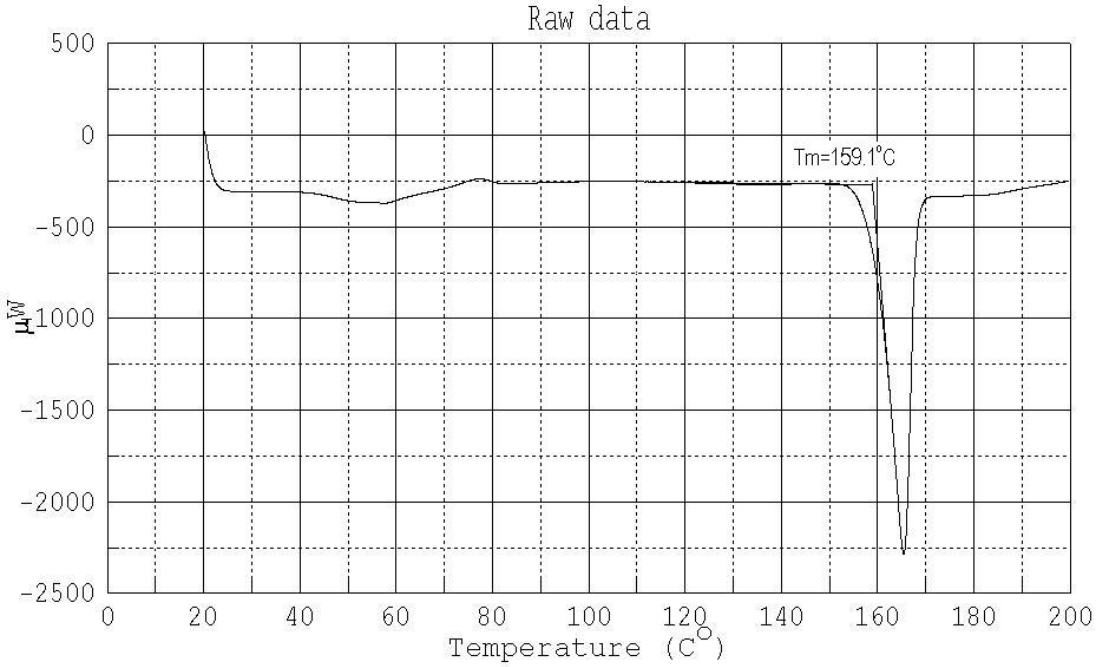

Figure 4.7 DSC results of cast PLA film at 0.4 °C/min heating rate (in channel 2 of MS-DSC 4100).

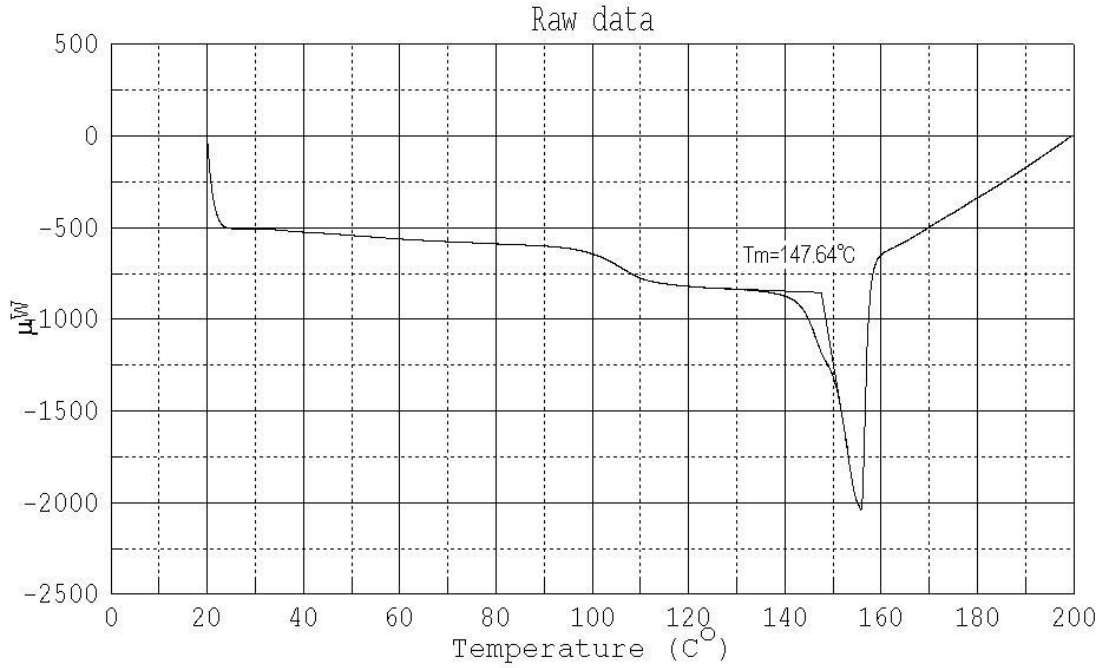

Figure 4.8 DSC results of cast PLAG film at 0.4 °C/min heating rate (in channel 3 of MS-DSC 4100).

The purpose of DSC testing was to optimize the operating temperature of hot press. Generally, the melting points of PLA and PLAG were lower than 160°C. References in the literature have used a processing temperature of 170-220°C for 2-10 min during hot pressing of a PLA composites [22, 84, 85, 127, 128]. Higher temperatures (over 190°C) would degrade the PLA and cellulose while lower temperatures reduce the fluidity of molten PLA. Therefore, the operating temperature was set at 180°C and the operating time used was 3 min.

Glass transition (T_g) stages of PLA have been shown on above curves (Figure 4.1, Figure 4.4, Figure 4.5, Figure 4.6 and Figure 4.7). The thermal history of polymeric material influences the T_g [119, 123]. The final materials had the procedure of hot pressing and cooling. Therefore, the T_g must different with the raw materials. The T_g of final materials could be measured out by DMA, therefore, T_g of PLAs would not be discussed in this section.

A Matlab programme was developed to calculate the DSC results. This programme is shown in Appendix B. Exactly, not all of DSC results are shown in this section. Most of curves based on 2.0 °C/min scan rate were not presented due to the results with 0.4 °C/min scan rate were more accurate than the results with 2.0 °C/min scan rate. None useful parameter for the melting point of PLA was shown on the cooling results. Those curves would be presented in the Appendix C.

4.2 Microstructure of bacterial cellulose (BC)

Due to the ultrafine microstructure of the bacterial cellulose, it was difficult to observe the microfibrils of wet BC pellicle by light microscopy (Figure 4.9). A layered structure can be scarcely seen in the dried BC pellicle by optical microscopy (Figure 4.10). Freeze-drying is a water removal method in which the structure of the material is largely retained [129]. Freeze-dried BC pellicles could be observed by FE-SEM (Figure 4.11). The microfibrils and ultrafine network structure could be seen clearly and the layered structure of BC could also be identified. The SEM images of air dried BC (Figure 4.12) showed not only the layers of BC, but also the network structure of microfibrils within the layer.

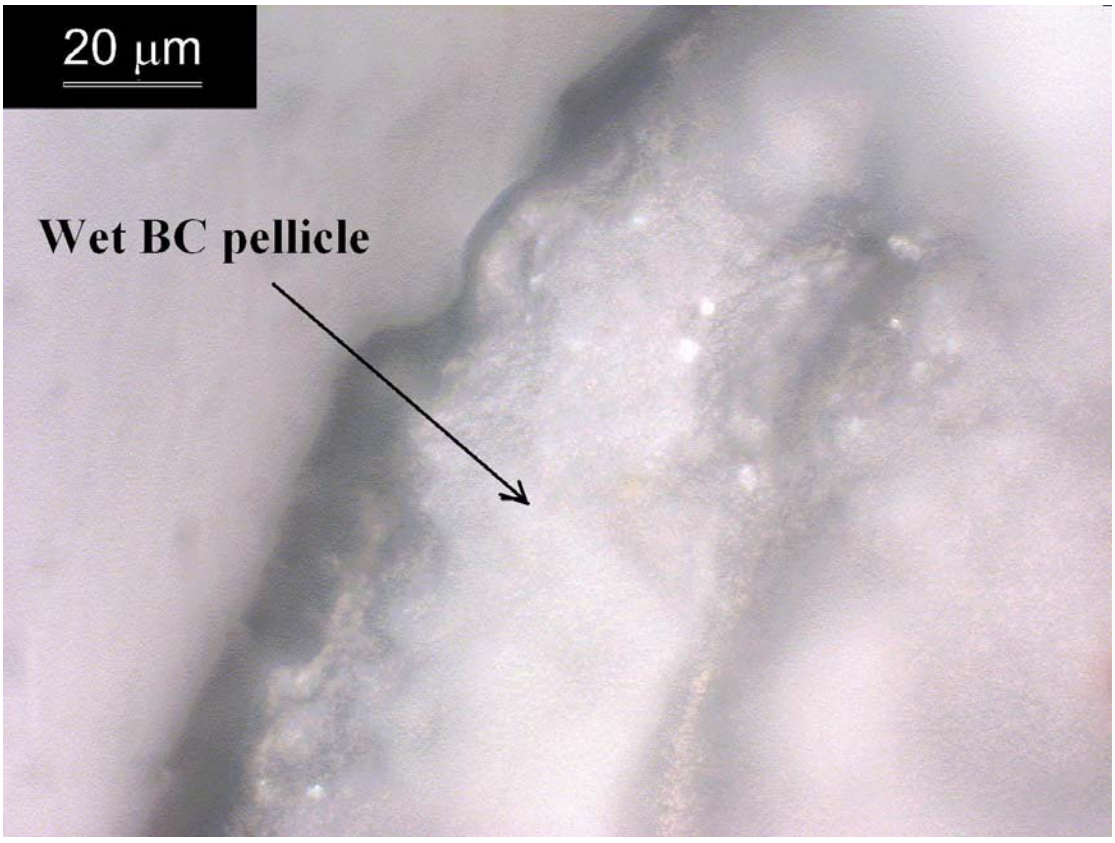

Figure 4.9 Optical micrography of wet BC pellicle (1,000 ×).

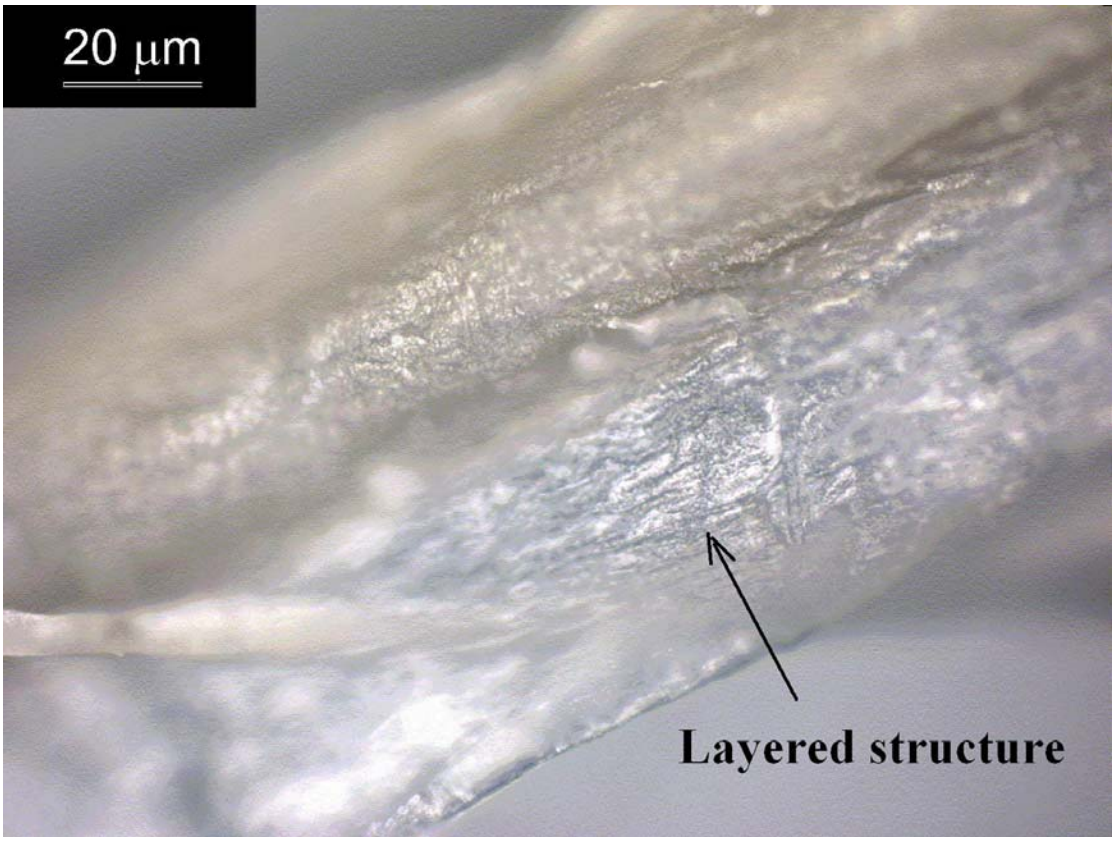

Figure 4.10 Optical micrography of air dried BC pellicle (1,000 ×).

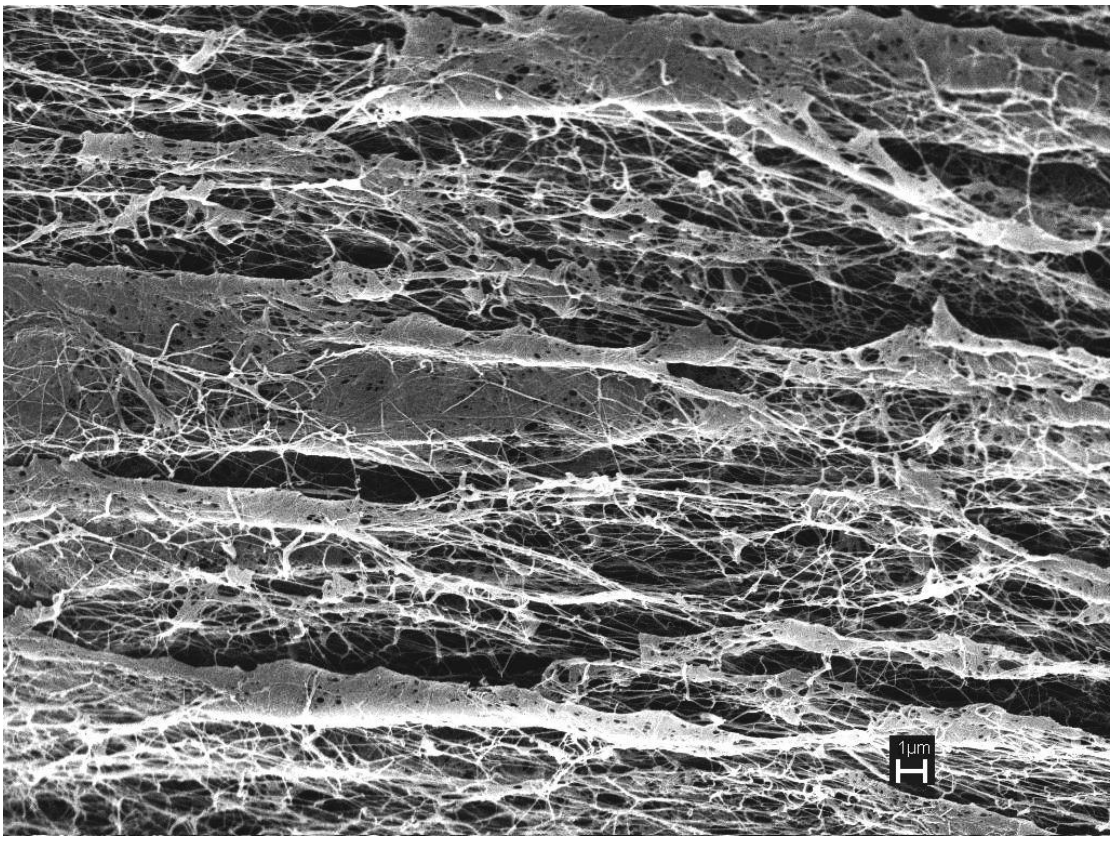

Figure 4.11 FE-SEM micrography of freeze dried BC pellicle (10,000 ×).

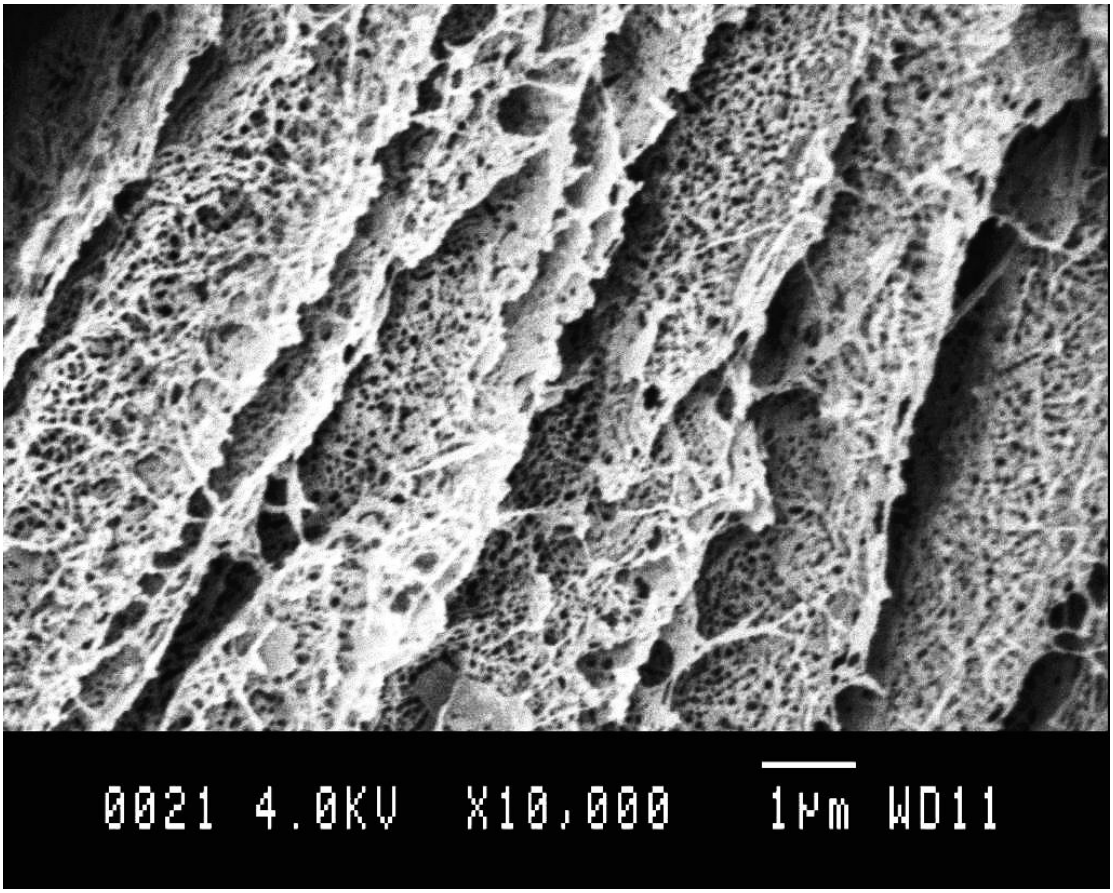

Figure 4.12 SEM micrography of air dried BC pellicle (10,000 ×)

The highly networked structure of the top surface of the bacterial cellulose, as imaged by the Atomic Force Microscope, is shown in Figure 4.13. The native BC is composed of microfibrils approximately 5-10 μm in length with diameters on the order of 50 nm. It is apparent in the higher magnification of Figure 4.13b, that these fibres are agglomerates of smaller subfibrils with diameters on the order of 10-20 nm.

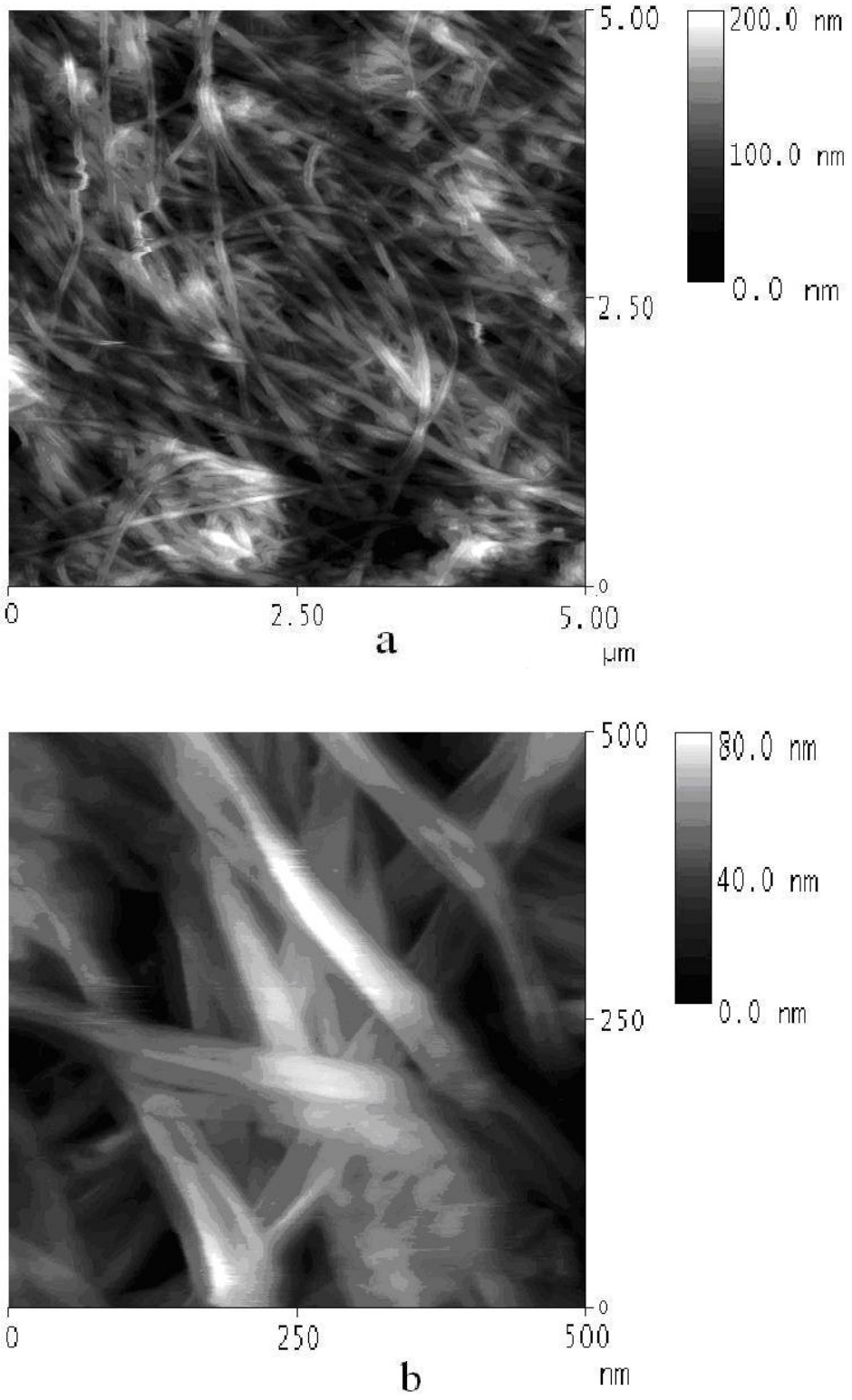

Figure 4.13 Atomic force micrographs of the top surface of the dried bacterial cellulose. At lower magnification (a) details of the highly networked structure can be observed while at higher magnification (b) the structure of the individual fibres can be seen.

4.3 Influence of different water exchange methods on the microstructure of composites before hot pressing

As described in section 3.2.1.2, two kind of water exchange route were used: (i) acetone-ethanol-1,4 dioxane and (ii) 1,4 dioxane-only. Figure 4.14 shows the freeze-fracture cross section of composites without hot pressing. The BC-PLA composite in which the BC pellicle was processed by the acetone-ethanol-dioxane route had a lower void content (Figure 4.14a and b) had lower void content than the BC-PLA composite in which the BC pellicle was processed by dioxane-only route (Figure 4.14c and d).

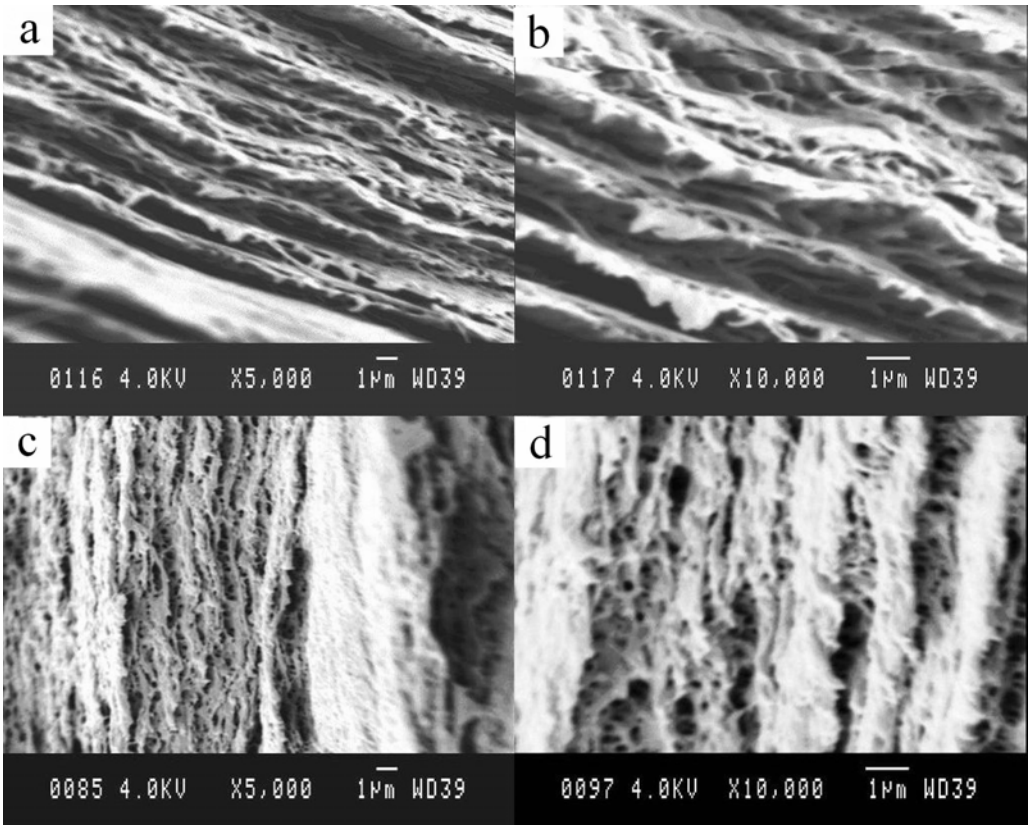

Figure 4.14 Scanning electron micrographs of the cross section of freeze-fractured BC-PLA composites before hot pressing. In (a) and (b) the BC pellicle was processed using the acetone-ethanol-dioxane water exchange route. In (c) and (d) the BC pellicle was processed *via* the dioxane-only water exchange route.

The void content would reduce the strength of the composite [1]. Therefore, hot pressing was used as a final step in the preparation of the composites. Furthermore, the dioxane-only route was used for water exchange in order to save the time on the preparation of composite.

4.4 The influence of different vaporisation rates and plasticizer on void content

A total of three different vaporisation rates were carried for drying the composites and cast films as described in the Section 3.2.3. The first one was fast rate, samples were dried under the vacuum condition. The second one was normal rate, samples were opened to air and dried. The third one was slow rate, samples were placed in Petri dish with a cover, and a small gap was kept between the dish and the cover. The solvent vaporised very quickly under a vacuum, so that the composites prepared by this higher vaporisation rate crinkled and shrunk. Some large bubbles were also present on the surface of the cast films. Therefore, the higher vaporisation rates were avoided to improve the quality of the samples.

Normal vaporisation rates also led to bubbles (or voids) or uneven surfaces on the cast films. A slow vaporisation rate yielded flat surfaces on the cast films and no visible bubbles in the samples. However, composites were flat with shrunken edges under both normal and slow vaporisation rates.

High magnification micrographs better described the microstructures. Optical micrographs (Figure 4.15) show the surface status of cast PLA film and cast PLAG

films that were dried under a slow vaporisation rate. The surface of the PLA film was slightly rough but no bubbles were visible (Figure 4.15a). With glycerol added to the PLA, voids were easily produced, even though a slow vaporisation rate was used on the cast films. Bubbles in the PLAG film can be seen under the optical microscope (Figure 4.15b).

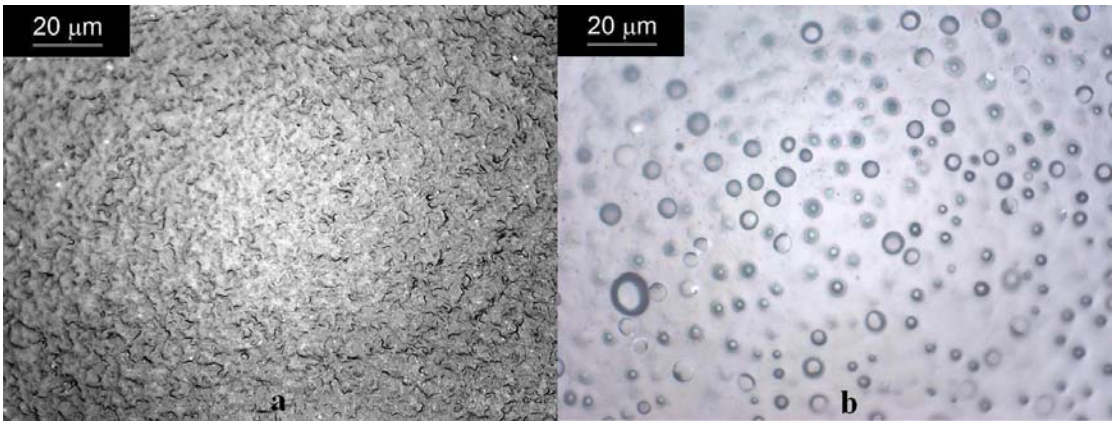

Figure 4.15 Optical micrographs of the as-cast a) PLA and b) PLAG film surfaces (1,000 ×).

A lower magnification with the optical microscope does not reveal the fine scale microstructure. Scanning electron microscopy was required to observe the fine microstructure of the cast films. Figure 4.16a shows a freeze fractured cross section of the cast PLA film which was dried under a slow vaporisation rate. Many voids are distributed within the film with a size of ~ 200-400 nm. Similar size voids were also seen in the freeze fractured cross section of cast PLAG film which was dried under a slow vaporisation rate (Figure 4.16b). However, the number of voids in the PLAG film was less than the PLA film. Larger voids (~1-2 μm) were present in the PLAG film. The comparison of these two images suggests that glycerol reduces the amount of voids but increases the size of the voids. In addition, a slow vaporisation rate could

not prevent the occurrence of very fine voids. Therefore, it was necessary to hot press the as-cast PLA films to reduce the void content.

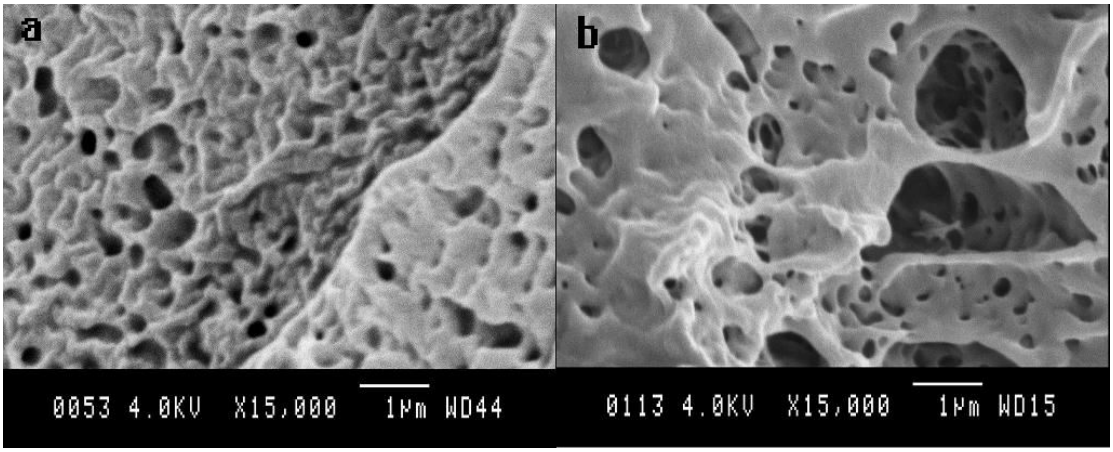

Figure 4.16 Scanning electron micrographs of the freeze fractured cross sections of cast films of a) PLA and b) PLAG, dried under a slow vaporisation rate.

Voids also formed in the composites when the vaporisation rate was normal or fast. Figure 4.17a and b show the freeze fractured cross section of the BC-PLA composite which was dried by normal vaporisation rate. Figure 4.17c and d show the freeze fractured cross section of BC-PLA composite which was dried by a slow vaporisation rate. Compare with these images, a slow vaporisation rate tends to reduce the size of voids in the composite, although the composite still has many voids.

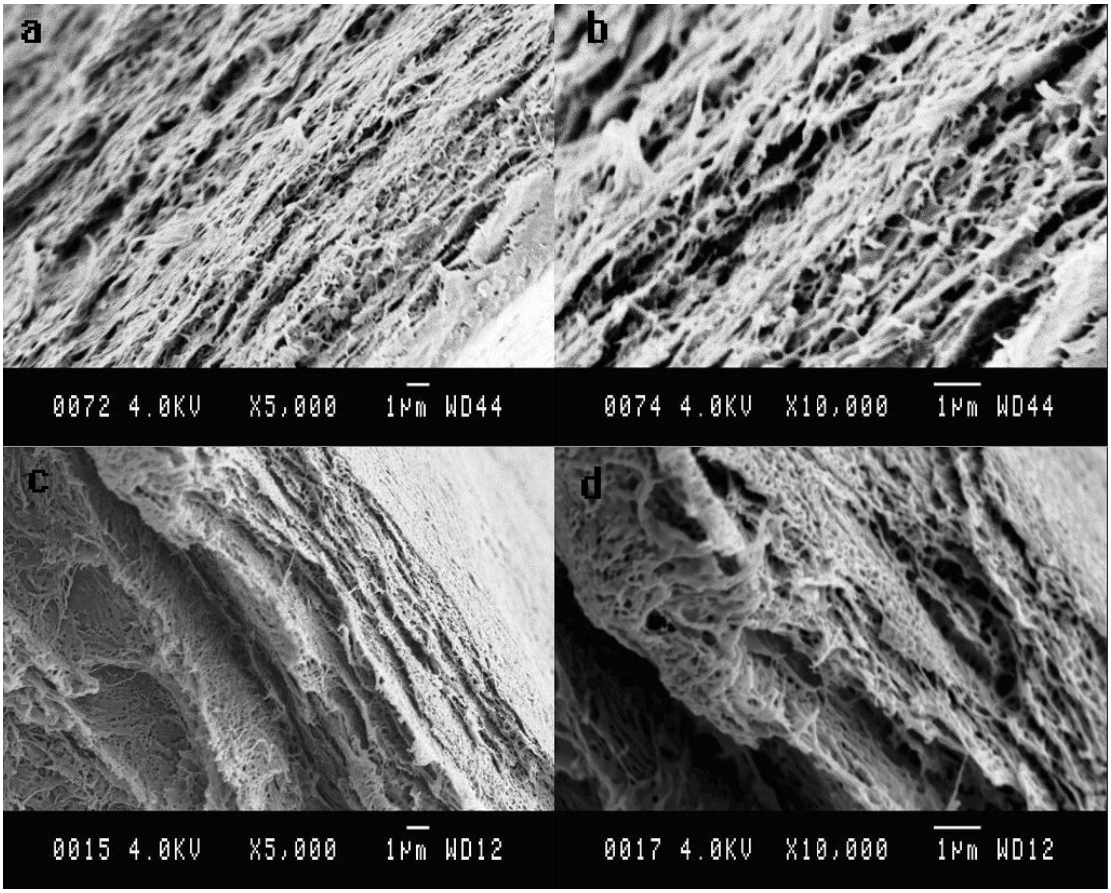

Figure 4.17 Scanning electron micrographs of freeze fracture cross section of BC-PLA composites, dried by normal (a and b) and slow (c and d) vaporisation rates.

Glycerol had a similar action in the composites as in the cast polymer film. Figure 4.18 shows the freeze fracture section of composites in which the matrix material was PLAG but with different drying speeds. The size of the voids hardly differed between the two different composites.

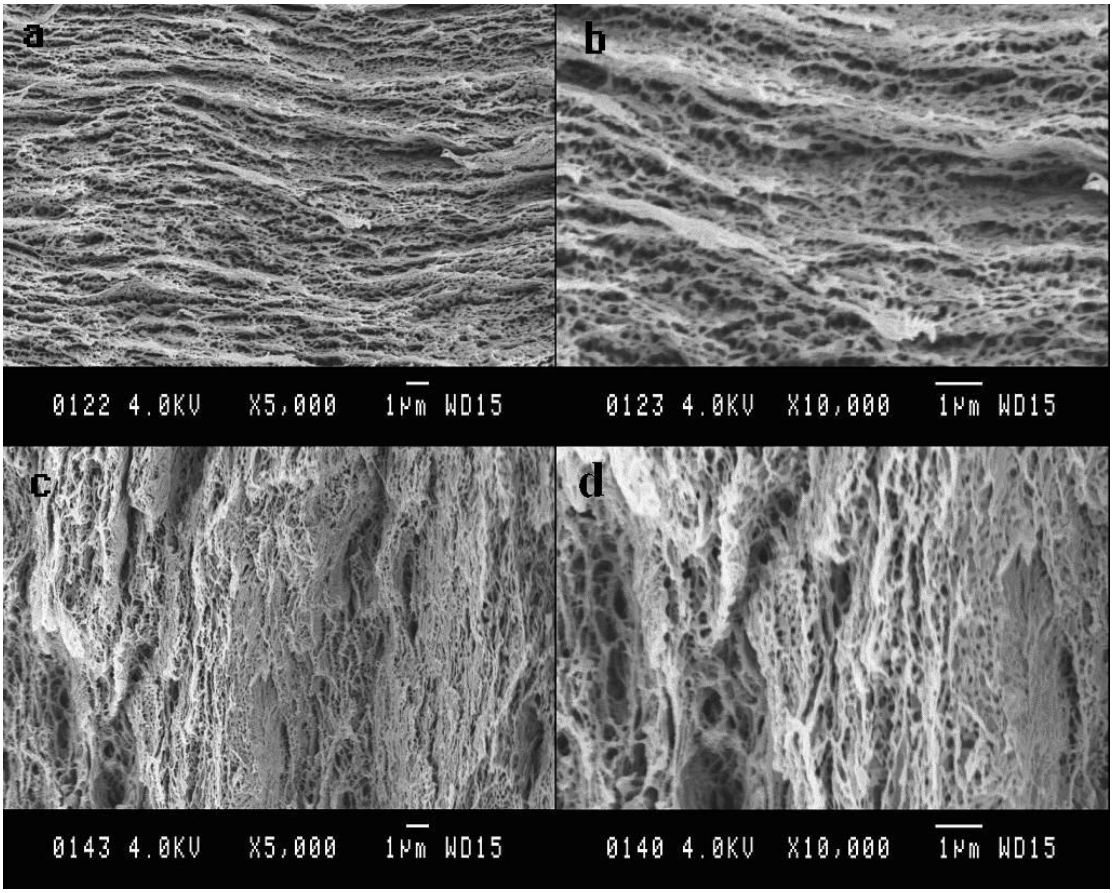

Figure 4.18 Scanning electron micrographs of freeze fracture cross section of BC-PLAG composites, dried by normal (a and b) and slow (c and d) vaporisation rates.

4.5 The influence of hot pressing on the composite microstructure

The main purpose of hot pressing was to reduce the void content and provide smooth, flat samples for testing. A comparison of the microstructure before and after hot pressing verified the action of the hot pressing. The polished cross sections of BC-PLA are shown Figure 4.19. A layered structure can be observed in the BC-PLA composites whether hot pressed or not. Furthermore, the layered structure of the hot

pressed BC-PLA composite (Figure 4.19a and b) was denser than before pressing (Figure 4.19c and d). This suggests that hot pressing is useful for reducing the void content of the BC-PLA composites. However, the microfibrils of BC cannot be identified in the micrographs. It was presumed that the polishing treatment smeared PLA over the surface of the samples, obscuring the cellulose microfibrils.

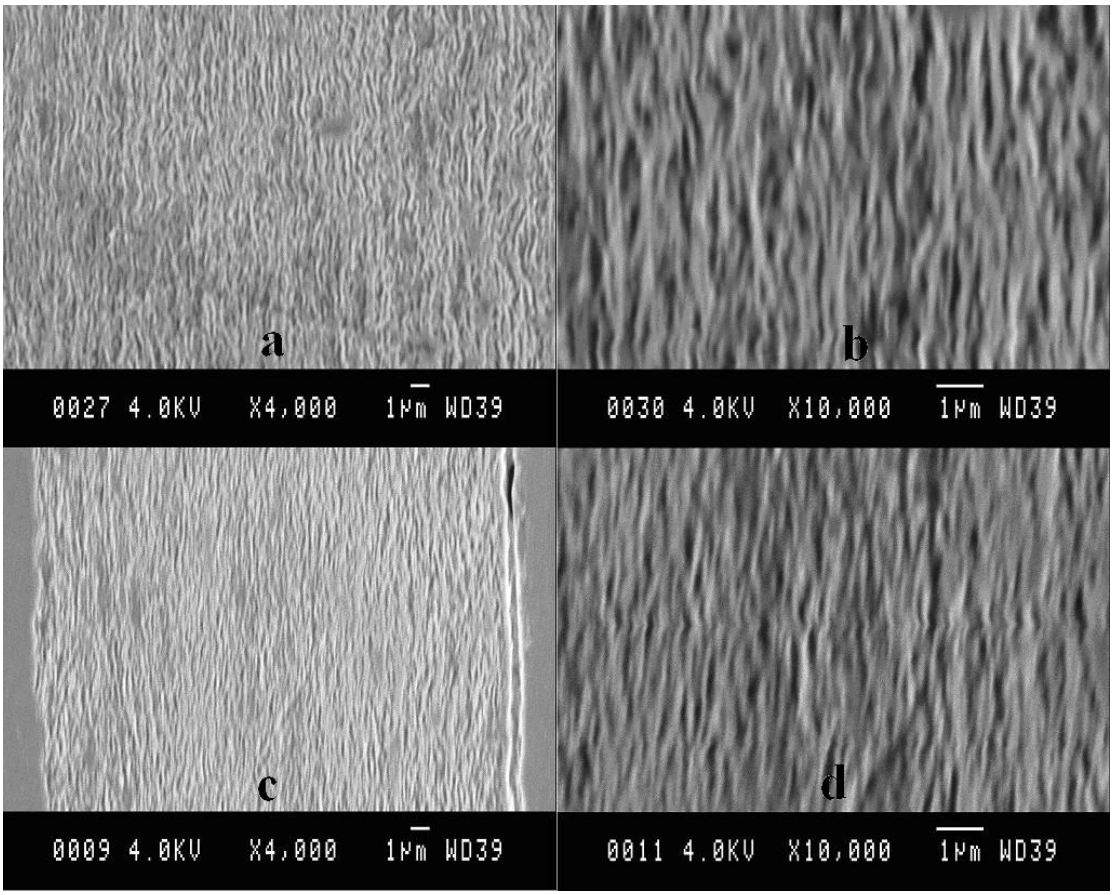

Figure 4.19 Scanning electron micrographs of polished cross section of BC-PLA composites before pressing (a and b) and after hot pressing (c and d).

The TEM images of BC-PLA and BC-PLAG present the difference between the composites before and after hot pressing. Cellulose microfibrils pulled out from the edge of an as-cast BC-PLA sample can be identified clearly in (Figure 4.20). The dark grey area on the top right corner of Figure 4.20a and top left corner of Figure 4.20b is

the embedding material (epoxy resin). The layered structure also can be identified in the centre of BC-PLA either as-cast (Figure 4.21) or hot pressed (Figure 4.22). The dark layers in the TEM images of pressed or as-cast BC-PLA are likely to be cellulose layers as cellulose is revealed by staining. In addition, the layered structure of the pressed BC-PLA was denser than the as-cast composite (Figure 4.19). The structure of the as-cast BC-PLAG (Figure 4.23) seemed loose. It is presumed that the loose structure of the as-cast BC-PLAG was due to the higher void content which was confirmed in Figure 4.18. Therefore, it is assumed that the light areas in the TEM images of as-cast BC-PLAG are voids. As expected, hot pressed BC-PLAG (Figure 4.24) had a tighter and more orderly structure than as-cast BC-PLAG due to the hot pressing reduced the reduced the void content with the high temperature and vacuum condition. However, some light areas remain in the TEM images since layers are still present in the pressed BC-PLAG. In addition, there are light areas in layer or spot form in the images of as-cast and pressed BC-PLA. The light areas in the as-cast one is more than in the pressed one. It also is assumed that the light areas are voids in the BC-PLA. However, it was difficult to differentiate the light areas as being PLA or voids in the hot pressed composites.

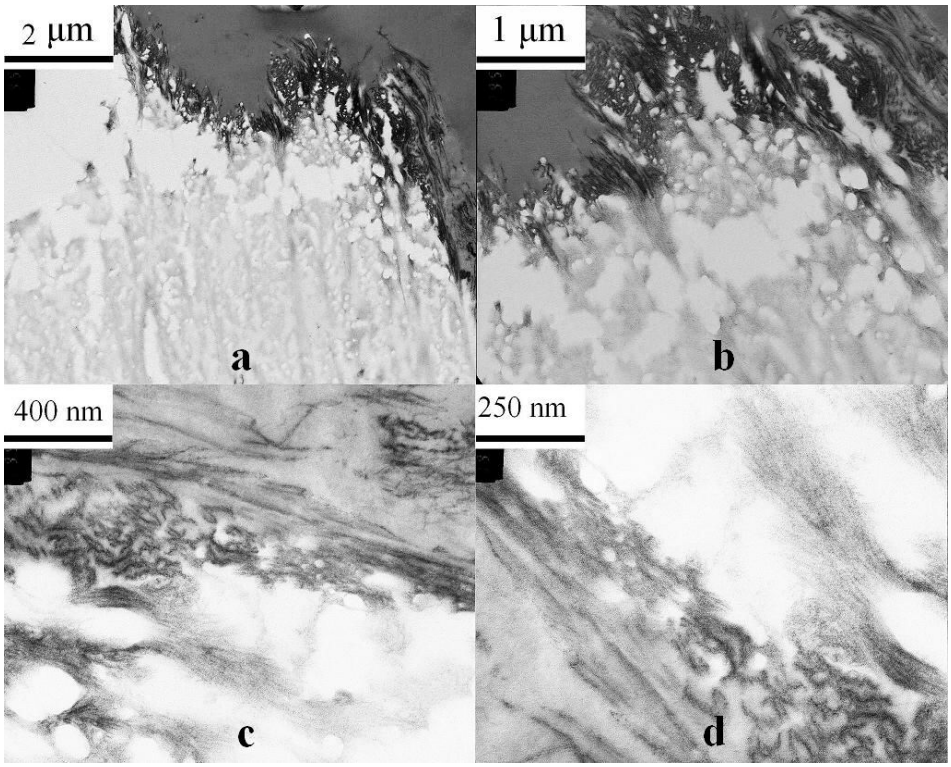

Figure 4.20 TEM micrographs of as-cast BC-PLA composite at the edge of the sample (a) 10000×, (b) 20000×, (c) 50000× and (d) 80000×.

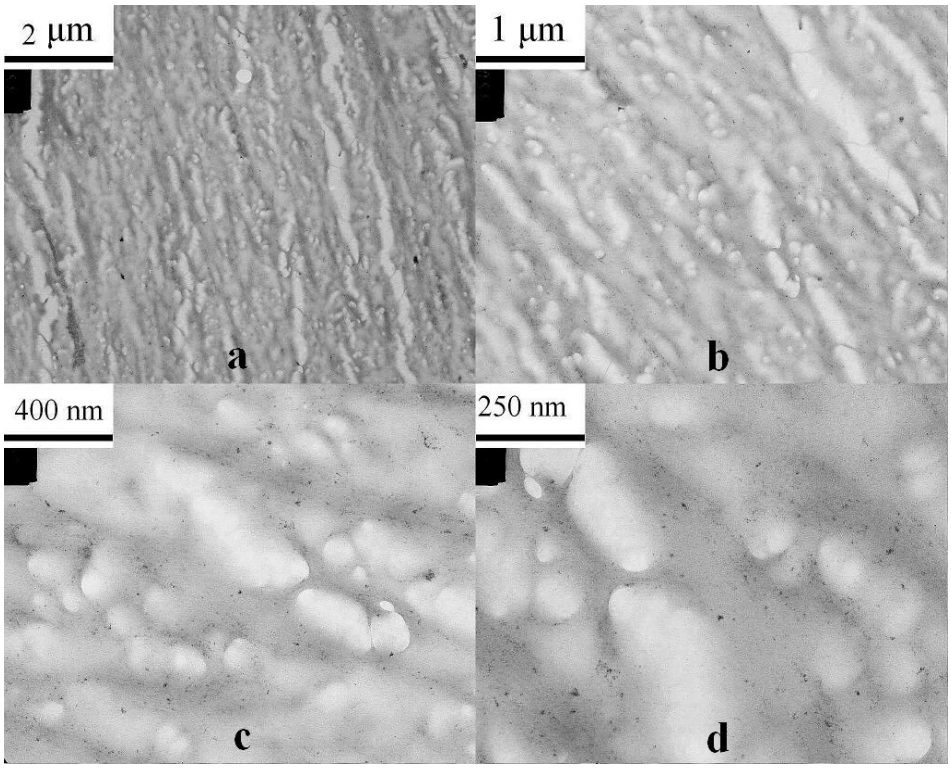

Figure 4.21 TEM micrographs of as-cast BC-PLA composite at the centre of the sample. (a) 10000×, (b) 20000×, (c) 50000× and (d) 80000×.

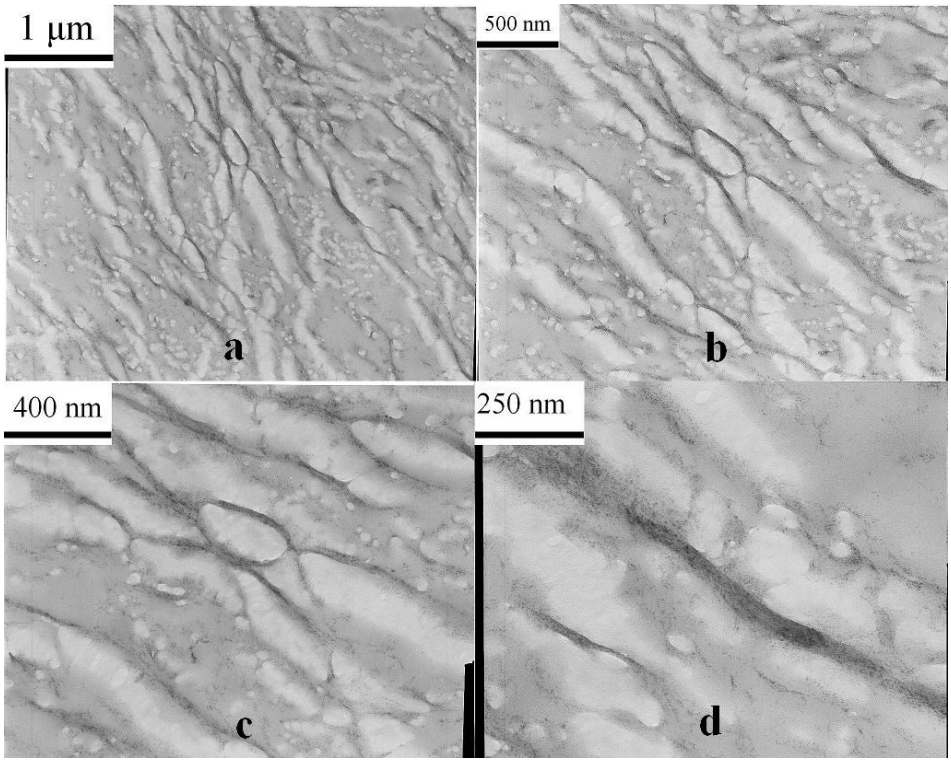

Figure 4.22 TEM micrographs of hot pressed BC-PLA composite at the centre of the sample. (a) 20000×, (b) 30000×, (c) 50000× and (d) 80000×.

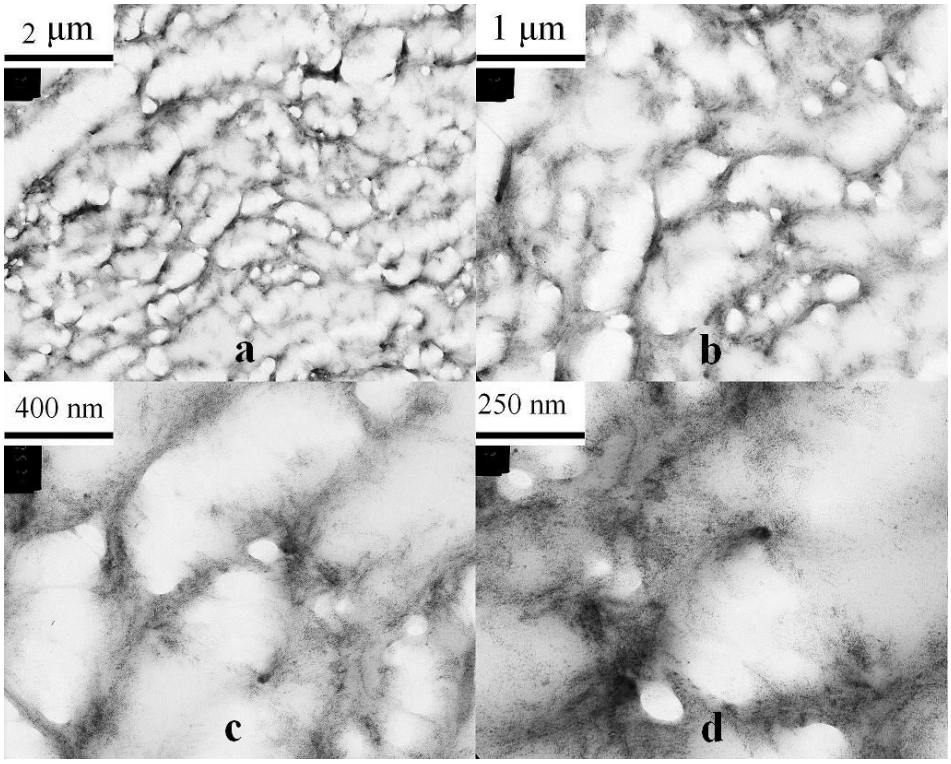

Figure 4.23 TEM micrographs of as-cast BC-PLAG composite at the centre of the sample. (a) 10000×, (b) 20000×, (c) 50000× and (d) 80000×.

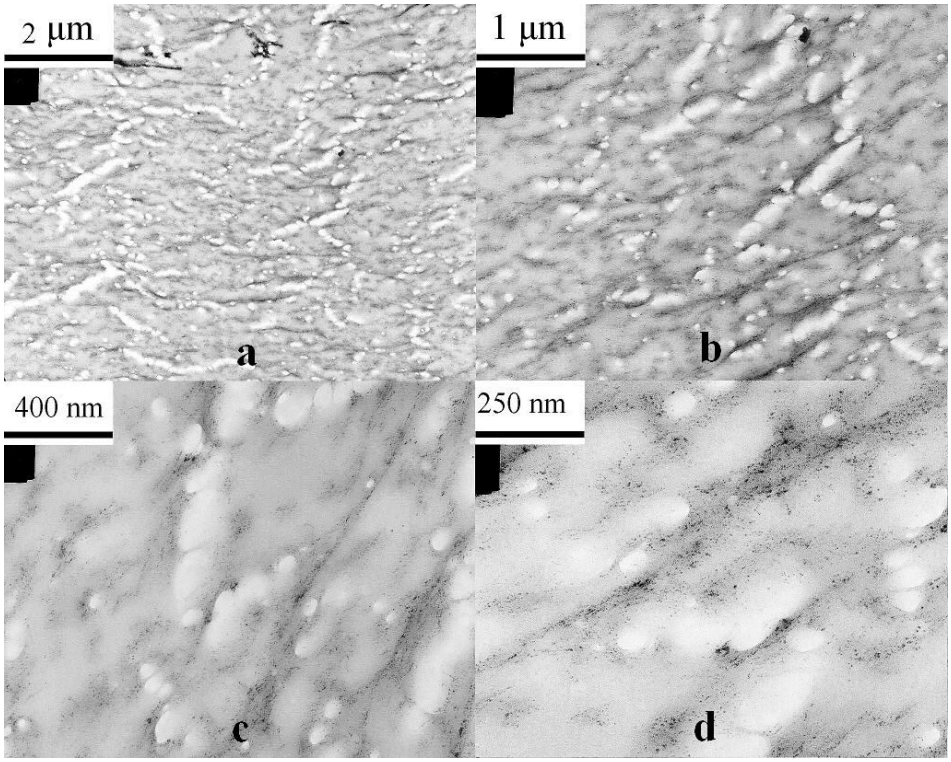

Figure 4.24 TEM micrographs of hot pressed BC-PLA composite at the centre of the sample. (a) 10000×, (b) 20000×, (c) 50000× and (d) 80000×.

4.6 Tensile properties

The tensile behaviour of all samples is shown in Table 4.1, Figure 4.25, Figure 4.26 and Figure 4.27. The Young's modulus (14-15.2 GPa) and tensile strength (245-303 MPa) of BC were very close to the literature values of Young's modulus (16.9 GPa) and tensile strength (260 MPa), respectively [55]. Because of the hydrophilicity of cellulose and the strong surface tension of water, the microfibrils of air dried BC (Figure 4.28) are seen to be denser than ABC (Figure 4.29) [100]. It is presumed that the Young's modulus of ABC (11.5 GPa) was lower than BC due to the less dense network structure. In addition, the diameter of ABC microfibrils became smaller than BC. This change is considered to result from increased hydrophobicity of the acetylated surfaces [100].

The surface morphology of SBC (Figure 4.30) was different compared with BC (Figure 4.28) or ABC (Figure 4.29). The microfibrils appeared to be coated with the some material (*i.e.* silanol-containing oligomers) which is probably the result of the reaction between the coupling agent and cellulose.

Table 4.1 Static tensile behaviours of PLA and its composites.

Material	Tensile strength (MPa)	Young's modulus (GPa)	Break elongation (%)		
			Overall	Elastic	Plastic
BC	245 – 303	14 – 15.2	1.8 –2.2	1.8 – 2.2	0
ABC	223 – 290	7.8 – 11.5	2.1 – 2.9	2.1 – 2.9	0
PLA	29 – 31	1.8 – 1.9	2.1 – 2.8	1.8 – 2.0	0.3 – 0.8
PLAG	16 – 20	1.3 – 1.7	3.4 – 5.8	1.1 – 1.8	2.3 – 4.0
BC-PLA	69 – 75	4.3 – 4.6	1.7 – 2.3	1.7 – 2.3	0
BC-PLAG	39 – 44	2.3 – 2.8	2.0 – 2.8	2.0 – 2.8	0
ABC-PLA	26 – 38	3.3 – 4.8	0.7 – 1.0	0.7 – 1.0	0
ABC-PLAG	23 – 28	1.6 – 2.1	2.2 – 3.2	1.0 – 1.5	1.2 – 1.7
SBC-PLA	58 – 72	4.1 – 4.5	2.2 – 2.7	2.1 – 2.3	0.1 – 0.4
SBC-PLAG	20 – 25	1.4 – 1.8	3.3 – 6.8	1.3 – 1.5	2.0 – 5.3

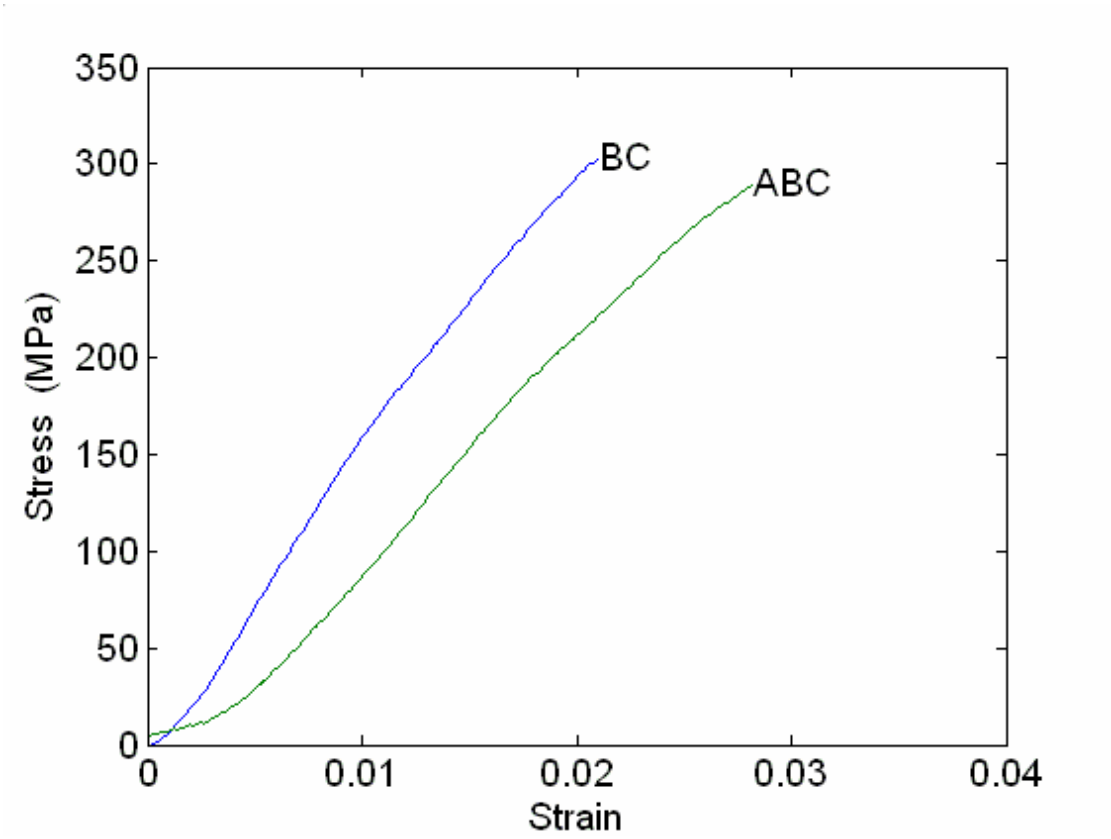

Figure 4.25 Tensile stress-strain behaviour of air dried BC and ABC.

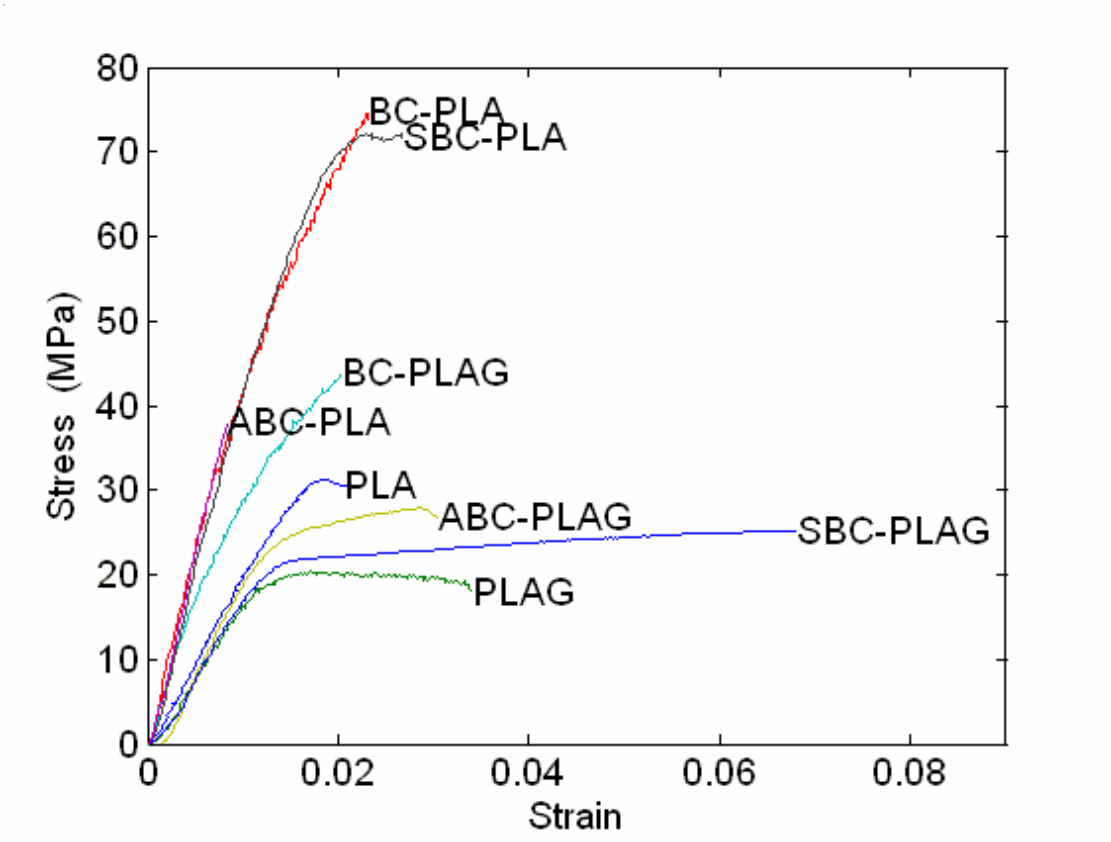

Figure 4.26 Tensile stress-strain behaviour of PLA and its composites.

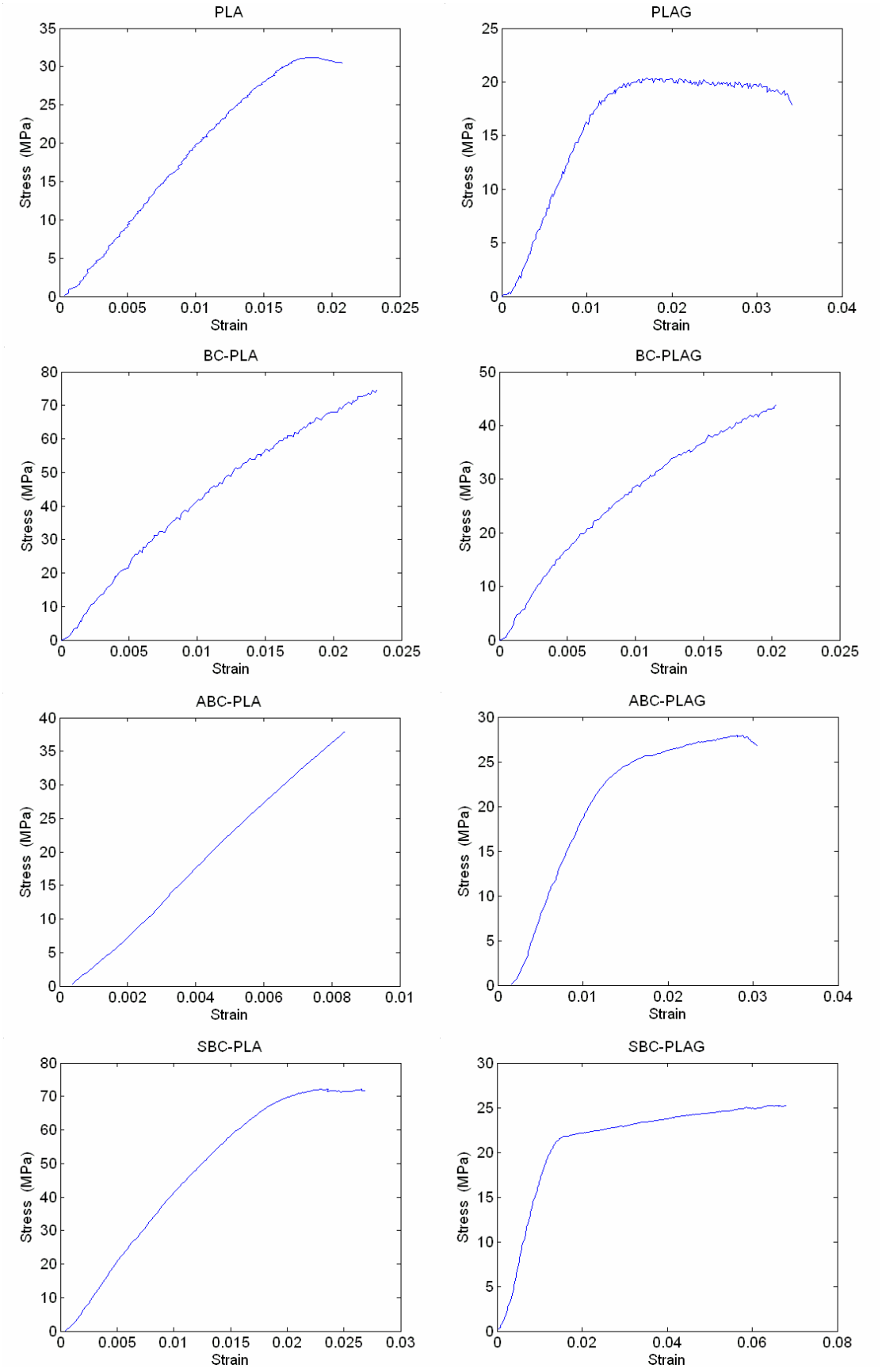

Figure 4.27 Tensile stress-strain behaviour of PLA and its composites.

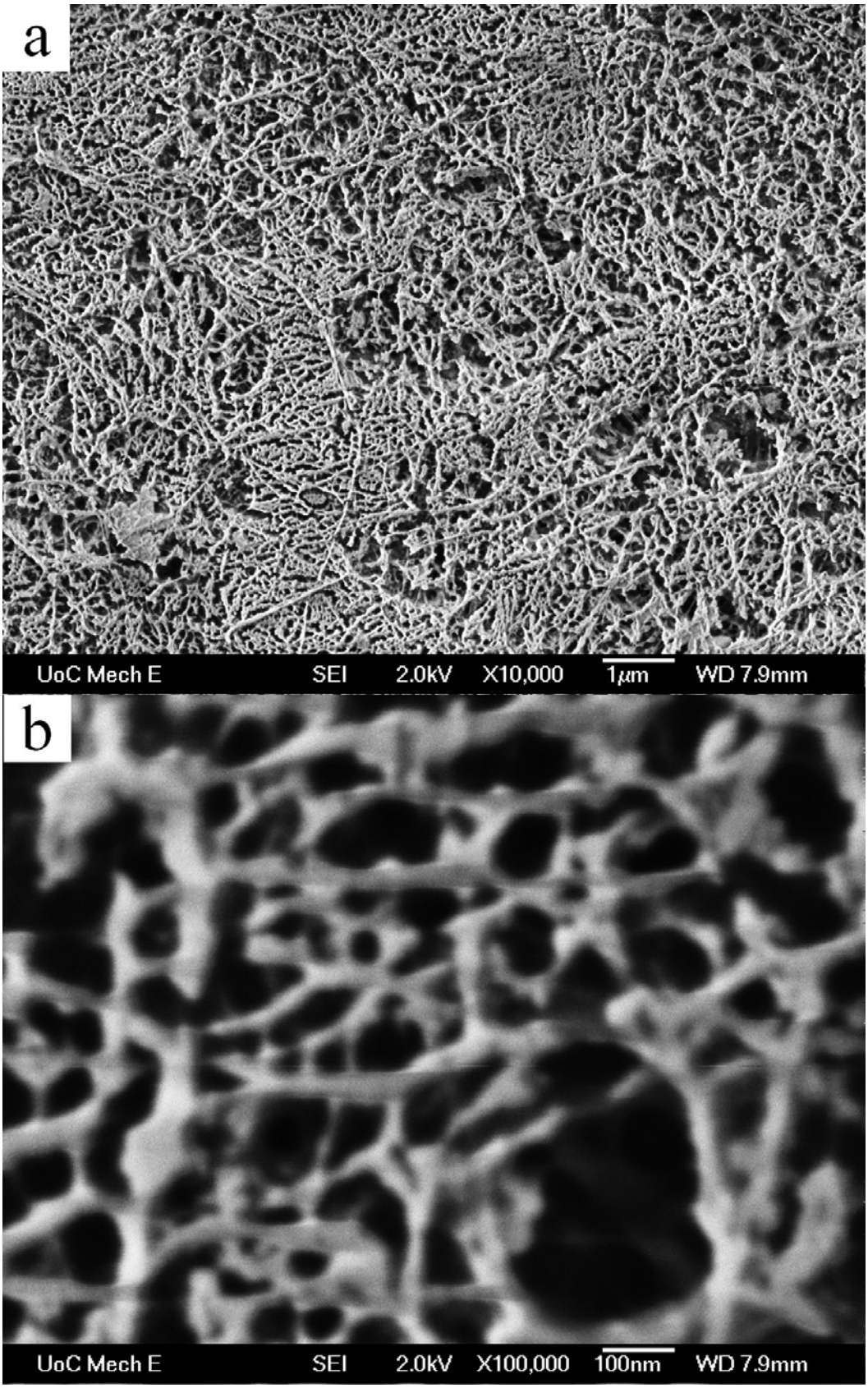

Figure 4.28 Surface morphology of air dried BC at magnifications of (a) 10000× and (b) 100000×

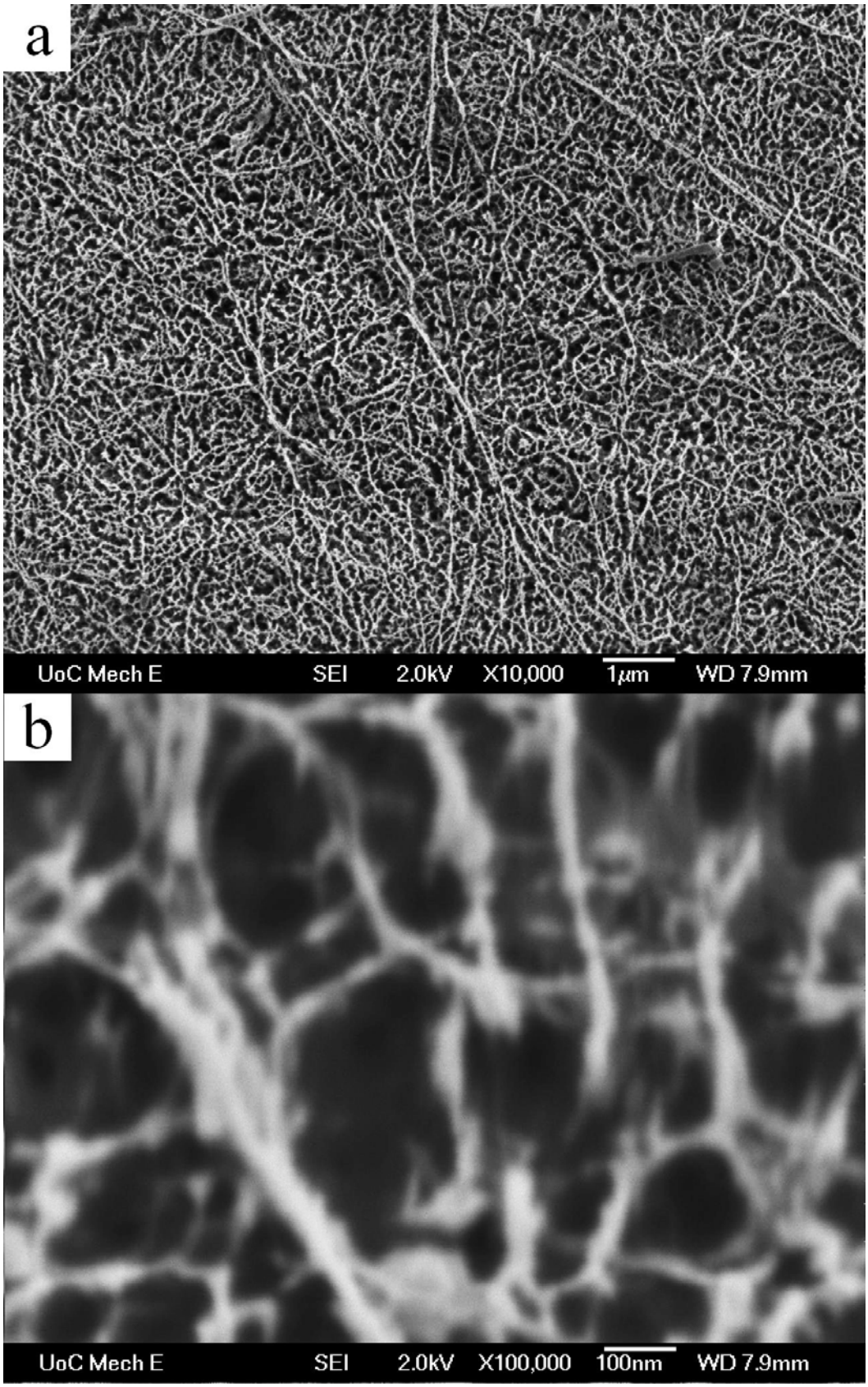

Figure 4.29 Surface morphology of air dried acetylated BC at magnifications of (a) 10000× and (b) 100000×.

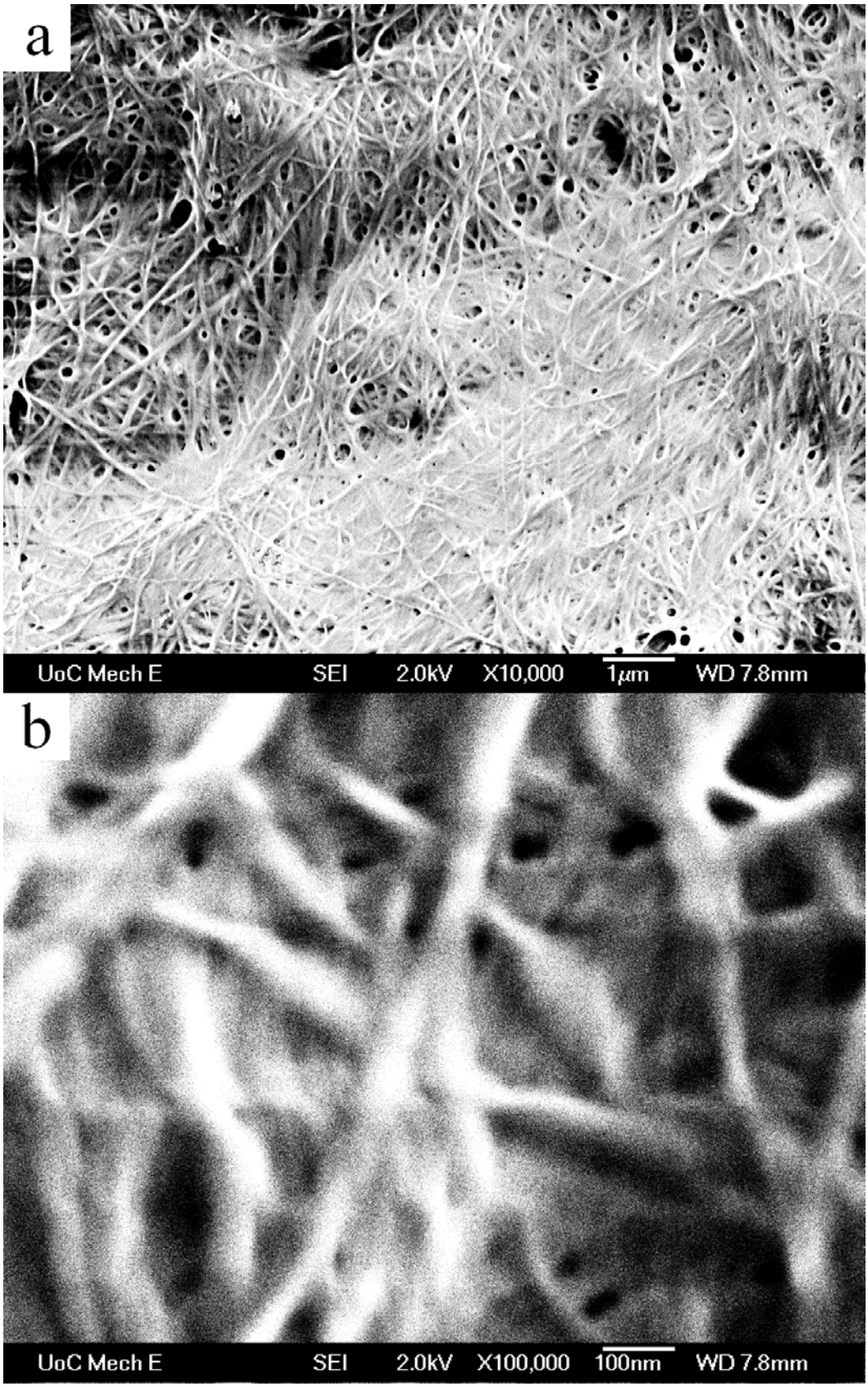

Figure 4.30 Surface morphology of air-dried silane-treated BC at magnifications of (a) 10000× and (b) 100000×.

PLA failed soon after yielding, demonstrating that PLA is a relatively brittle polymer. The brittle behaviour of PLA was observed in the micrographs of fracture surfaces (Figure 4.31). The fracture surface was smooth, aside from some small voids present in the hot pressed PLA. The void size was ~100-200 nm which is smaller than the voids in the as-cast PLA (Figure 4.16a). Most of the voids were close to the surface of the PLA film, with less voids at the centre of the PLA film. This suggests that the vacuum applied during hot pressing reduces the void content of PLA. The main reason for residual voids is presumed to be due to the short hot pressing time of 3 min. However, longer pressing times (10 min.) led to severe degradation of the PLA.

The Young's modulus and tensile strength of PLAG were lower than PLA. However, it exhibited much larger failure strains (2.3% plastic deformation region). Thus, the toughness of PLA was increased by the addition of glycerol. The plastically deformed material on the surface of PLAG film is visible in the SEM images (Figure 4.32). However, most regions of the tensile fracture surface of PLAG presented a brittle behaviour, suggesting that glycerol is not an efficient plasticizer of PLA. Similar conclusions were made by Martin *et al.* using thermal analysis [111]. A large amount of voids also are visible in the SEM images that are also likely to be responsible for the reduced strength of PLAG.

BC reinforcement greatly enhances the modulus and strength of PLA even though the fibre contents were not particularly high as shown in Table 3.3 in this work. The cellulose microfibrils appear to have good mechanical bonding with the PLA matrix in BC-PLA. This is observed in Figure 4.33; where only a few microfibrils were

pulled out under tensile load. In addition, PLA impregnated BC microfibrils networks also prevented the pulling out of microfibrils. Therefore, BC-PLA has the excellent mechanical properties and the highest tensile strength of 75 MPa of all the composites. The fracture surface appears rougher than pure PLA due to the addition of BC reinforcements, suggesting improved fracture and impact properties.

There were many of small voids in BC-PLAG as for PLAG (Figure 4.34). It is presumed that the voids reduce the strength of BC-PLAG. Furthermore, very few microfibrils were pulled out from the matrix. It is difficult to differentiate between the porous structure of the PLAG matrix and the network structure of the BC, suggesting that the BC microfibrils also had good adhesion to the PLAG matrix. Therefore, no plastic elongation appeared in the tensile test on the BC-PLAG.

ABC-PLA had the highest Young's modulus (4.8 GPa) of all the composites while its tensile strength was only half of that of BC-PLA. It appears that the strength of the BC was reduced, although the Young's modulus was not changed after acetylation. Similar phenomena have been described by Zafeiropoulos *et al*. on flax fibres [130]. The acetylated flax fibres retained their original Young's modulus while the tensile strength was lower than before the acetylation [130]. And also, acetylation treatment can reduce the crystallinity of high purity cellulose fibre such as cotton [36]. In addition acetylation can reduce the crystallite size of BC [100]. These observations may explain the lower tensile strength of the BC measured in this work.

As expected, the tensile strength of ABC-PLAG was lower than ABC-PLA. Extensive microfibril pull-out was observed on the fracture surface (Figure 4.36), suggesting

that poor bonding between the ABC microfibrils and PLAG matrix was the cause. In addition, ABC-PLA had a yield region under tension. Its yield behaviour was similar to PLAG. It is presumed that ABC failed first, followed by the PLAG matrix. The lower strength of ABC-PLAG is also due to the presence of large voids.

The Young's modulus and tensile strength of SBC-PLA were very close to BC-PLA. The tensile fracture surface of SBC-PLA (Figure 4.37) was similar to BC-PLA, suggesting that the bonding between the reinforcement and matrix was good. However, a few voids appeared on the fracture surface of SBC-PLA and the amount of pulled out microfibrils were slight more than BC-PLA. Therefore, Young's modulus and tensile strength of SBC-PLA were slight lower than BC-PLA.

SBC-PLAG elongated extensively compared with the other composites, especially those with a PLAG matrix. A large number of microfibrils were pulled out under tension (see Figure 4.38).). The elastic elongation of SBC-PLAG was close to PLAG and ABC-PLAG. It also is presumed that matrix failure occurred before reinforcement failure.

Furthermore, the yield elongation of SBC-PLAG was 3.5 times that of the elastic elongation. Extensive yielding occurred in SBC-PLA which is in contrast to BC-PLA and ABC-PLA. Bengtsson *et al*. reported that silane could act as a plasticizer led to a lower the strength of the neat silane crosslinking polyethylene (XLPE) than neat high density polyethylene (HDPE) [102]. Suzuki et al. also suggested that the mono-functional coupling agents with long alkyl units worked as a plasticizer of rubber

molecules [131]. Therefore, it is presumed that the silanol-containing oligomers acted the role of plasticizer further increased the toughness of PLA or PLAG.

The materials with glycerol had much more voids, whereas the materials without glycerol had less voids. Therefore, the glycerol led to formation of larger number of voids in PLA. In addition, compared with the materials without glycerol (PLA, BC-PLA, ABC-PLA and SBC-PLA), the materials with glycerol (PLAG, BC-PLAG, ABC-PLAG and SBC-PLAG) had a rougher fracture surface. Thus, glycerol appears to increase the ductility of PLA slightly

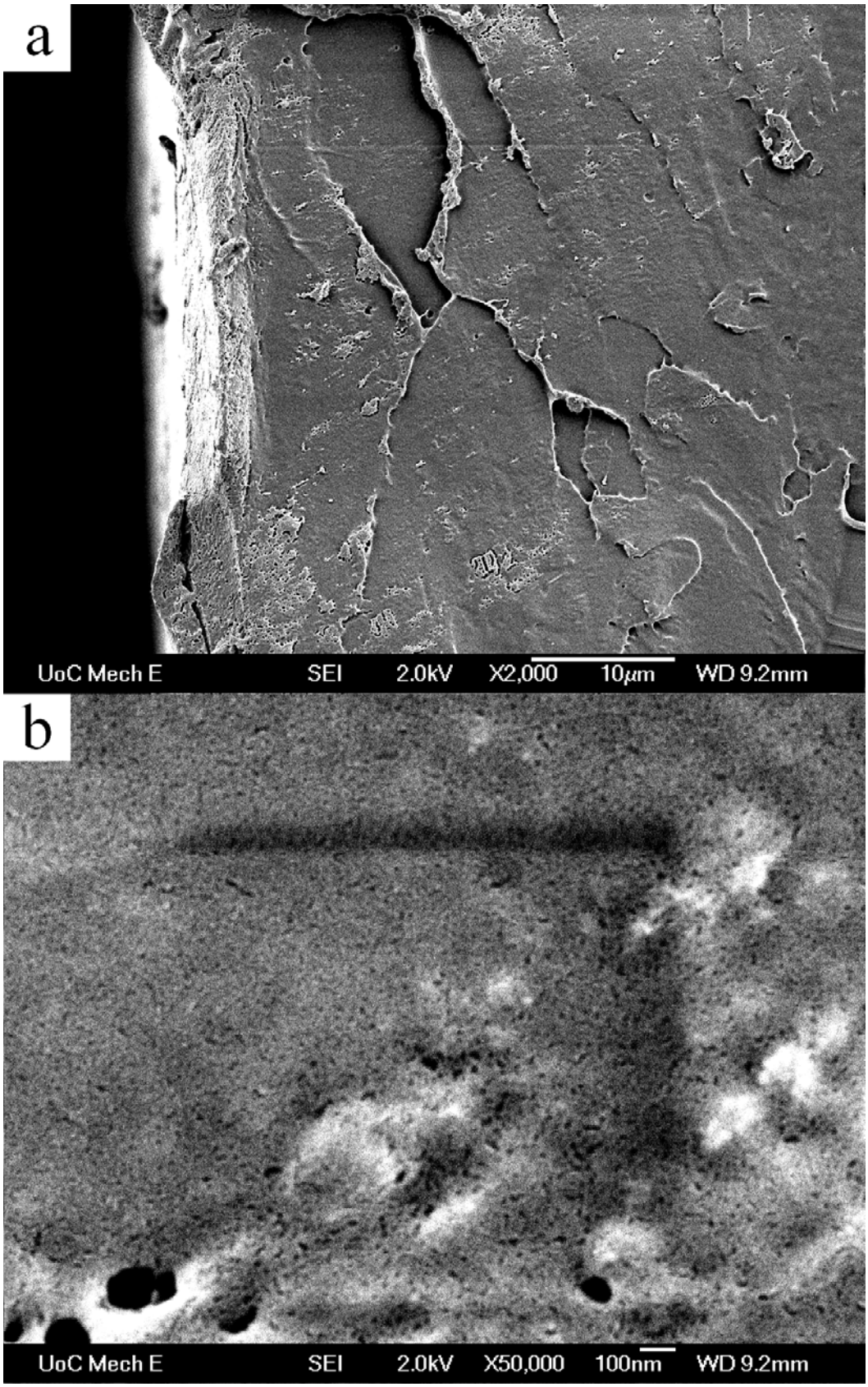

Figure 4.31 Scanning electron micrographs of tensile fracture surface of PLA at magnifications of (a) 2000× and (b) 50000×.

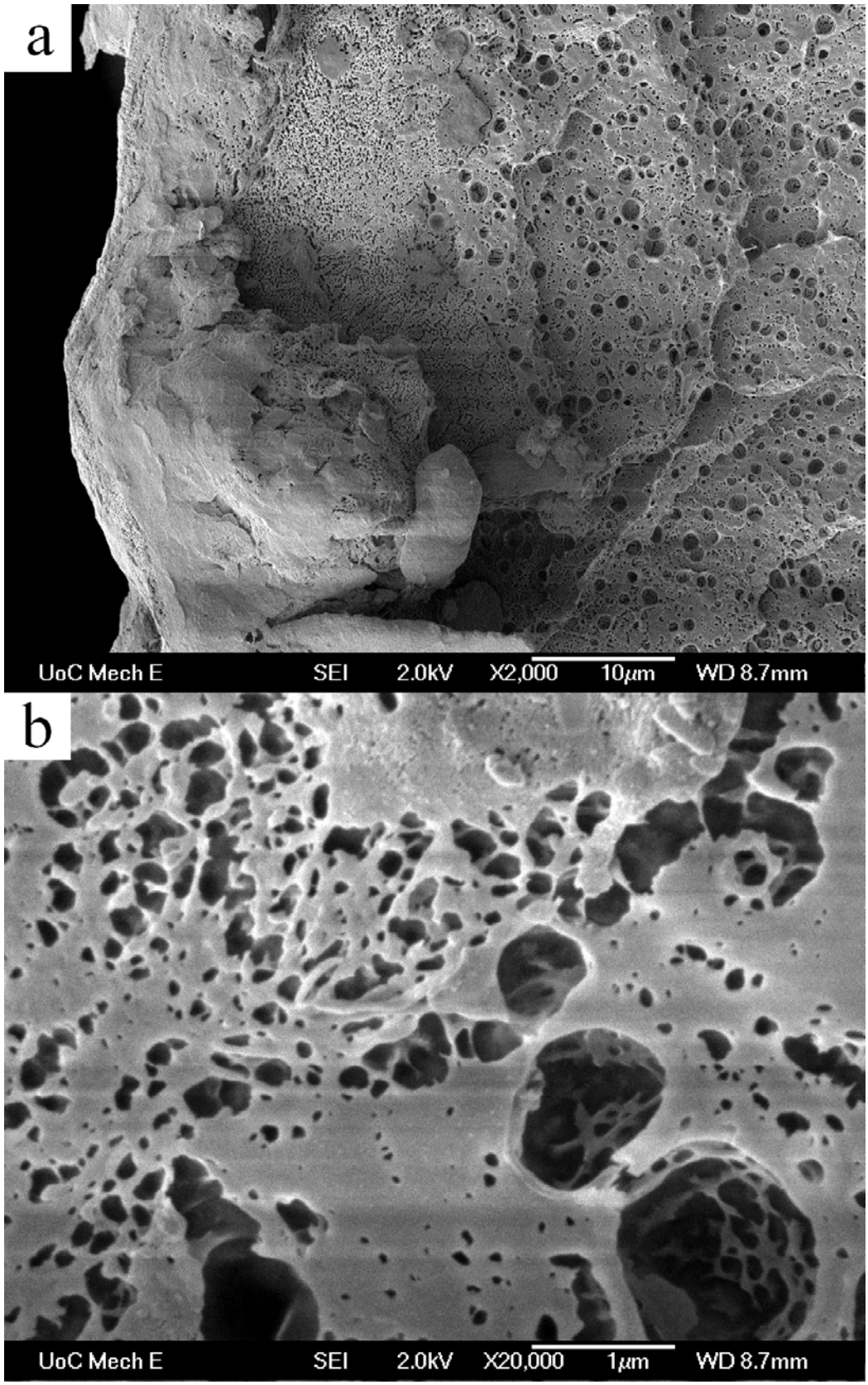

Figure 4.32 Scanning electron micrographs of tensile fracture surface of PLAG at magnifications of (a) 2000× and (b) 20000×.

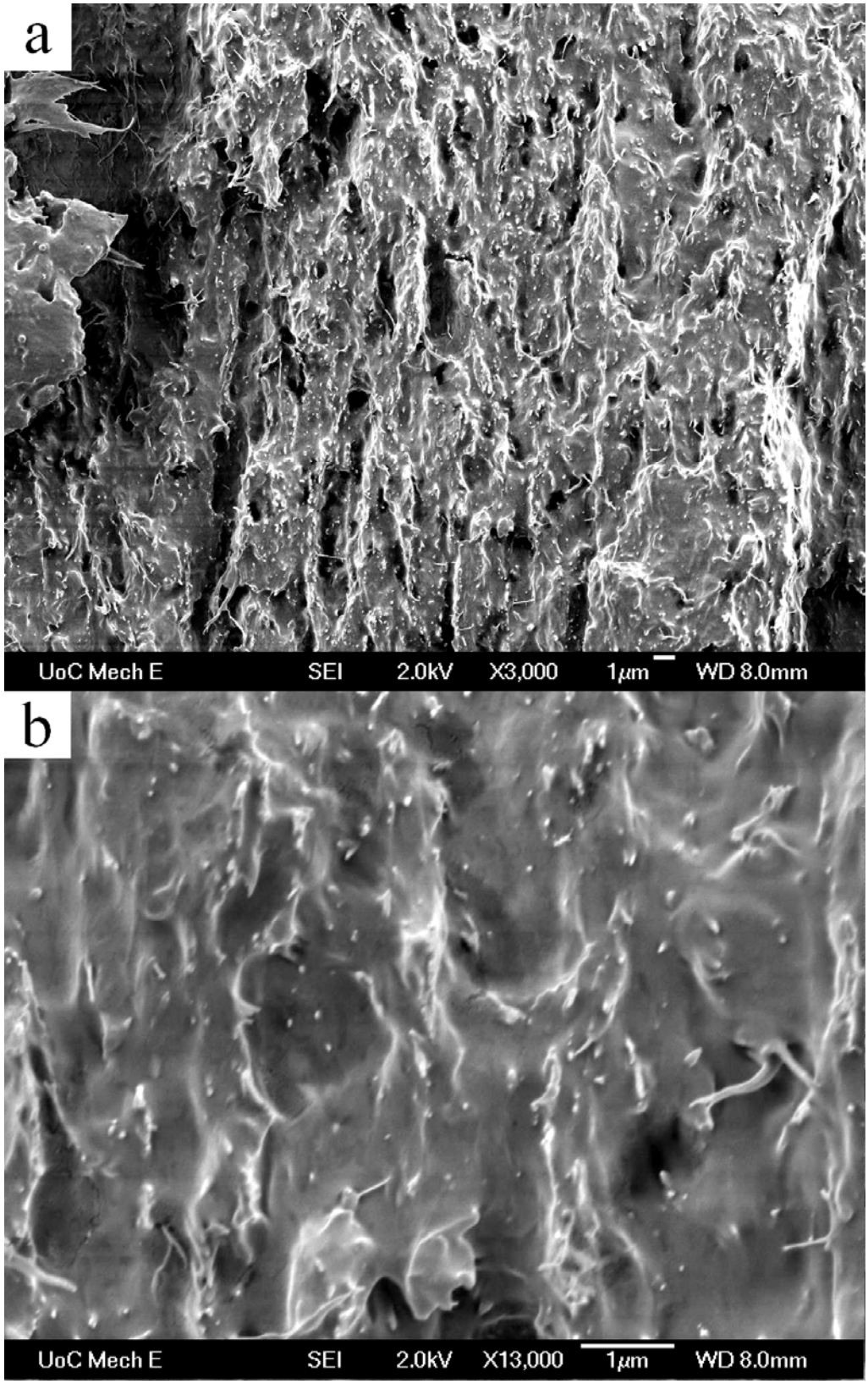

Figure 4.33 Scanning electron micrographs of tensile fracture surface of BC-PLA at magnifications of (a) 3000× and (b) 13000×.

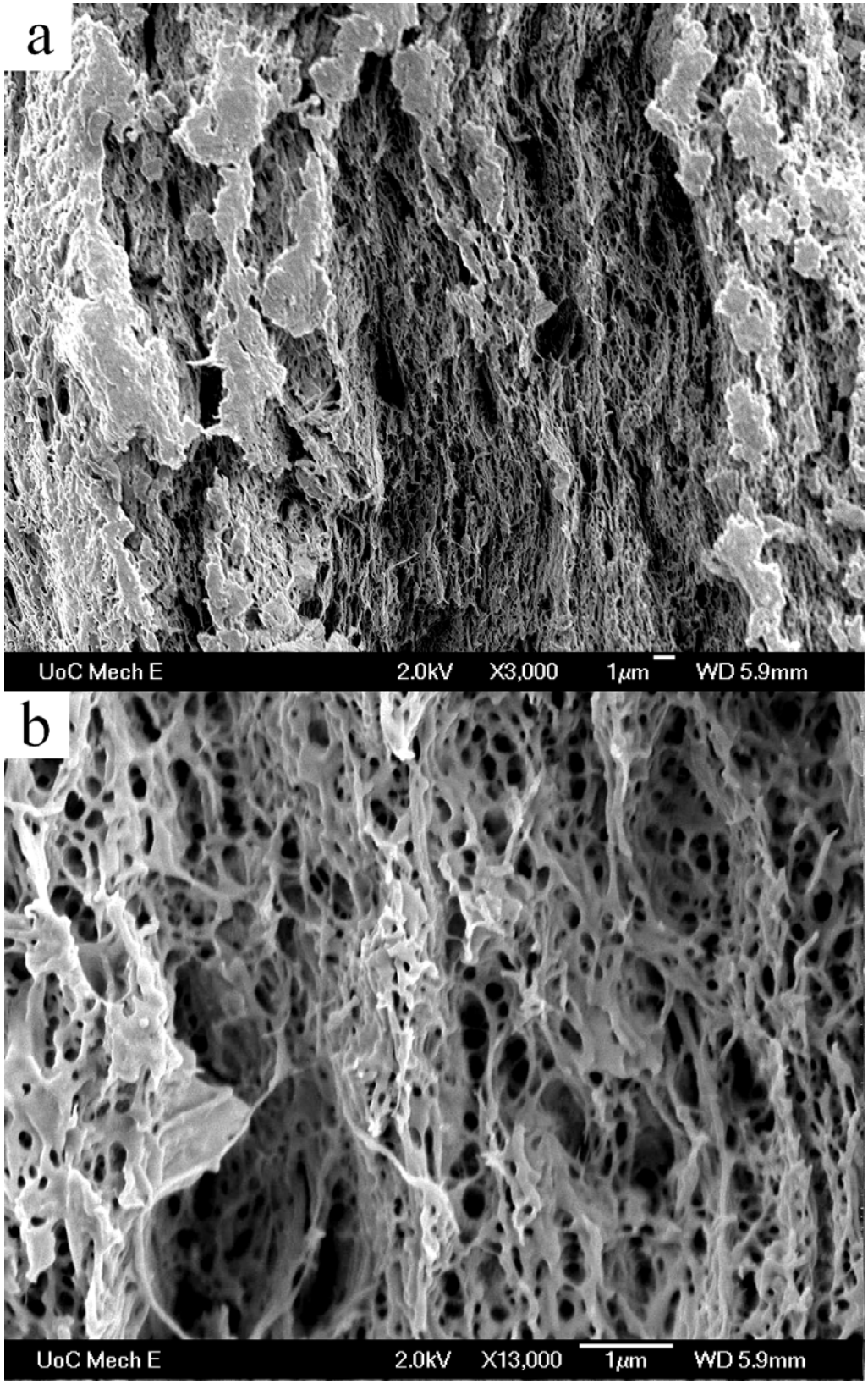

Figure 4.34 Scanning electron micrographs of tensile fracture surface of BC-PLAG at magnifications of (a) 3000× and (b) 13000×.

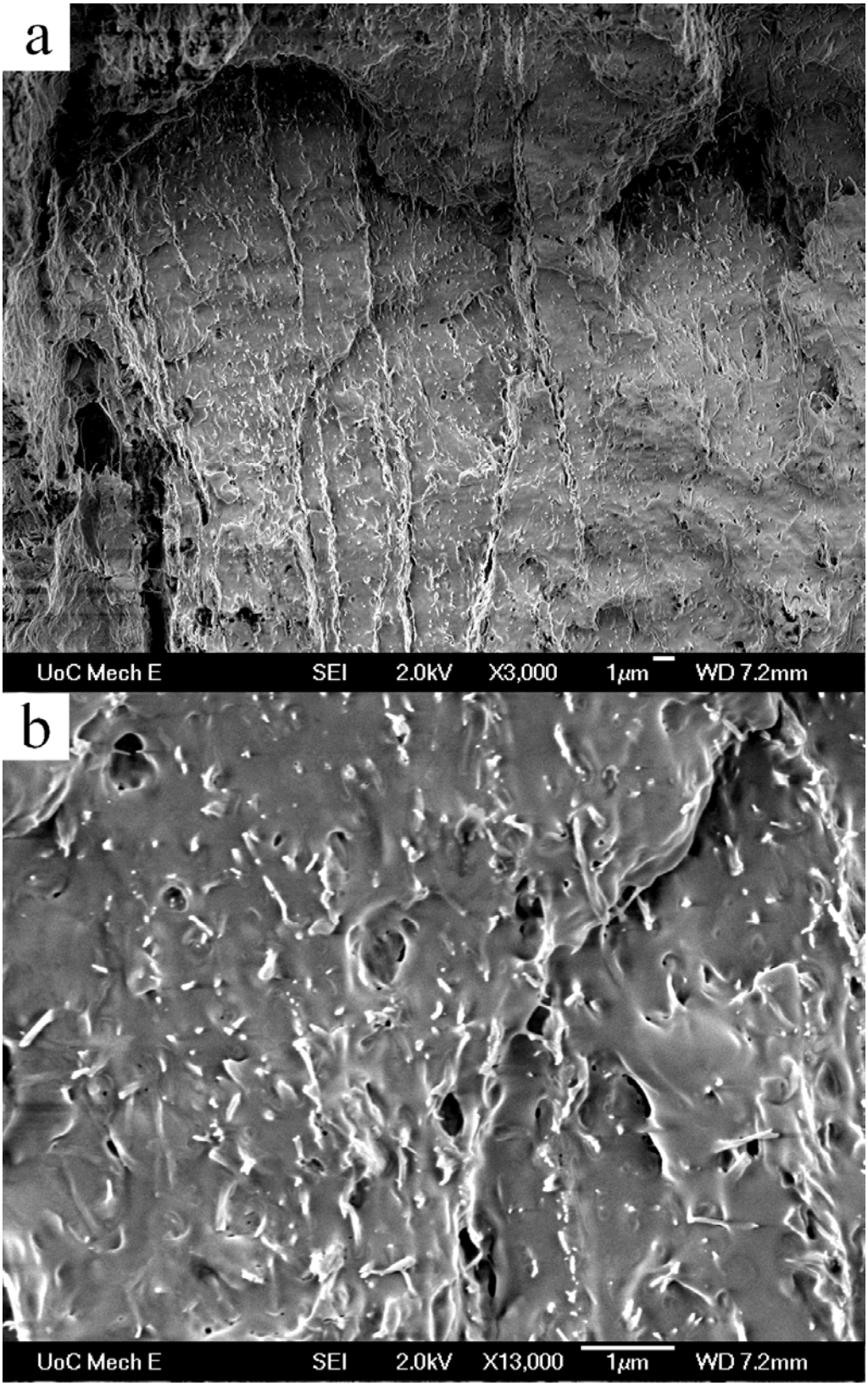

Figure 4.35 Scanning electron micrographs of tensile fracture surface of ABC-PLA at magnifications of (a) 3000× and (b) 13000×.

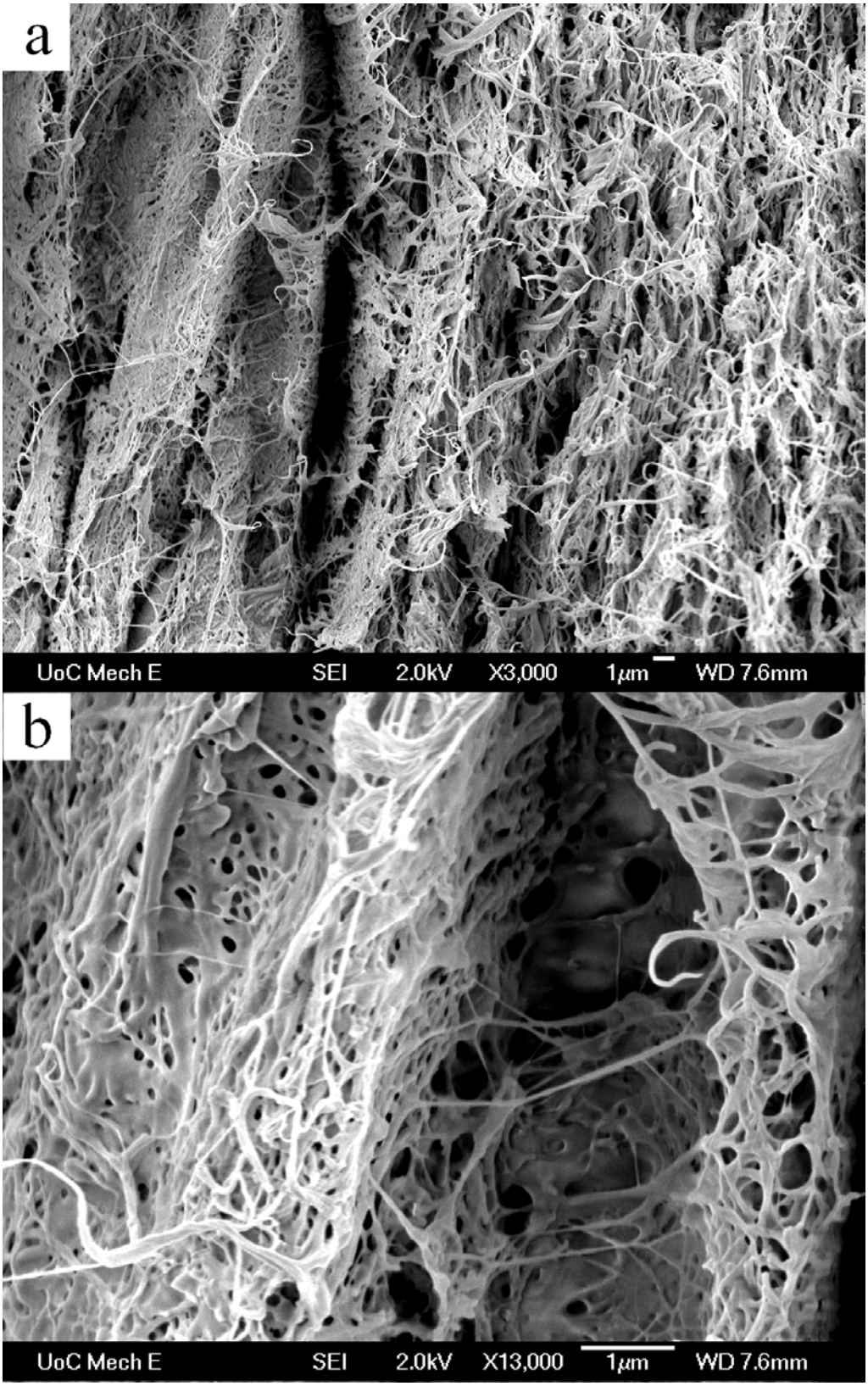

Figure 4.36 Scanning electron micrographs of tensile fracture surface of ABC-PLAG at magnifications of (a) 3000× and (b) 13000×.

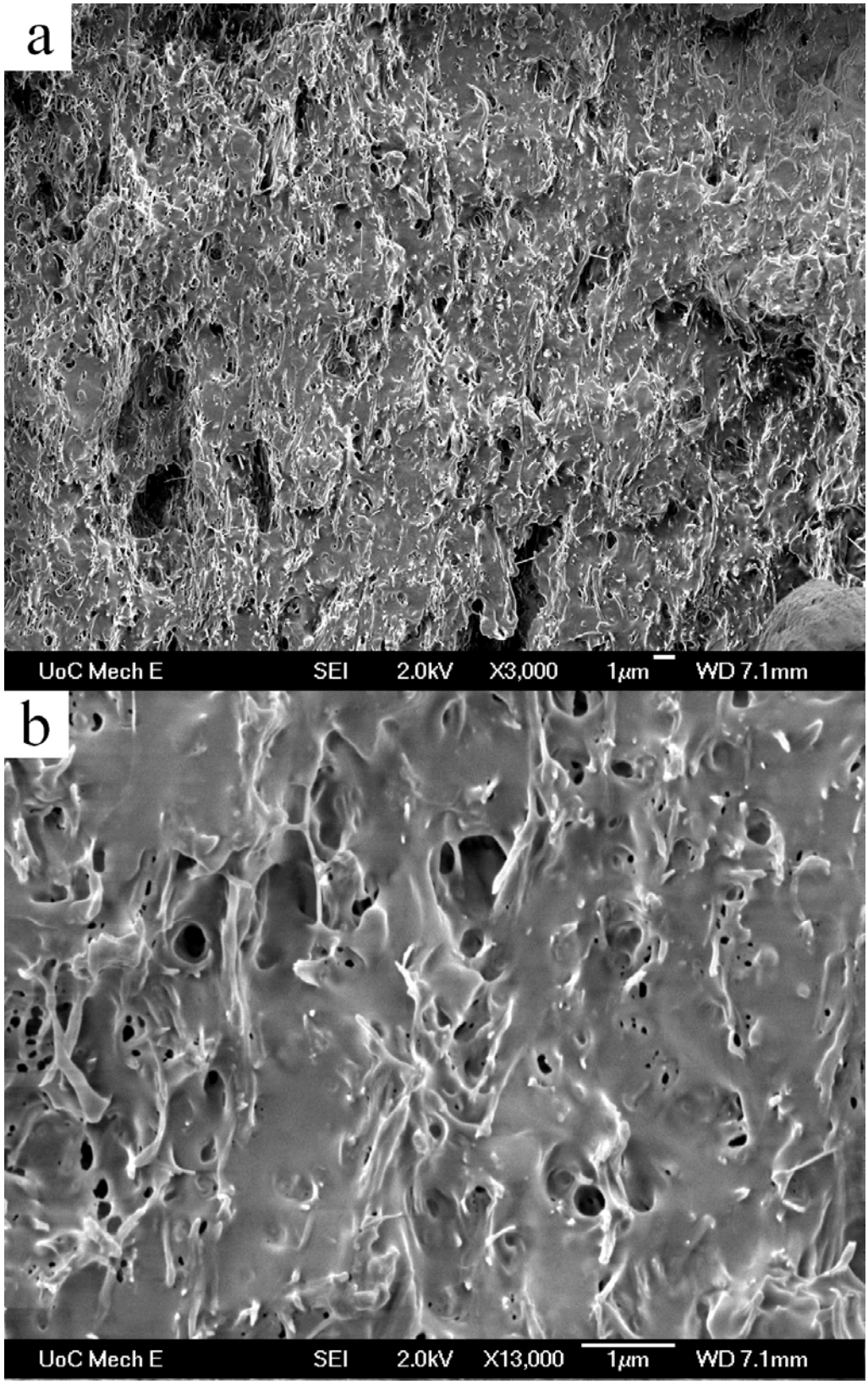

Figure 4.37 Scanning electron micrographs of tensile fracture surface of SBC-PLA at magnifications of (a) 3000× and (b) 13000×.

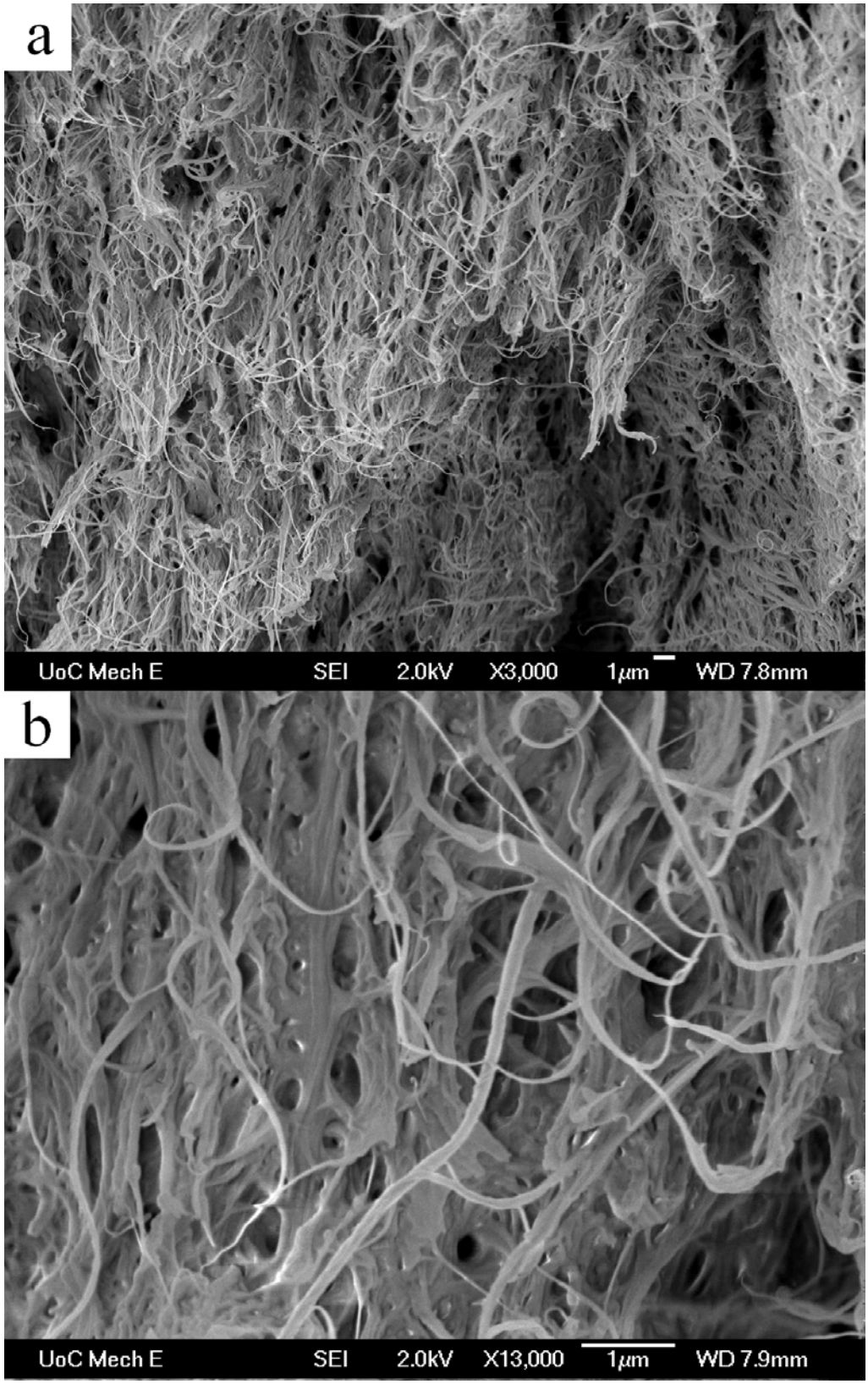

Figure 4.38 Scanning electron micrographs of tensile fracture surface of SBC-PLAG at magnifications of (a) 3000× and (b) 13000×.

4.7 Crystallisation Behaviour of PLA and BC-PLA Composites.

Thermograms of PLA and PLA-based composites (without glycerol) at a cooling rate of 5°C/min are shown in Figure 4.39. The crystalline peak of BC-PLA and SBC-PLA disappeared dramatically. However, a crystallisation peak was observed on the original PLA film with 0.4°C/min cooling rate as shown Figure 4.5. Hu *et al.* described that the crystallisation enthalpy of PLA decreased as the cooling rate increased [132] such that for a cooling rate of 5°C/min there was not enough time for crystal formation.

Regardless of formulation, the introduction of cellulose fibre into a semicrystalline polymer melt leads to a change in the morphology of the crystallizing polymer [133, 134]. The cellulose fibre provides a surface upon which polymer crystals may heterogeneously nucleate. With sufficiently high nucleation density, the embryonic crystals may impinge on one another as they grow radially from the fibre surface. The resulting interphase morphology is termed the transcrystalline layer and is commonly found in semicrystalline thermoplastic composites with many different synthetic and natural fibre types [133]. PLA is a semicrystalline polymer [135], therefore, the crystallisation peaks observed for BC-PLA and ABC-PLA due to the addition of BC or ABC increased the tendency for crystallisation in PLA.

However, the crystallisation peak was not observed for SBC-PLA. It had been suggested that the fibre surfaces with higher roughness cause thermal stress concentration and enhance the crystalline nucleating process [136]. SBC microfibrils had smoother surface compared with BC (Figure 4.28) or ABC (Figure 4.29) which

might be a reason for reduced tendency for crystallisation in SBC-PLA during cooling at 5°C/min.

In addition, Martins *et al*. reported that acetylation produced a rough surface on sisal fibre [137]. Native BC was found to have a surface area of 2.7 m^2/g while acetylated BC had almost 10 times this surface area (25 m^2/g) [100]. It can be observed that the crystallisation peak is in fact larger for ABC-PLA compared with that for BC-PLA (Figure 4.39).

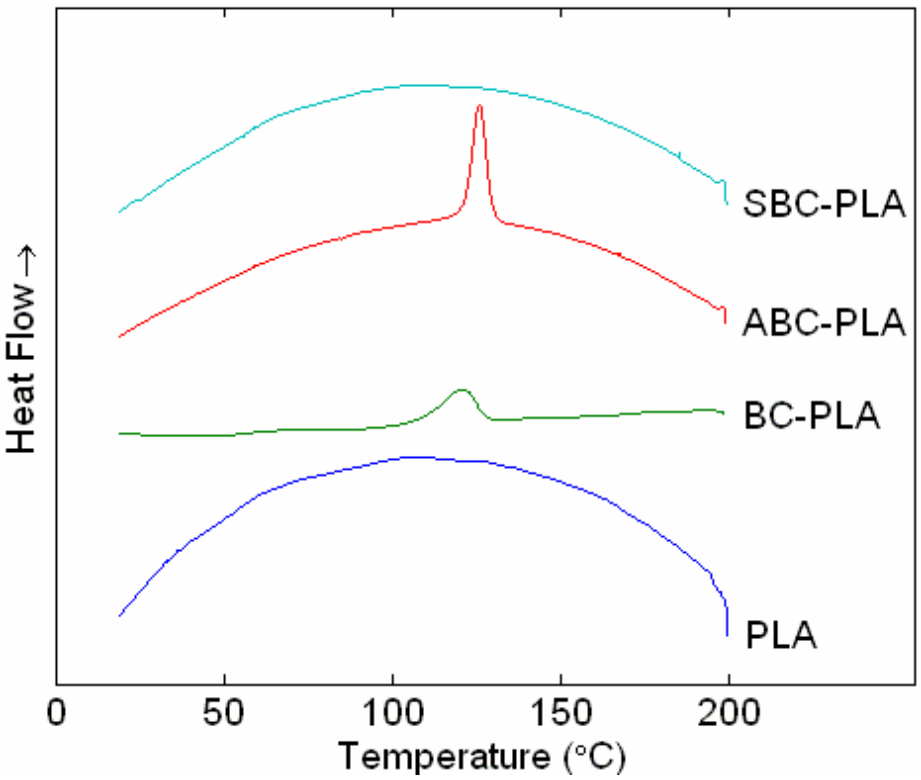

Figure 4.39 Thermograms of PLA and BC-PLA composites at a cooling rate of 5°C/min.

The subsequent thermograms of neat PLA and PLA-based composites (without glycerol) at a heating rate of 5°C/min are shown in Figure 4.40. Cold crystallisation occurs in PLA if the material is rapidly cooled from the melt. The cold crystallisation

can be measured during the heating. Cao *et al*. have reported that PLA does not crystallise at higher cooling rates and that crystallisation occurs during heating [138]. Hu *et al.* [132] also reported that the melting enthalpy corresponded to the crystallisation enthalpy in the cooling thermogram. The strong endothermic cold crystallisation peak of PLA on subsequent heating corresponded with higher cooling rates. Solarski *et al*. concluded that the higher the degree of cristallinity of PLA fibres, the higher the decrease in the cold crystallisation temperature and the lower the cold crystallisation enthalpy. For PLA fibres with a low degree of crystallinity, the cold crystallisation peak was located at 96°C [139]. Therefore, the peaks on the DSC curves of neat PLA and SBC-PLA at ~110 °C in the Figure 4.40 are due to cold crystallisation. In addition, the cold crystallisation peak of neat PLA was observed at 108 °C, suggesting that the degree of crystallinity was much lower in the neat PLA or SBC-PLA. The cold crystallisation phenomena of neat PLA and SBC-PLA explained the disappeared crystalline peaks of neat PLA and SBC-PLA in the thermograms with 5°C/min cooling rate (Figure 4.39). Furthermore, no cold crystallisation peak was observed on the DSC curves of ABC-PLA with heating due to the higher crystallisation; a slight cold crystallisation peak was observed on the DSC curves of BC-PLA with heating due to the lower crystallisation.

Yasuniwa *et al*. [135] reported "double-melting" behaviour of PLA where double-melting peaks appear in the DSC curve with heating rates of 0.5 to 10°C/min. In general, the first endotherm is attributed to the melting of some amount of the original crystals, while the second endotherm is attributed to the melting of crystals formed through a melt-recrystallisation process during the DSC heating scan. The exothermic peak between the double-melting peaks is attributed to the recrystallisation [139].

Nano-clay/PLA composites have also been reported to exhibit a double-melting peak [140]. Ogata *et al*. reported the structure and physical properties of cellulose acetate/PLLA blends where a double-melting peak was observed for neat PLLA. However, only a single melting peak was observed on the DSC curve of cellulose acetate/PLLA blends [141]. Therefore, cellulose acetate, an acetylated product of cellulose, possibly induces a single melting peak on the DSC curve of ABC-PLA upon heating.

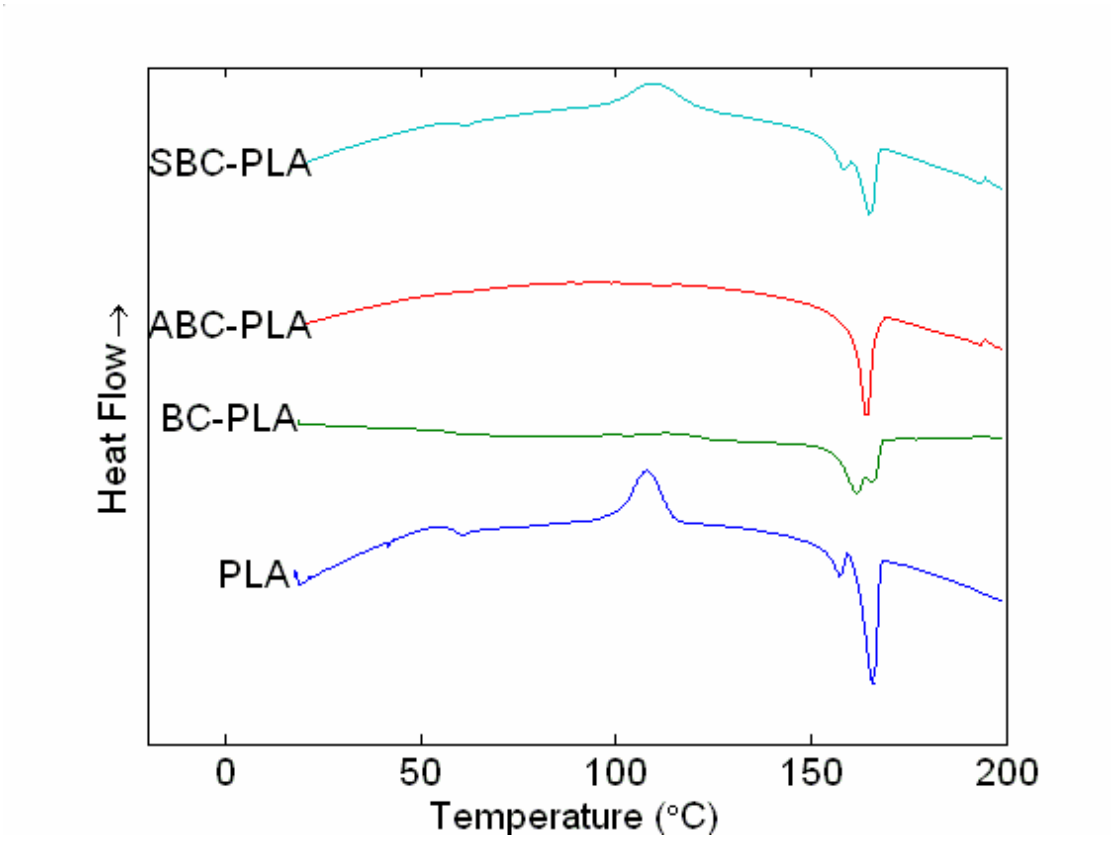

Figure 4.40 The subsequent thermograms of PLA and PLA-based composites at heating rate of 5°C/min.

The crystallinity of PLA and its composites was determined from the crystallisation enthalpies in cooling thermograms and from the enthalpies of cold-crystallisation and melting in subsequent heating thermograms. The values are shown in Table 4.2. The percentage crystallinity was calculated from the melting enthalpy of 100% crystalline

PLA given in the literature as 93.7 J/g for PLA [120]. With the addition of BC or ABC to the PLA matrix, the melting points of the composites were increased ~ 4-7 °C. However, the crystallinity did not change significantly. On the other hand, the crystallinity of SBC-PLA composite decreased from 31.9 % to 26.9 % with only a slight change of ~ 1 °C in the melting point with the addition of SBC.

Table 4.2 Crystallinity of PLA and PLA-based composites

Materials	Cooling			subsequent heating					
	PLA crystallisation			PLA cold crystallisation			PLA melting		
	T_c (°C)	ΔH (J/g)	X_c (%)	T_c (°C)	ΔH (J/g)	X_c (%)	T_m (°C)	ΔH (J/g)	X_c (%)
PLA	-	-	0	108	-32.5	34.7	157.5 165.9	29.9	31.9
BC-PLA	120.4	-17.9	19.1	113	-6.8	7.3	161.8 165.7	30.1	32.1
ABC-PLA	126	-29.4	31.4	-	-	0	164.2	29.6	31.6
SBC-PLA	-	-	0	110	-27.1	28.9	158.6 165.4	25.2	26.9

T_c, the temperature of crystallisation peak; T_m, temperatures of the melting peaks; ΔH, the enthalpy of cold crystallisation or melting; X_c, the crystallinity.

4.8 Dynamic Mechanical Analysis (DMA) of PLA and BC-PLA Composites

The storage modulus (E') as a function of temperature for PLA and its composites was determined from dynamic mechanical analysis (Table 4.3, Figure 4.41 and Figure 4.42). Fibrous reinforcements have a large effect in enhance the modulus of materials, due to the combination of the effect of the fibres embedded in a viscoelastic matrix and to the mechanical limitation introduced by the fibrous reinforcements which reduce the mobility and deformation of the matrix [1].

The increase in E' due to the BC reinforcement over the PLA was found to be even greater at higher temperatures. For example, at 25°C the increase in E' from 4.66 to 8.49 GPa is almost doubled; in contrast, increase of E' from 0.337 to 4.092 GPa at ~100°C – an increase of ~12 times. Only slight increase on E' of PLA and PLAG after relaxation (T_g) can be observed. The broad peaks in E' observed at ~100°C for all composites can be attributed to crystallisation *via* molecular rearrangement [142]. It appears that the BC microfibrils provide favourable nucleation sites for crystallisation since a nearly nil crystallisation peak appears in the PLA and the PLAG [143]. The storage modulus of PLAG was reduced because of the action of glycerol. However, BC-PLAG presented higher storage modulus than the PLAG; also greater at higher temperature. The storage modules of every material from DMA kept similar trend as static testing results. For example, the storage modulus of ABC-PLA was higher than SBC-PLA; the storage modulus of all of materials with glycerol was lower than the materials with glycerol.

Table 4.3 Storage modulus as a function of temperature for PLA and composites.

Material	Storage modulus (GPa)		T_g (°C)
	At 25 °C	At 100 °C	
PLA	4.66	0.337	58.68
PLAG	2.794	0.076	56.69
BC-PLA	8.49	1.092	63.87
BC-PLAG	4.216	2.128	63.06
ABC-PLA	8.986	2.438	50.23
ABC-PLAG	3.819	0.85	62.19
SBC-PLA	7.528	1.945	57.04
SBC-PLAG	2.731	0.68	58.37

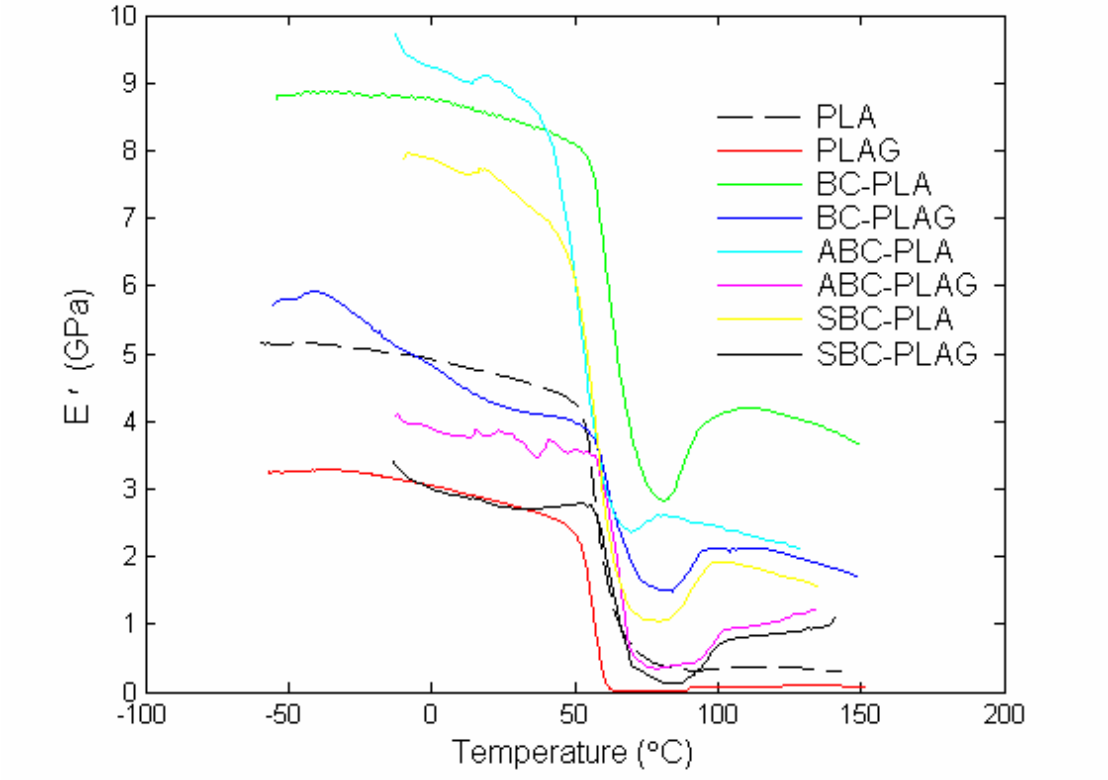

Figure 4.41 Storage modulus (E') of PLA and its composites as a function of temperature (frequency: 1 Hz).

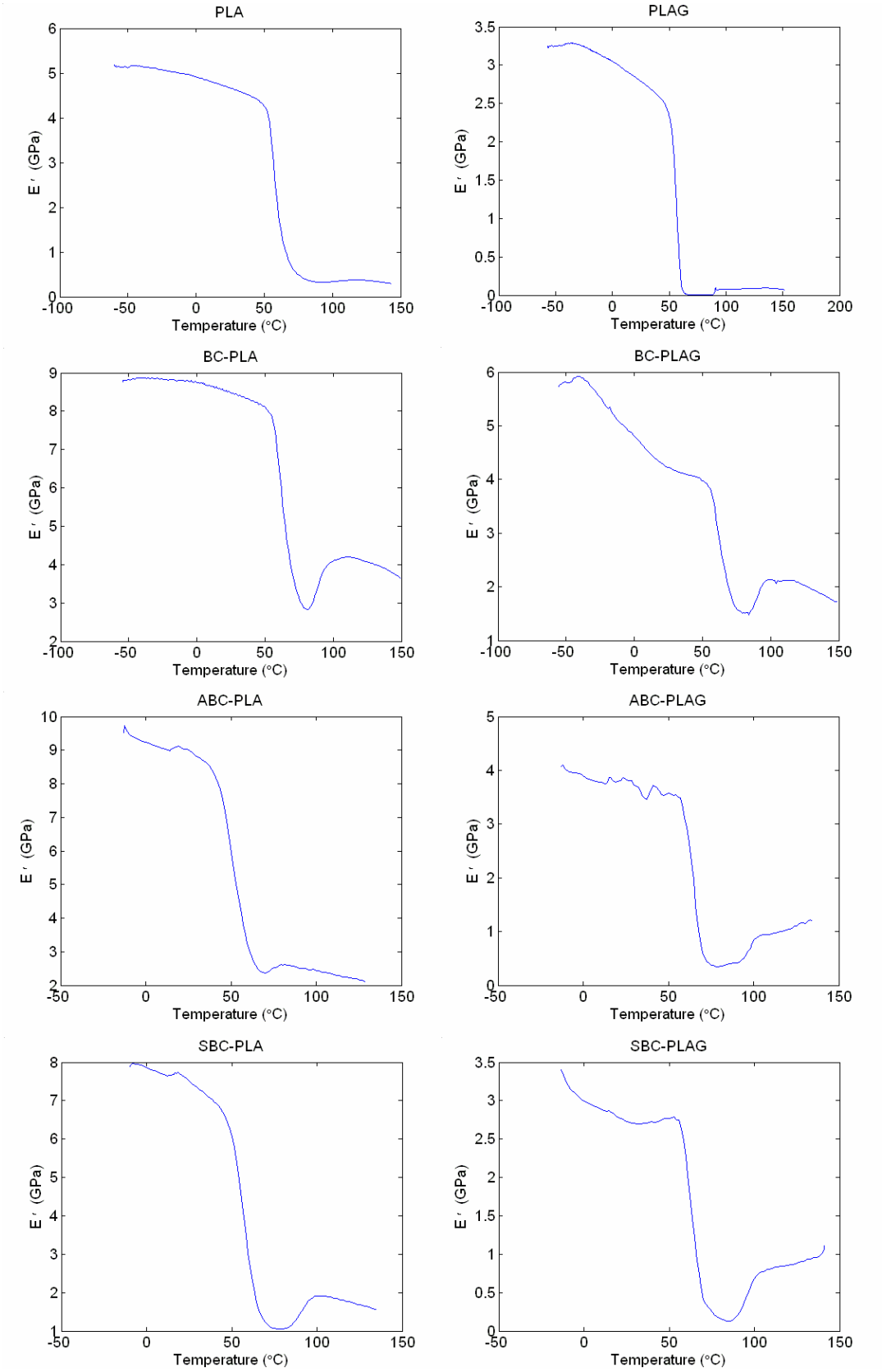

Figure 4.42 Storage modulus (E') of PLA and its composites as a function of temperature (frequency: 1 Hz).

Figure 4.43 and Figure 4.44 show the loss modulus (E") of PLA and its composites. The loss modulus indicates the ability of material to dissipate mechanical energy, which is proportional to viscous behaviour and impact resistance of the material. It can be seen from the peak of the loss modulus (E") that the T_g (58.68 °C) of the PLA was shifted to the T_g of the BC-PLA (63.87 °C) because of the reinforcing of BC and shifted to the T_g of PLAG 56.69 °C because of the addition of glycerol. However, the difference of T_g between PLA and PLAG was not so much. Similar result was discovered by Martin *et al.* with DSC analysis [111]. The BC reinforcement also increased the T_g of PLAG to 63.06 °C.

An increase was observed on the curve of every composite the when the temperature was over T_g, however, none increase can be found on the curve of PLA or PLAG. Ray *et al*. reported that a large increment occurred in loss modulus of PLA/Layered clay nanocomposites above T_g, indicating the flocculation enhanced the loss component due to the large anisotropy of the dispersed clay particles [84]. The cellulose microfibrils which dispersed in the matrix also presented the anisotropy [144]. Therefore, the loss modulus was increased when the temperature past T_g.

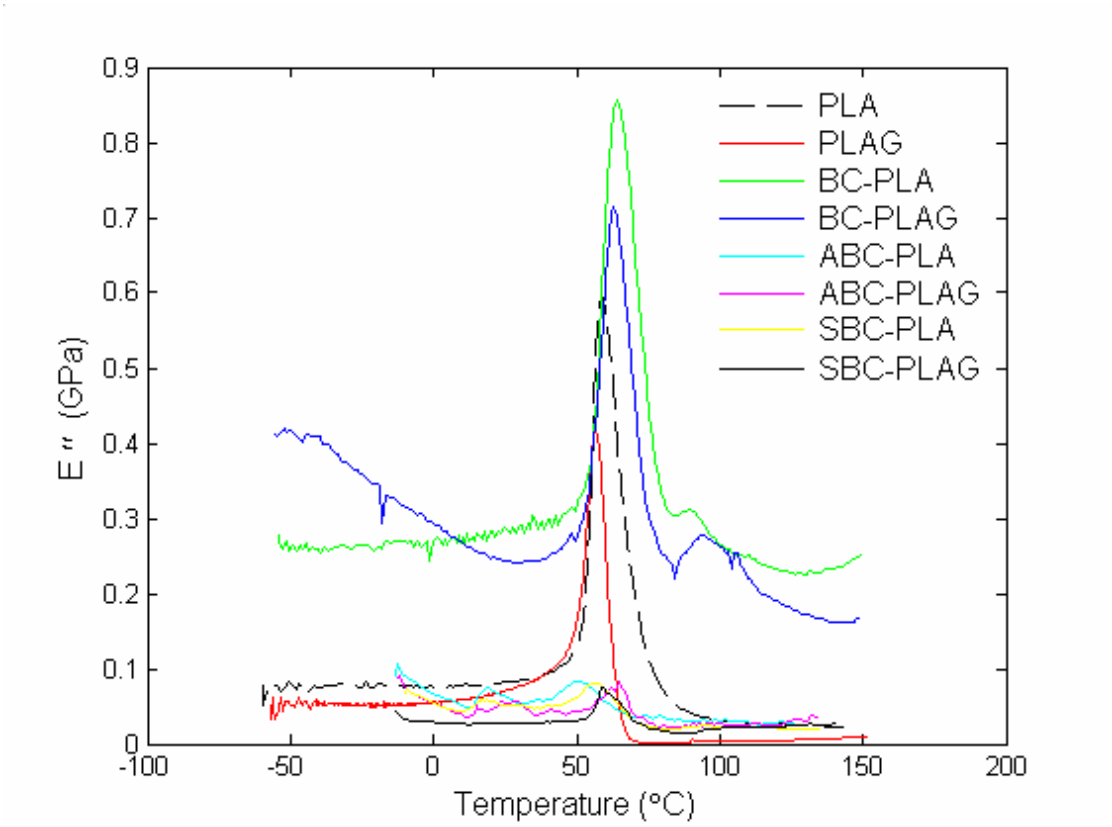

Figure 4.43 Loss modulus (E") of PLA and its composites as a function of temperature (frequency: 1 Hz).

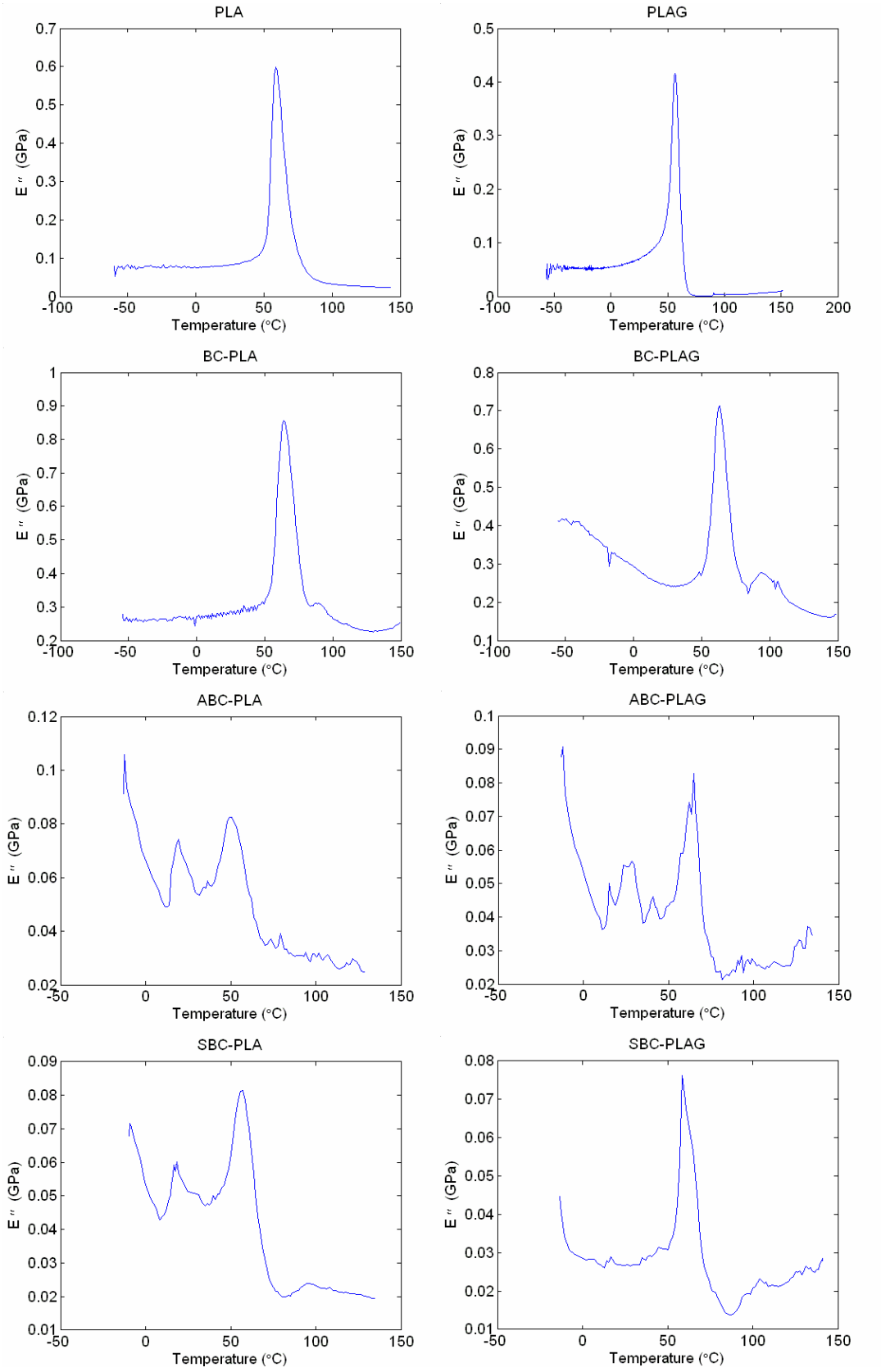

Figure 4.44 Loss modulus (E") of PLA and its composites as a function of temperature (frequency: 1 Hz).

Loss factors (Tan δ) of PLA and its composites are shown in Figure 4.45 and Figure 4.46. The addition of BC to the PLA or PLAG reduced the height of the tan δ peak, indicating that the energy damping ability of the composites was significantly decreased. Generally, if fibres have a good adhesion with the polymeric matrix, the fibres carry a greater extent of stress and allow only a small part of it to strain the interface [3]. Therefore, energy dissipation will occur in the polymer matrix while the well bonded interface contributes less to energy dissipation in the structure [145]. Therefore, the lowest loss factor of BC-PLA is due to strong bonding between the microfibrils and PLA matrix as shown in Figure 4.33. On the other hand, less fibre pull-out was found in Figure 4.34, suggesting that the adhesion between BC and PLAG was good. Similarly, the loss factor of BC-PLAG was lower than PLAG.

Moroni *et al.* decribed that with increasing porosity of 3D fibre-deposited scaffolds for tissue engineering, dynamic mechanical analysis (DMA) revealed a decrease in elastic properties such as dynamic stiffness and equilibrium modulus, and an increase of the viscous parameters like damping factor. There were a few voids in the materials without glycerol, leading to a lower loss factor. In contrast, a large loss factor was measured for materials with glycerol due to their porous structure as show in the Figure 4.32, Figure 4.34, Figure 4.36 and Figure 4.38.

In addition, the increase of the loss factor above T_g corresponded the enhancement of the loss modulus.

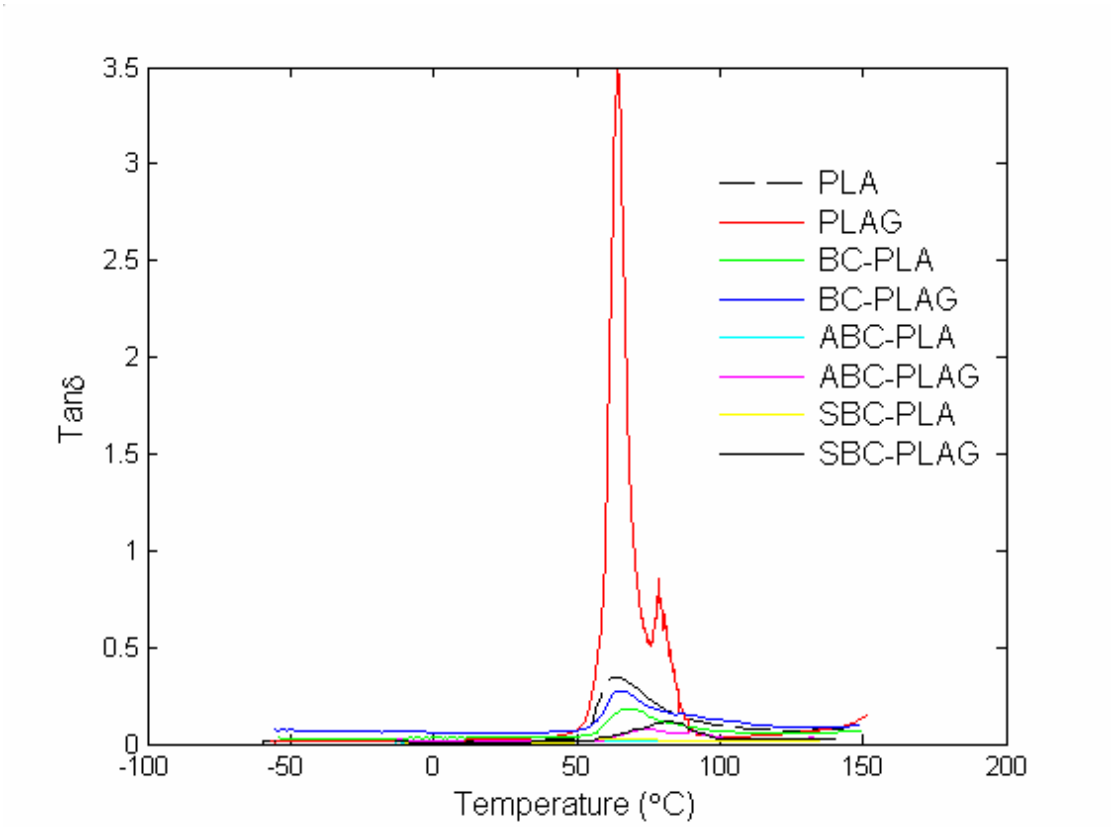

Figure 4.45 Loss factor (Tan δ) of PLA and its composites as a function of temperature (frequency: 1 Hz).

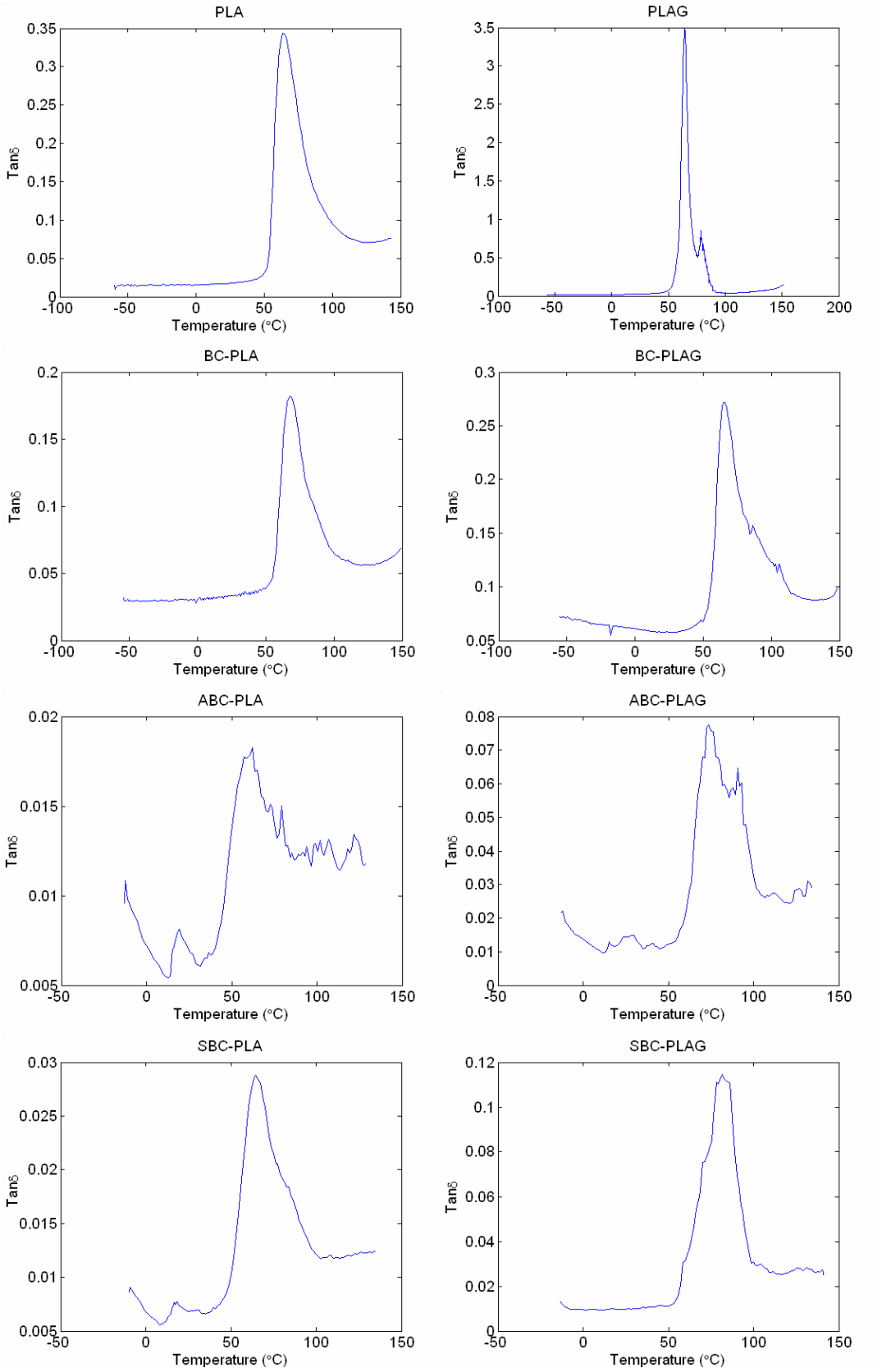

Figure 4.46 Loss factor (Tan δ) of PLA and its composites as a function of temperature (frequency: 1 Hz).

4.9 Comparison with other cellulosic nanocomposites

A comparison of the tensile behaviour of the nanocomposites in the present work and that for nanocomposites utilising cellulosic reinforcements in the literature is shown in Table 4.4. Some workers have used BC as the reinforcements for their composites [51, 71, 75]. Nanoscale cellulose microfibrils (also referred to as DNC) obtained from disintegrated plant fibres have also been used as reinforcement in various polymeric matrices [30, 146].

The enhancement of the tensile behaviour of BC-PLA, ABC-PLA and SBC-PLA were similar to other nanocomposites with cellulose reinforcements. For example, the Young's modulus of the composites in this research was ~2-3 times that of the neat PLA; a BC-cellulose acetate butyrate (CAB) composite with 10 vol. % fibre content was ~ 2.7 times that of neat CAB [51]; and a DNC-hydroxypropyl cellulose (HPC) composite with 10 wt. % fibre content was ~ 2 times that of neat HPC [146].

Grunert *et al*. reported an increase on BC nanocrystals reinforced CAB. The storage modulus of CAB varied from 0.9 to 0.004 GPa with temperatures of 81°C and 124°C, respectively. The storage modulus of composite, reinforced by 10 wt. % BC was found to be 1.75 and 0.104 GPa, respectively. This composite system exhibited a greater storage modulus at high temperature [50]. The nanocomposites of current research also exhibited a high storage modulus at elevated temperature. For example, the storage modulus of PLA varied from 4.6 to 0.337 GPa with temperatures of 50°C and 100°C, respectively, while the storage modulus of BC-PLA was 8.49 and 2.128 GPa, respectively.

Table 4.4 Comparison of the tensile behaviours of cellulose based nanocomposite

Composite system	Young's modulus (GPa)	Tensile strength (MPa)	Reference
PLA with	1.8-1.9	29-31	
11.39 wt. % (9.4 vol. %) BC	4.3-6.6	69-75	Current research
10.24 wt. % (8.4 vol. %) ABC	3.3-4.8	26-38	
10.62 wt. % (8.7 vol. %) SBC	4.1-4.5	58-72	
Cellulose acetate butyrate (CAB) with	1.2	25.9	
10 vol. % BC	3.2	52.6	[51]
32 vol. % BC	5.8	128.9	
Phenolformaldehyde (PF) with	0.375	10	[76]
87.6 wt. % BC	28	420	[75]
87.5 wt. % disintegrated BC	19	350	
Epoxy with	3-6	35-100	[1]
65 wt. % BC	20	325	[71]
poly(styrene-co-butyl acrylate) with	0.55×10^{-3}	7.1	[30]
10 wt. % DNC from Opuntia ficus-indica	34.46×10^{-3}	14.5	
Hydroxypropyl cellulose (HPC) with	~ 0.4		
10 wt. mechanical DNC from sulphite pulp	~ 0.8		
10 wt. chemical DNC from sulphite pulp	~ 0.7		[146]
Polyvinyl alcohol (PVA) with	~ 0.6		
10 wt. mechanical DNC from sulphite pulp	~ 0.45		
10 wt. Chemcal DNC from sulphite pulp	~ 0.8		

Note: In order to compare the BC-CAB nanocomposites system [51] with the nanocomposites of current research, the fibre content of the nanocomposites of current research can be converted with follows equation,

$$V_f = (W_f/D_{bc})/((1-W_f)/D_{PLA}) \times 100\%$$

where V_f is the fibre content in volume, W_f is the fibre content in weight; D_{bc} is the density of cellulose which literature value is 1.55 g/mm^3 [52], and the D_{PLA} is the density of PLA which is 1.25 g/mm^3 from manufacturer

5 Conclusions

There are several conclusions that can be derived from this research:

Tensile properties were strongly enhanced by the addition of BC based reinforcement. The Young's modulus values of PLA-based composites with varieties of reinforcement were up to ~1.7 - 2.5 times that of neat PLA; the Young's modulus values of PLAG-based composites with varieties of reinforcement were up to ~1.2 - 2 times that of PLAG. The tensile strength values of PLA-based composites with varieties of reinforcement were up to ~1.3 - 2.5 times that of neat PLA; the tensile strength values of PLAG-based composites with varieties of reinforcement were up to ~1.2 - 2.2 times that of PLAG.

PLAG exhibited lower tensile properties, Young's modulus and tensile strength values were ~ 50 % - 90 % that of neat PLA, respectively; and larger tensile failure strains up to 1.5 times that of neat PLA. However, glycerol is not an efficient plasticizer of PLA concluded from the forming of large amount of voids and the continued brittle behaviour after the addition of glycerol. A large amount of voids also were caused with glycerol in the PLAG based composites. The porous structure of the PLAG based composites reduced the tensile properties.

An enhancement in the storage modulus (E') of the neat PLA and PLAG, especially, when the temperature above the glass transition temperature (T_g) presented due to the addition of varieties of BC based reinforcements. The DMA results showed that the

presence of BC based reinforcements significantly reduced the damping properties of the composites. However, the porous structure of PLAG based materials led to a lower loss factor than PLA based materials.

Either native BC or surface treated BC exhibited a good adhesion with PLA matrix. A few number of cellulose microfibrils were pulled out under the tensile load. However, a large amount of microfibrils were pulled out from ABC-PLAG and SBC-PLAG composites under the tensile load.

The addition of BC or ABC increased the tendency for crystallisation in PLA during the cooling down procedure. Further more, BC or ABC increased the melt points of the composites. However, the crystallinity did not change significantly. On the other hand, crystallinity of SBC-PLA composite decreased with a slight changed melting point for the presence of SBC. PLA, BC-PLA and ABC-PLA also presented a double-melting behaviour.

Reference

1. Hull, D. and T.W. Clyne, *An introduction to composite materials*. 2 ed. 1996, Cambridge ; New York: Cambridge University Press. 326.
2. Jang, B.Z. and ASM International., *Advanced polymer composites*. 1994, Materials Park, Ohio: ASM International. ix, 297.
3. Jones, F.R., *Handbook of polymer-fibre composites*. Polymer science and technology series. 1994, Burnt Mill, Harlow, Essex: Longman Scientific & Technical. xiv, 418.
4. Netravali, A.N. and S. Chabba, *Composites get greener.* Materials Today, 2003. 6(4): p. 22-29.
5. Scott, G., *'Green' polymers.* Polymer Degradation and Stability, 2000. 68(1): p. 1-7.
6. Schlechter, M., *Biodegradable Polymer*. 2001, Norwalk: Communications Co., Inc.
7. Kolybaba, M., et al. *Biodegradable Polymers: Past, Present, and Future*. in *2003 CSAE/ASAE Annual Intersectional Meeting*. 2003.
8. Peijs, T., *Composites turn green.* e-Polymers, 2002. 2: p. 1-12.
9. Marklund, E., *Micromechanism Based Material Models for Natural Fiber Composites*, in *Department of Applied Physics and Mechanical Engineering, Division of Polymer Engineering.* 2005, Luleå University of Technology.
10. Bledzki, A.K. and J. Gassan, *Composites reinforced with cellulose based fibres.* Progress in Polymer Science, 1999. 24: p. 221-274.
11. Nishino, T., et al., *Kenaf reinforced biodegradable composite.* Composites Science and Technology, 2003. 63: p. 1281-1286.
12. Herrmann, A.S., J. Nickel, and U. Riedel, *Construction materials based upon biologically renewable resources—from components to finished parts.* Polymer Degradation and Stability, 1998. 59(1-3): p. 251-261.
13. Ray, S.S. and M. Bousmina, *Biodegradable polymers and their layered silicate nanocomposites: In greening the 21st century materials world.* Progress in Materials Science, 2005. 50(8): p. 962-1079.
14. Andrady, A.L., *Plastics and the environment*. 2003, Hoboken: Wiley-Interscience.
15. S‰derg┐rdb, A. and M. Stolta, *Properties of lactic acid based polymers and their correlation with composition.* Progress in Polymer Science, 2002. 27: p. 1123-1163.
16. Kasuga, T., et al., *Preparation and mechanical properties of polylactic acid composites containing hydroxyapatite fibers.* Biomaterials, 2001. 22(1): p. 19-23.
17. Gomes, M.E., *Biodegradable polymers and composites in biomedical applications: From catgut to tissue engineering Part 1 Available systems and their properties.* International Materials Reviews, 2004. 12(4): p. 65-81.
18. Ray, S.S. and M. Okamoto, *Polymer/layered silicate nanocomposites: a review from preparation to processing.* Progress in Polymer Science, 2003. 28(11): p. 1539-1641.
19. Oksmana, K., M. Skrifvarsb, and J.F. Selinc, *Natural Fibres as reinforcement in polylactic acid (PLA) composites.* Composites Science and Technology, 2003. 63: p. 1317-1324.

20. Lee, S.M., et al., *Novel silk/poly(butylene succinate) biocomposites: the effect of short fibre content on their mechanical and thermal properties.* Composites Science and Technology, 2005. 65(3-4): p. 647-657.
21. Taib, R.M., *Cellulose Fiber-Reinforced Thermoplastic Composites: Processing and Product Characteristics*. 1998, Virginia Polytechnic Institute and State University.
22. Plackett, D., et al., *Biodegradable composites based on L-polylactide and jute fibres.* Composites Science and Technology, 2003. 63(9): p. 1287-1296.
23. Joseph, P.V., et al., *The thermal and crystallisation studies of short sisal fibre reinforced polypropylene composites.* Composites: Part A, 2003. 34(3): p. 253-266.
24. Ganster, J., H.P. Fink, and M. Pinnow, *High-tenacity man-made cellulose fibre reinforced thermoplastics - Injection moulding compounds with polypropylene and alternative matrices.* Composites Part A: Applied Science and Manufacturing, 2005. In Press, Corrected Proof.
25. Hepworth, D.G. and D.M. Bruce, *The mechanical properties of a composite manufactured from non-fibrous vegetable tissue and PVA.* Composites: Part A, 2000. 31: p. 283-285.
26. Salmen, L., *Micromechanical understanding of the cell-wall structure.* Comptes Rendus Biologies, 2004. 327(9-10): p. 873-880.
27. Biermann, C.J., *Handbook of pulping and papermaking*. 1996, San Diego: : Academic Press.
28. Lundquist, L., et al., *Novel pulp fibre reinforced thermoplastic composites.* Composites Science and Technology, 2003. 63(1): p. 137-152.
29. Molder, T. and O. Trass, *Grinding of waste paper and rice hulls with the Szego Mill for use as plastics fillers.* International Journal of Mineral Processing, 1996. 44-45: p. 583-595.
30. Malainine, M.E., M. Mahrouz, and A. Dufresne, *Thermoplastic nanocomposites based on cellulose microfibrils from Opuntia ficus-indica parenchyma cell.* Composites Science and Technology, 2005. 65(10): p. 1520-1526.
31. Bruce, D.M., et al., *High-performance composites from low-cost plant primary cell walls.* Composites Part A: Applied Science and Manufacturing, 2005. 36(11): p. 1486-1493.
32. Dufresne, A. and M.R. Vignon, *Improvement of Starch Film Performances Using Cellulose Microfibrils.* Macromolecule, 1998. 31: p. 2693-2696.
33. Dufresne, A., D. Dupeyre, and M.R. Vignon, *Cellulose microfibrils from potato tuber cells: Processing and characterization of starch-cellulose microfibril composites.* Journal of Applied Polymer Science, 2000. 76(14): p. 2080-2092.
34. Dufresne, A., J.-Y. CavailĬ, and M.R. Vignon, *Mechanical behavior of sheets prepared from sugar beet cellulose microfibrils.* Journal of Applied Polymer Science, 1997. 64(6): p. 1185-1194.
35. Nakagaito, A.N. and H. Yano, *The effect of morphological changes from pulp fiber towards nano-scale fibrillated cellulose on the mechanical properties of high-strength plant fiber based composites.* Applied Physics A: Materials Science and Processing, 2004. 78(4): p. 547-552.
36. Berthold, F., et al. *Strategies for the disintegration/fibrillation of wood-fibre cell walls*. in *Proceedings of the 23rd International Symposium on materials*

Science: Sustainable natural and polymeric Composites - Science and Technolodge.
37. Chazeau, L., M. Paillet, and J.Y. Cavaille, *Plasticized PVC Reinforced with Cellulose Whiskers. I. Linear Viscoelastic Behavior Analyzed through the Quasi-Point Defect Theory.* Journal of Polymer Science: Part B, 1999. 37: p. 2151–2164.
38. Chazeau, L., J.Y. Cavaille, and J. Perez, *Plasticized PVC reinforced with cellulose whiskers. II. Plastic behavior.* Journal of Polymer Science, Part B: Polymer Physics, 2000. 38(3): p. 383-392.
39. Azizi Samir, M.A.S., et al., *POE-based nanocomposite polymer electrolytes reinforced with cellulose whiskers.* Electrochimica Acta, 2005. 50(19): p. 3897-3903.
40. Mathew, A.P. and A. Dufresne, *Morphological Investigation of Nanocomposites from Sorbitol Plasticized Starch and Tunicin Whiskers.* Biomacromolecules, 2002. 3: p. 609-617.
41. Angle`s, M.N. and A. Dufresne, *Plasticized Starch/Tunicin Whiskers Nanocomposites. 1. Structural Analysis.* Macromolecules, 2000. 33: p. 8344-8353.
42. Angle`s, M.N. and A. Dufresne, *Plasticized Starch/Tunicin Whiskers Nanocomposites. 2. Mechanical Behavior.* Macromolecules, 2001. 34: p. 2921-2931.
43. Dufresne, A., M.B. Kellerhals, and B. Witholt, *Transcrystallization in Mcl-PHAs/Cellulose Whiskers Composites.* Macromolecules, 1999. 32: p. 7396-7401.
44. Vandamme, E.J., et al., *Improved production of bacterial cellulose and its application potential.* Polymer Degradation and Stability, 1998. 59: p. 93-99.
45. Jonas, R. and L.F. Farah, *Production and application of microbial cellulose.* Polymer Degradation and Stability, 1998. 59: p. 101-106.
46. Czaja, W., et al., *Microbial cellulose--the natural power to heal wounds.* Biomaterials, 2006. 27(2): p. 145-151.
47. Svensson, A., et al., *Bacterial cellulose as a potential scaffold for tissue engineering of cartilage.* Biomaterials, 2005. 26(4): p. 419-431.
48. Klemm, D., et al., *Bacterial synthesized cellulose -- artificial blood vessels for microsurgery.* Progress in Polymer Science, 2001. 26(9): p. 1561-1603.
49. Grunert, M. and W.T. Winter. *Progress in the Development of Cellulose Reinforced Nanocomposites*. in *Polymeric Materials: Science and Engineering (PMSE) National Meeting, American Chemical Society (ACS).* 2000. San Francisco, USA.
50. Grunert, M. and W.T. Winter, *Nanocomposite of cellulose acetate butyrate reinforced with cellulose nanocrystals.* Journal of polymers and the Environment, 2002. 10: p. 28-30.
51. Gindl, W. and J. Keckes, *Tensile properties of cellulose acetate butyrate composites reinforced with bacterial cellulose.* Composites Science and Technology, 2004. 64(15): p. 2407-2413.
52. Krässig, H., et al., *Cellulose*. 2004, Weinheim: Wiley-VCH Verlag GmbH & Co. KGaA.
53. Hendrik, H.P., *Physics and chemistry of cellulose fibres*. 1949, New York: Elsevier Pub. Co.
54. Bayer, E.A., et al., *Cellulose, cellulases and cellulosomes.* Current Opinion in Structural Biology, 1998. 8: p. 548-557.

55. Iguchi, M., S. Yamanaka, and A. Budhiono, *Review Bacterial cellulose - a masterpiece of nature's arts.* Journal of Materials Science, 2000. 35: p. 261-270.
56. Son, H., et al., *Optimization of fermentation conditions for the production of bacterial cellulose by a newly isolated Acetobacter sp. A9 in shaking cultures.* Biotechnol. Appl. Biochem, 2001. 33: p. 1-5.
57. Steinbüchel, A. and Y. Doi, *Biotechnology of Biopolymers*. 2004, Weinheim: Wiley-VCH.
58. Sutherland, I., *A sticky business. Microbial polysaccharides:current products and future trends.* Microbiology Today, 2002. 29: p. 70-71.
59. BROWN, R.M., *Cellulose: Structural and functional aspects*. 1989: Ellis Horwood Ltd.
60. Steinbüchel, A., E.J. Vandamme, and S.D. Baets, *Biopolymers*. 2002, Germany: Wiley-VCH.
61. Watanabe, K., et al., *Structural features and properties of bacterial cellulose produced in agitated culture.* Cellulose, 1998. 1998: p. 187-200.
62. Krystynowicz, A., et al., *Factors affecting the yield and properties of bacterial cellulose.* Journal of Industrial Microbiology and Biotechnology, 2002. 29(4): p. 189-195.
63. Phillips, G.O. and P.A. Williams, *Handbook of Hydrocolloids*. 2000, Williams: Woodhead Publishing.
64. Yamanaka, S., et al., *The Structure and Mechanical Properties of Sheets Prepared from Bacterial Cellulose.* Journal of Materials Science, 1989. 24: p. 3141-3145.
65. Guhados, G., W. Wan, and J.L. Hutter, *Measurement of the Elastic Modulus of Single Bacterial Cellulose Fibers Using Atomic Force Microscopy.* Langmuir, 2005. 21: p. 6642-6646.
66. Astley, O.M., et al., *Tensile deformation of bacterial cellulose composites.* International Journal of Biological Macromolecules, 2003. 32(1-2): p. 28-35.
67. Kacurakova, M., et al., *Molecular interactions in bacterial cellulose composites studied by 1D FT-IR and dynamic 2D FT-IR spectroscopy.* Carbohydrate Research, 2002. 337(12): p. 1145-1153.
68. Dammstrom, S., L. Salmen, and P. Gatenholm, *The effect of moisture on the dynamical mechanical properties of bacterial cellulose/glucuronoxylan nanocomposites.* Polymer, 2005. 46(23): p. 10364-10371.
69. Dubey, V., L.K. Pandey, and C. Saxena, *Pervaporative separation of ethanol/water azeotrope using a novel chitosan-impregnated bacterial cellulose membrane and chitosan-poly(vinyl alcohol) blends.* Journal of Membrane Science, 2005. 251(1-2): p. 131-136.
70. Pandey, L.K., C. Saxena, and V. Dubey, *Studies on pervaporative characteristics of bacterial cellulose membrane.* Separation and Purification Technology, 2005. 42(3): p. 213-218.
71. Yano, H., et al., *Optically transparent composites reinforced with networks of bacterial nanofibers.* Advanced Materials, 2005. 17(2): p. 153-155.
72. Seifert, M., et al., *Controlling the Water Content of Never Dried and Reswollen Bacterial Cellulose by the Addition of Water-Soluble Polymers to the Culture Medium.* Journal of Polymer Science, Part A: Polymer Chemistry 2004. 42(3): p. 463-470.
73. Seves, A., et al., *Characterization of Native Cellulose/Poly(ethylene glycol) Films.* Macromolecular Materiala and Engineering, 2001. 286: p. 524-528.

74. Yasuda, K., et al., *Biomechanical properties of high-toughness double network hydrogels.* Biomaterials, 2005. 26(21): p. 4468-4475.
75. Nakagaito, A.N., S. Iwamoto, and H. Yano, *Bacterial cellulose: The ultimate nano-scalar cellulose morphology for the production of high-strength composites.* Applied Physics A: Materials Science and Processing, 2005. 80(1): p. 93-97.
76. Sreekala, M.S., et al., *The mechanical performance of hybrid phenol-formaldehyde-based composites reinforced with glass and oil palm fibres.* Composites Science and Technology, 2002. 62(3): p. 339-353.
77. Hutmacher, D.W., *Scaffolds in tissue engineering bone and cartilage.* Biomaterials, 2000. 21: p. 2529-2543.
78. *www.biofill.co.br*.
79. Krystynowicz, A., et al., *The Evaluation of Usefulness of Microbial Cellulose as A Wound Dressing Material.* Proceedings Mededelingen Faculteit Landbouwkundige Biologische Wetenschappen, 2000. 65: p. 213-220.
80. Mormino, R. and H. Bungay, *Composites of bacterial cellulose and paper made with a rotating disk bioreactor.* Applied Microbiology And Biotechnology, 2003. 62(5-6): p. 503-506.
81. Jacobsen, S., et al., *New developments on the ring opening polymerisation of polylactide.* Industrial Crops and Products, 2000. 21: p. 265-275.
82. Velde, K.V.d. and P. Kiekens, *Biopolymers: overview of several properties and consequences on their applications.* Polymer Testing, 2002. 21: p. 433-442.
83. Eichhorn, S.J., et al., *Review-current international research into cellulosic fibres and composites.* Journal of Materials Science, 2001. 36: p. 2107-2131.
84. Ray, S.S., et al., *New Polylactide/Layered Silicate Nanocomposites. 1. Preparation, Characterization, and Properties.* Macromolecules, 2002. 35: p. 3104-3110.
85. Ray, S.S. and M. Okamoto, *Biodegradable Polylactide and Its Nanocomposites: Opening a New Dimension for Plastics and Composites.* Macromolecular Rapid Communicanitions, 2003. 24: p. 815-840.
86. Yew, G.H., et al., *Water absorption and enzymatic degradation of poly(lactic acid)/rice starch composites.* Polymer Degradation and Stability, 2005. 90(36): p. 488-500.
87. Li, L., S. Ding, and C. Zhou, *Preparation and degradation of PLA/Chitosan composite materials.* Journal of Applied Polymer Science, 2004. 91(1): p. 274-277.
88. Suyatma, N.E., et al., *Mechanical and Barrier Properties of Biodegradable Films based on Chitosan and Poly(lactic acid) for Food Packaging Application.*
89. Leo, E., et al., *In vitro evaluation of PLA nanoparticles containing a lipophilic drug in water-soluble or insoluble form.* International Journal of Pharmaceutics, 2004. 278: p. 133-141.
90. Seala, B.L., T.C. Oterob, and A. Panitch, *Polymeric biomaterials for tissue and organ regeneration.* Materials Science and Engineering: R: Reports, 2001. 34: p. 147-230.
91. Kricheldorf, H.R., *Syntheses and application of polylactides.* Chemosphere, 2001. 43: p. 49-54.

92. Schwach, G. and M. Vertb, *In vitro and in vivo degradation of lactic acid-based interference screws used in cruciate ligament reconstruction.* International Journal of Biological Macromolecules, 1999. 25: p. 283-291.
93. Sarazin, P., X. Roy, and B.D. Favis, *Controlled preparation and properties of porous poly(-lactide) obtained from a co-continuous blend of two biodegradable polymers.* Biomaterials, 2004. 25: p. 5965-5978.
94. Thomson, R.C., et al., *Hydroxyapatite fiber reinforced poly(a-hydroxy ester) foams for bone regeneration.* Biomaterials, 1998. 19: p. 1935-1943.
95. Serafica, Mormino, and Bungay, *Inclusion of solid particles in bacterial cellulose.* Applied Microbiology and Biotechnology, 2002. 58(6): p. 756-760.
96. Harris, J.R., *Electron microscopy in biology : a practical approach*. The Practical approach series. 1991, Oxford ; New York: IRL Press. xix, 308.
97. Mwaikambo, L.Y., E. Martuscelli, and M. Avella, *Kapok/cotton fabric–polypropylene composites.* Polymer Testing, 2000. 19(8): p. 905-918.
98. Lee, S.-H., T. Ohkita, and K. Kitagawa, *Eco-composite from poly(lactic acid) and bamboo fiber.* Holzforschung, 2004. 58: p. 529-536.
99. Tserki, V., et al., *A study of the effect of acetylation and propionylation surface treatments on natural fibres.* Composites Part A: Applied Science and Manufacturing, 2005. 36(8): p. 1110-1118.
100. Kim, D.-Y., Y. Nishiyama, and S. Kuga, *Surface acetylation of bacterial cellulose.* Cellulose, 2002. 9: p. 361-367.
101. *Silane Coupling Agents: Connecting Across Boundaries*. 2004, Gelest Inc.
102. Bengtsson, M. and K. Oksman, *The use of silane technology in crosslinking polyethylene/wood flour composites.* Composites Part A: Applied Science and Manufacturing, 2006. 37(5): p. 752-765.
103. Herrera-Franco, P.J. and A. Valadez-Gonz?lez, *Mechanical properties of continuous natural fibre-reinforced polymer composites.* Composites Part A: Applied Science and Manufacturing, 2004. 35(3): p. 339-345.
104. Pickering, K.L., et al., *The effect of silane coupling agents on radiata pine fibre for use in thermoplastic matrix composites.* Composites Part A: Applied Science and Manufacturing, 2003. 34(10): p. 915-926.
105. Park, B.-D., et al., *X-ray photoelectron spectroscopy of rice husk surface modified with maleated polypropylene and silane.* Biomass and Bioenergy, 2004. 27(4): p. 353-363.
106. Misra, M., M.S. Huda, and L.T. Drzal. *The Effect of Fiber Surface Treatment on Laminated Biocomposites from Poly(lactic acid) (PLA) and Natural Fibers*. in *GPEC 2006: Global Plastics Environmental Conference - Creating Sustainability & Recycling in Action*. 2006. Atlanta, Georgia, USA.
107. Salon, M.-C.B., et al., *Silane adsorption onto cellulose fibers: Hydrolysis and condensation reactions.* Journal of Colloid and Interface Science, 2005. 289(1): p. 249-261.
108. Maeda, H., T. Kasuga, and L.L. Hench, *Preparation of poly(l-lactic acid)-polysiloxane-calcium carbonate hybrid membranes for guided bone regeneration.* Biomaterials, 2006. 27(8): p. 1216-1222.
109. Wong, S., R.A. Shanks, and A. Hodzic, *Poly(L-actic acid) Composites With Flax Fibers Modified by Plasticizer Absorption.* Polymer Engineering and Science, 2003. 43(9): p. 1566-1575.
110. Kulinski, Z. and E. Piorkowska, *Crystallization, structure and properties of plasticized poly(l-lactide).* Polymer, 2005. 46(23): p. 10290-10300.

111. Martin, O. and L. Averous, *Poly(lactic acid): plasticization and properties of biodegradable multiphase systems.* Polymer, 2001. 42(14): p. 6209-6219.
112. Thellen, C., et al., *Influence of montmorillonite layered silicate on plasticized poly(l-lactide) blown films.* Polymer, 2005. 46(25): p. 11716-11727.
113. Rahman, M. and C.S. Brazel, *The plasticizer market: an assessment of traditional plasticizers and research trends to meet new challenges.* Progress in Polymer Science, 2004. 29: p. 1223-1248.
114. Špitalský, Z., et al., *Controlled degradation of polyhydroxybutyrate via alcoholysis with ethylene glycol or glycerol.* Polymer Degradation and Stability, 2006. 91(4): p. 856-861.
115. Christoph, R., et al., *Glycerol*. 2000: Wiley-VCH Verlag GmbH & Co.
116. *Multi-cell Differential Scanning Calorimeter User's Manual*. 1999, Calorimetry Sciences Corporation.
117. Warrington, S.B. and G.u.W.H. Höhne, *Thermal Analysis and Calorimetry*. 2002: Wiley-VCH Verlag GmbH & Co.
118. Garlotta, D., *A Literature Review of Poly(Lactic Acid).* Journal of Polymers and the Environment, 2001. 9(2): p. 63-84.
119. Ehrenstein, G.W., G. Riedel, and P. Trawiel, *Thermal analysis of plastics : theory and practice*. 2004, Munich
120. Ouchi, T., S. Ichimura, and Y. Ohya, *Synthesis of branched poly(lactide) using polyglycidol and thermal, mechanical properties of its solution-cast film.* Polymer, 2006. 47(1): p. 429-434.
121. Amelinckx, S. and L. Reimer, *Microscopy*. 2005, Weinheim: Wiley-VCH Verlag GmbH & Co.
122. Bubert, H., et al., *Surface and Thin-Film Analysis*. 2005, Weinheim: Wiley-VCH Verlag GmbH & Co. KGaA.
123. Wunderlich, B., *Thermal analysis of polymeric materials*. 2005, Berlin: Springer. xvi, 894.
124. Menard, K.P., *Dynamic Mechanical Analysis Basics: Part 1 How It Works*. 2003, Perkin Elmer.
125. Menard, K.P., *Dynamic Mechanical Analysis Basics: Part 2 Thermoplastic Transitions and Properties*. 2003, Perkin Elmer.
126. Tomita, K., et al., *Degradation of poly(L-lactic acid) by a newly isolated thermophile.* Polymer Degradation and Stability, 2004. 84(3): p. 433-438.
127. Paul, M.-A.l., et al., *New nanocomposite materials based on plasticized poly(L-lactide) and organo-modified montmorillonites: thermal and morphological study.* Polymer, 2003. 44(2): p. 443-450.
128. Teramoto, N., et al., *Biodegradation of aliphatic polyester composites reinforced by abaca fiber.* Polymer Degradation and Stability, 2004. 86(3): p. 401-409.
129. Oetjen, G.-W., *Freeze-Drying*. 2004, Wiley-VCH Verlag GmbH & Co. KGaA: Germany.
130. Zafeiropoulos, N.E., G.G. Dijon, and C.A. Baillie, *A study of the effect of surface treatments on the tensile strength of flax fibres. Part I. Application of Gaussian statistics.* Composites Part A: Applied Science and Manufacturing, 2006.
131. Suzuki, N., M. Ito, and F. Yatsuyanagi, *Effects of rubber/filler interactions on deformation behavior of silica filled SBR systems.* Polymer, 2005. 46(1): p. 193-201.

132. Hu, Y., et al., *Crystallization and phase separation in blends of high stereoregular poly(lactide) with poly(ethylene glycol).* Polymer, 2003. 44(19): p. 5681-5689.
133. Harper, D. and M. Wolcott, *Interaction between coupling agent and lubricants in wood–polypropylene composites.* Composites Part A: Applied Science and Manufacturing, 2004. 35(3): p. 385-394.
134. Arbelaiz, A., et al., *Thermal and crystallization studies of short flax fibre reinforced polypropylene matrix composites: Effect of treatments.* Thermochimica Acta, 2006. 440(2): p. 111-121.
135. Yasuniwa, M., et al., *Thermal analysis of the double-melting behavior of poly(L-lactic acid).* Journal of Polymer Science Part B: Polymer Physics, 2003. 42(1): p. 25-32.
136. Quan, H., et al., *On transcrystallinity in semi-crystalline polymer composites.* Composites Science and Technology, 2005. 65(7-8): p. 999-1021.
137. Martins, M.A., et al., *solid state 13C high resolution NMR study of raw and chemically treated sisal fibers.* Carbohydrate Polymers, 2005.
138. Cao, X., et al., *DSC study of biodegradable poly(lactic acid) and poly(hydroxy ester ether) blends.* Thermochimica Acta, 2003. 406(1-2): p. 115-127.
139. Solarski, S., M. Ferreira, and E. Devaux, *Characterization of the thermal properties of PLA fibers by modulated differential scanning calorimetry.* Polymer, 2005. 46(25): p. 11187-11192.
140. Pluta, M., *Morphology and properties of polylactide modified by thermal treatment, filling with layered silicates and plasticization.* Polymer, 2004. 45(24): p. 8239-8251.
141. Ogata, N., et al., *Structure and physical properties of cellulose acetate/poly(L-lactide) blends.* Journal of Applied Polymer Science, 2002. 85(6): p. 1219-1226.
142. Liu, Z., K. Chen, and D. Yan, *Crystallization, morphology, and dynamic mechanical properties of poly(trimethylene terephthalate)/clay nanocomposites.* European Polymer Journal, 2003. 39(12): p. 2359-2366.
143. Lee, S.-H. and S. Wang, *Biodegradable polymers/bamboo fiber biocomposite with bio-based coupling agent.* Composites Part A: Applied Science and Manufacturing, 2006. 37(1): p. 80-91.
144. Nakayama, A., et al., *High mechanical strength double-network hydrogel with bacterial cellulose.* Advanced Functional Materials, 2004. 14(11): p. 1124-1128.
145. Mohanty, S., S.K. Verma, and S.K. Nayak, *Dynamic mechanical and thermal properties of MAPE treated jute/HDPE composites.* Composites Science and Technology, 2006. 66(3-4): p. 538-547.
146. Zimmermann, T., E. Pohler, and T. Geiger, *Cellulose fibrils for polymer reinforcement.* Advanced Engineering Materials, 2004. 6(9): p. 754-761.

Appendix A. Drawings of Mould for Hot Pressing

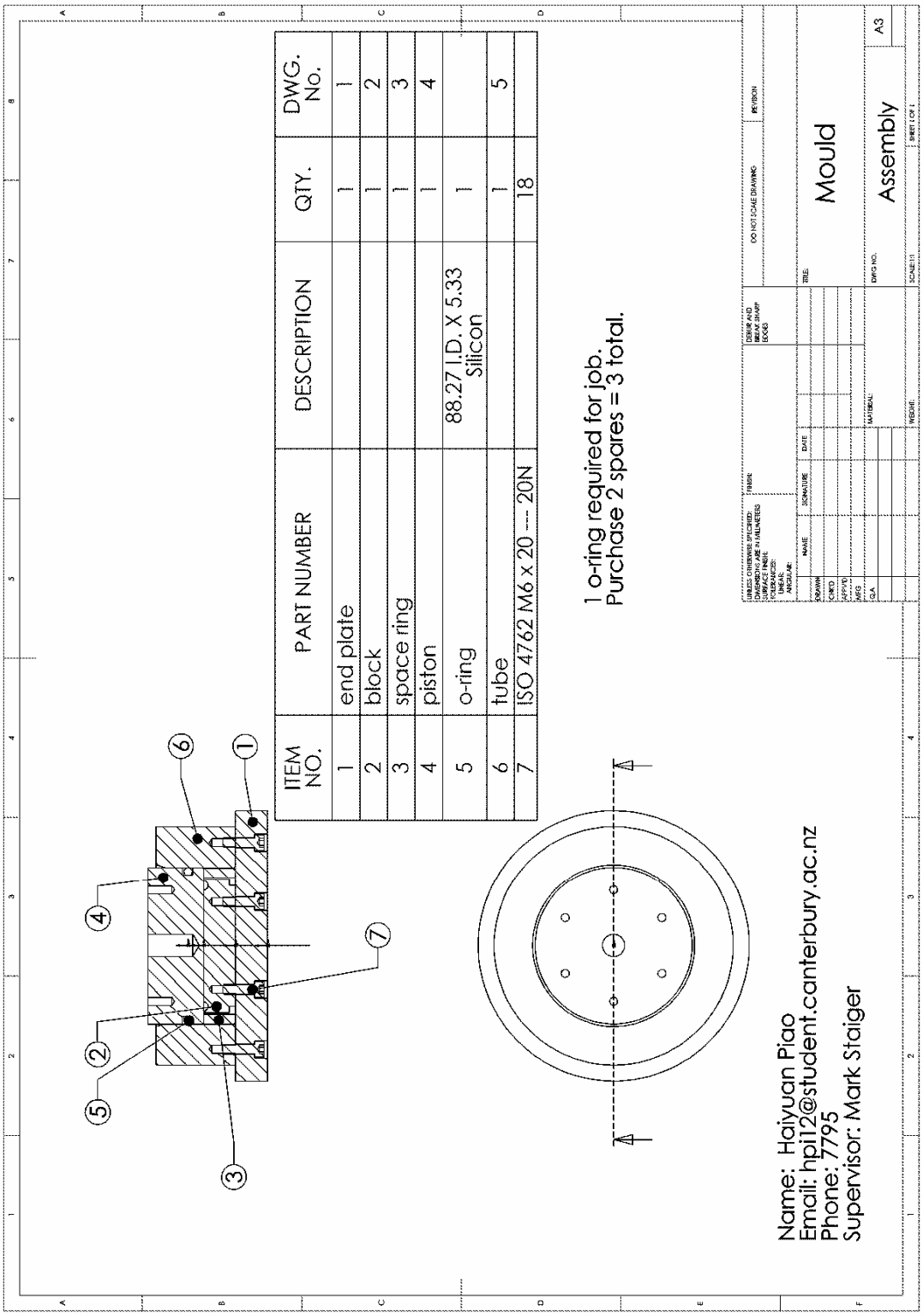

Figure A.1 Assembly drawing of mould

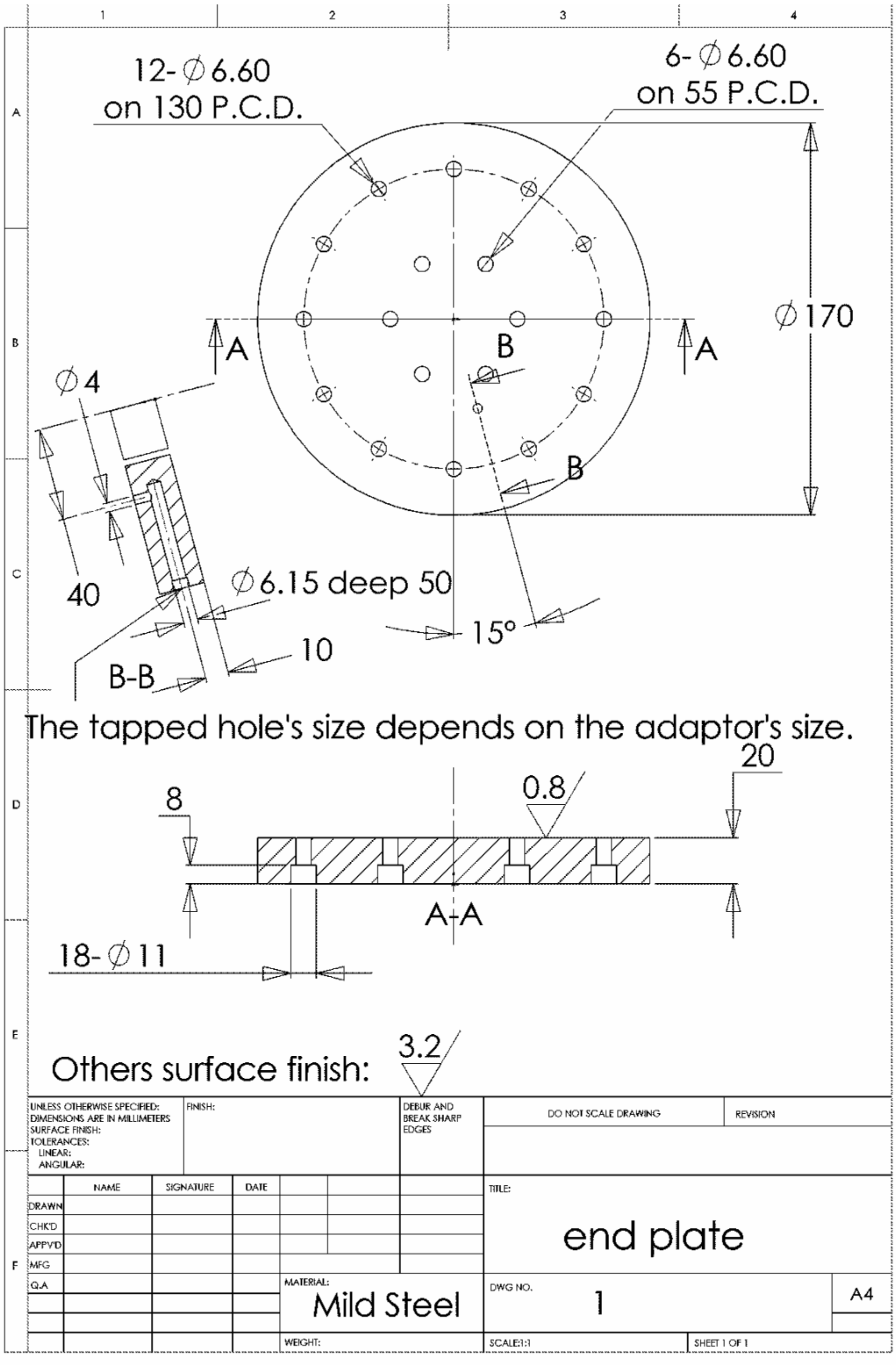

Figure A.2 Drawing of "end plate"

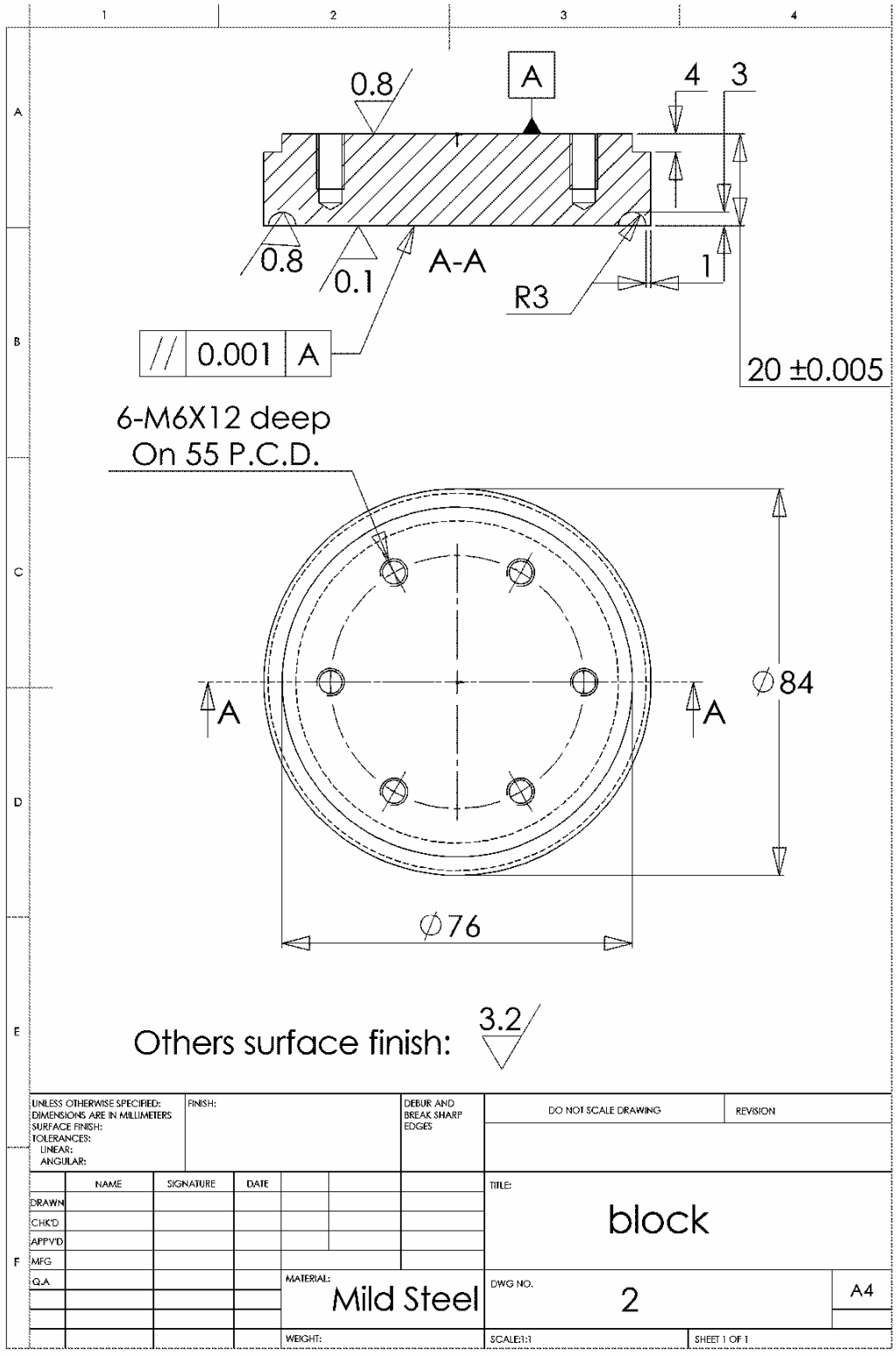

Figure A.3 Drawing of "block"

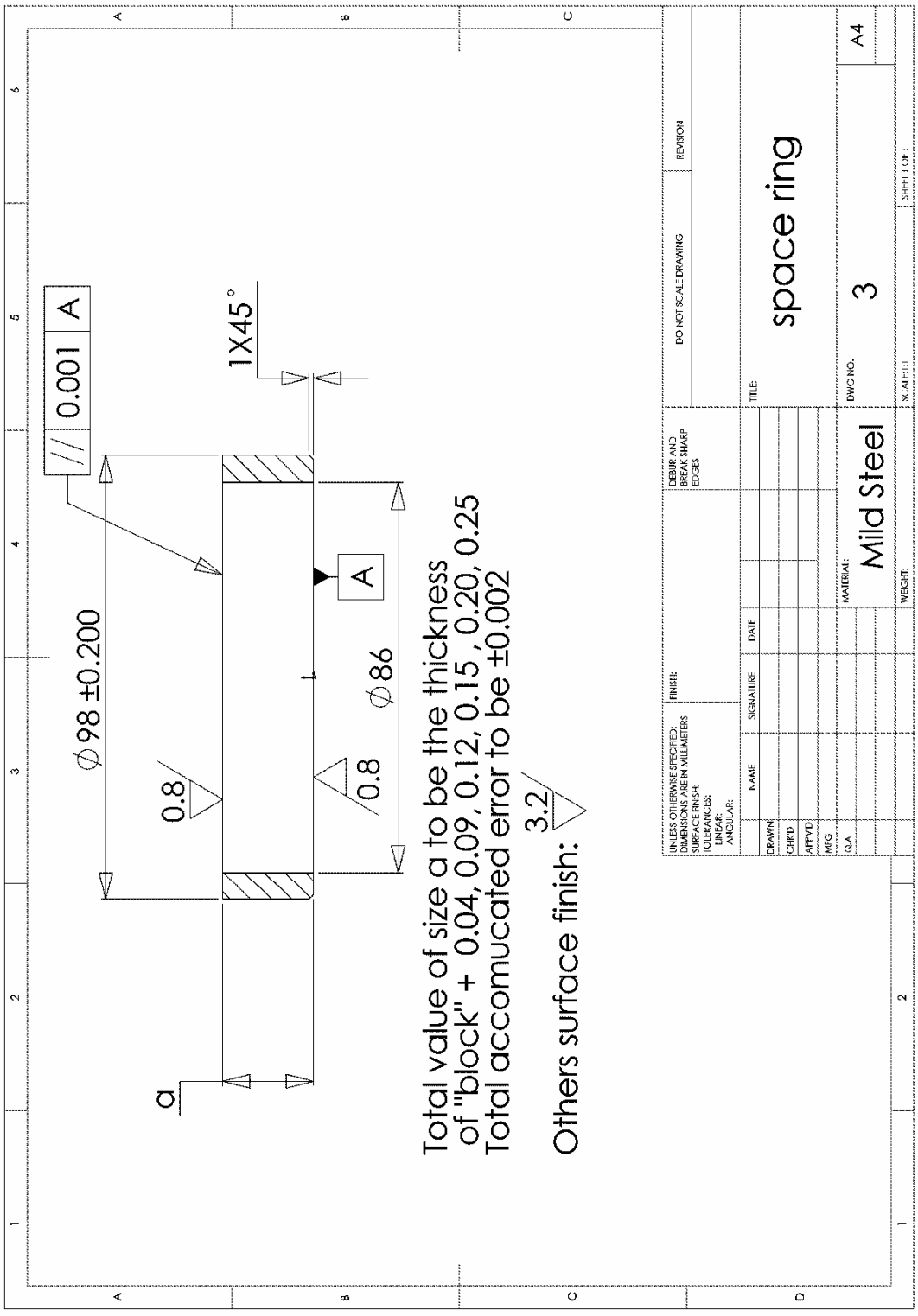

Figure A.4 Drawing of "space ring"

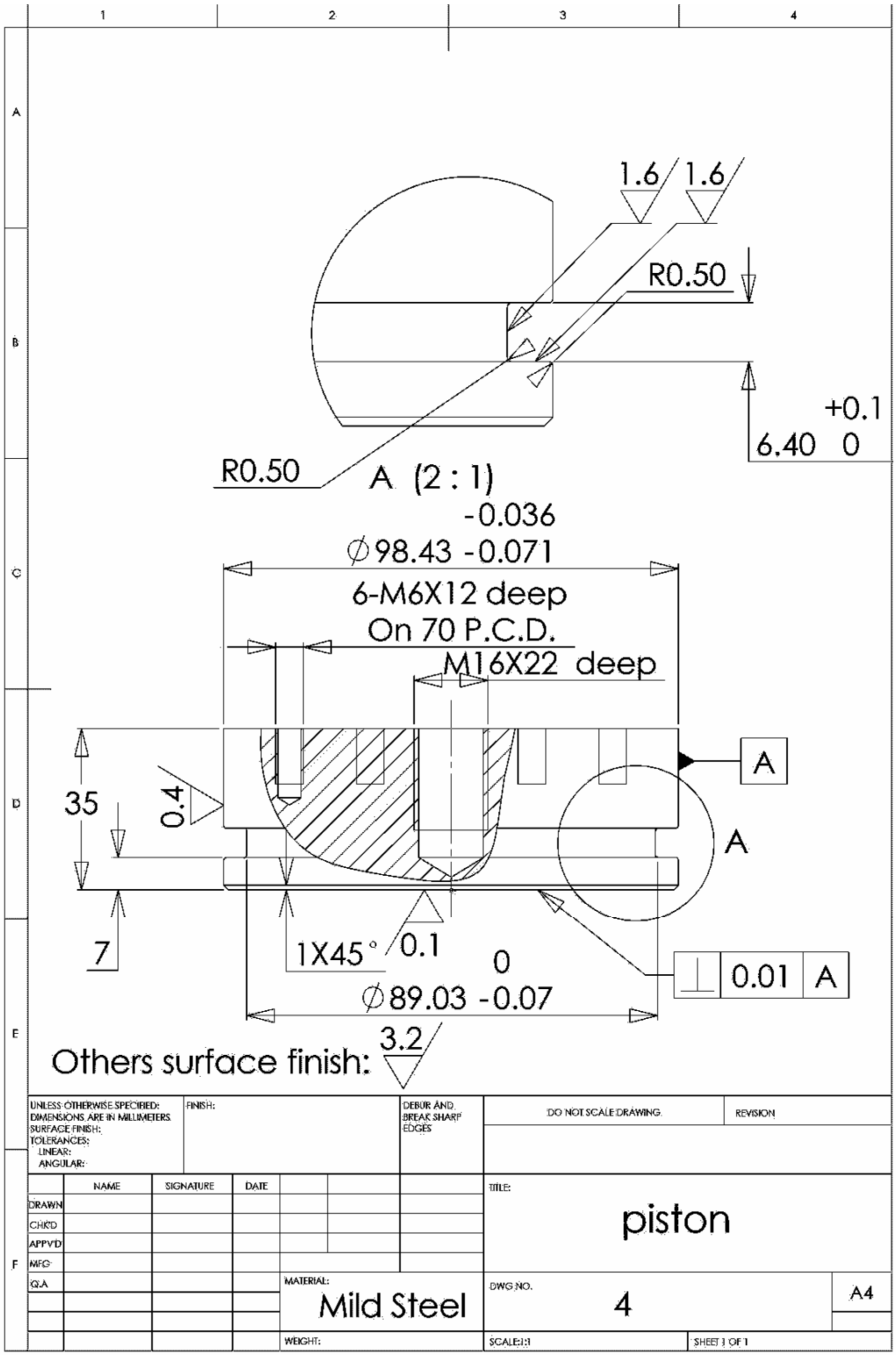

Figure A.5 Drawing of "piston"

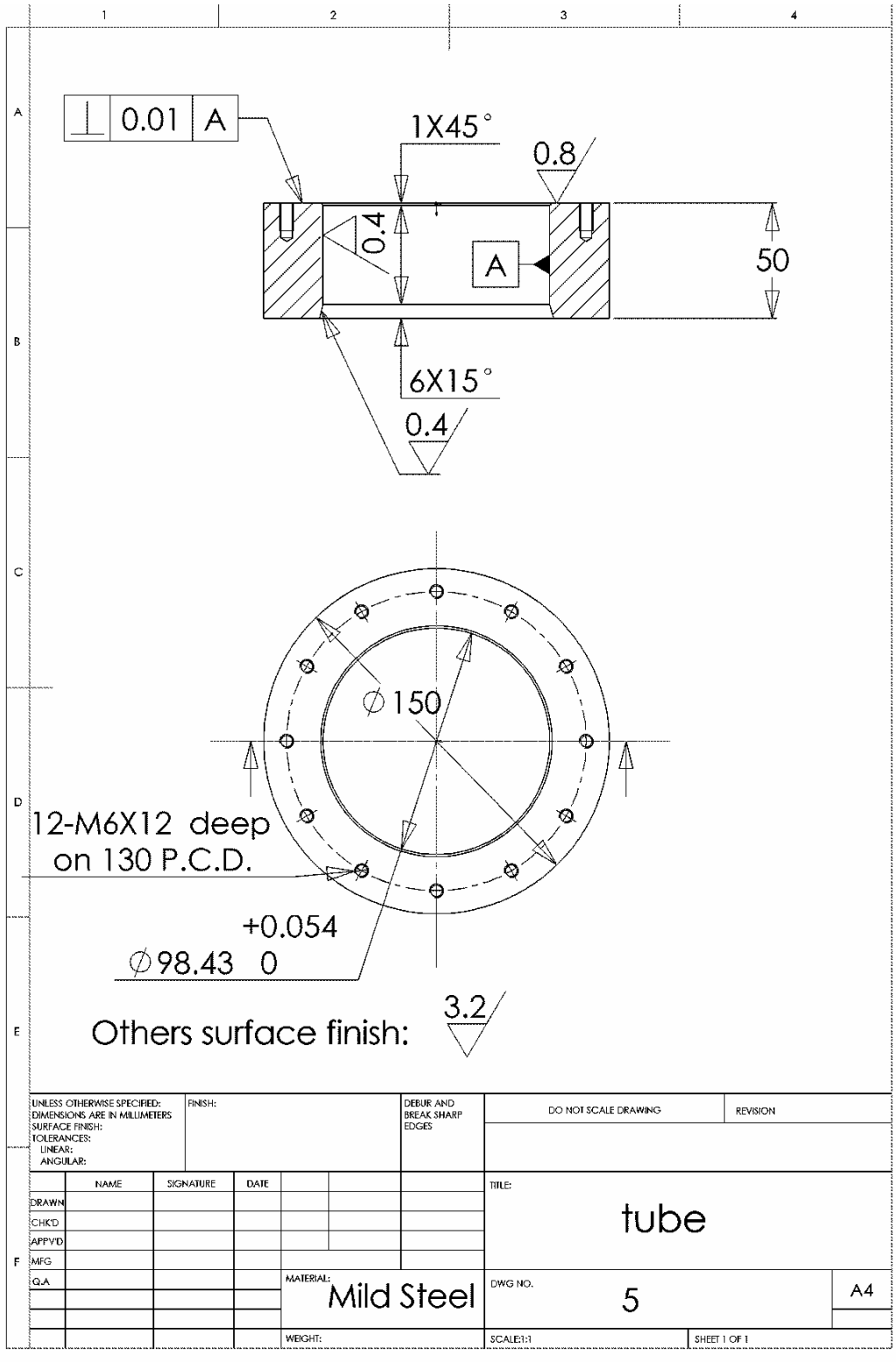

Figure A.6 Drawing of "tube"

Appendix B. Matlab Programme of Calculation for Melting Point of PLA

```
format long

clc

clear all


amp04heat(:,:,1)=load('amp0104heat.csv')    %load amp 1 baseline @ 0.4C/m heat

amp04heat(:,:,2)=load('amp0204heat.csv')    %load amp 2 baseline @ 0.4C/m heat

amp04heat(:,:,3)=load('amp0304heat.csv')    %load amp 3 baseline @ 0.4C/m heat

amp04cool(:,:,1)=load('amp0104cool.csv')    %load amp 1 baseline @ 0.4C/m cool

amp04cool(:,:,2)=load('amp0204cool.csv')    %load amp 2 baseline @ 0.4C/m cool

amp04cool(:,:,3)=load('amp0304cool.csv')    %load amp 3 baseline @ 0.4C/m cool


amp20heat(:,:,1)=load('amp0120heat.csv')    %load amp 1 baseline @ 2.0C/m heat

amp20heat(:,:,2)=load('amp0220heat.csv')    %load amp 2 baseline @ 2.0C/m heat

amp20heat(:,:,3)=load('amp0320heat.csv')   %load amp 3 baseline @ 2.0C/m heat

amp20cool(:,:,1)=load('amp0120cool.csv')   %load amp 1 baseline @ 2.0C/m cool

amp20cool(:,:,2)=load('amp0220cool.csv')    %load amp 2 baseline @ 2.0C/m cool

amp20cool(:,:,3)=load('amp0320cool.csv')    %load amp 3 baseline @ 2.0C/m cool


al04heat(:,:,1)=load('al0104heat.csv')    %load al 1 baseline @ 0.4C/m heat

al04heat(:,:,2)=load('al0204heat.csv')   %load al 2 baseline @ 0.4C/m heat

al04heat(:,:,3)=load('al0304heat.csv')   %load al 3 baseline @ 0.4C/m heat

al04cool(:,:,1)=load('al0104cool.csv')    %load al 1 baseline @ 0.4C/m cool
```

```
al04cool(:,:,2)=load('al0204cool.csv')    %load al 2 baseline @ 0.4C/m cool
al04cool(:,:,3)=load('al0304cool.csv')    %load al 3 baseline @ 0.4C/m cool

al20heat(:,:,1)=load('al0120heat.csv')    %load al 1 baseline @ 2.0C/m heat
al20heat(:,:,2)=load('al0220heat.csv')    %load al 2 baseline @ 2.0C/m heat
al20heat(:,:,3)=load('al0320heat.csv')    %load al 3 baseline @ 2.0C/m heat
al20cool(:,:,1)=load('al0120cool.csv')    %load al 1 baseline @ 2.0C/m cool
al20cool(:,:,2)=load('al0220cool.csv')    %load al 2 baseline @ 2.0C/m cool
al20cool(:,:,3)=load('al0320cool.csv')    %load al 3 baseline @ 2.0C/m cool

plla04heat(:,:,1)=load('plla0104heat.csv')     %load original pla @ 0.4C/m heat
plla04heat(:,:,2)=load('plla0204heat.csv')    %load cast pla @ 0.4C/m heat
plla04heat(:,:,3)=load('plla0304heat.csv')    %load cast plag @ 0.4C/m heat
plla04cool(:,:,1)=load('plla0104cool.csv')    %load original pla @ 0.4C/m cool
plla04cool(:,:,2)=load('plla0204cool.csv')    %load cast pla @ 0.4C/m cool
plla04cool(:,:,3)=load('plla0304cool.csv')    %load cast plag @ 0.4C/m cool

plla20heat(:,:,1)=load('plla0120heat.csv')    %load original pla @ 2.0/m heat
plla20heat(:,:,2)=load('plla0220heat.csv')    %load cast pla @ 2.0C/m heat
plla20heat(:,:,3)=load('plla0320heat.csv')    %load cast plag @ 2.0C/m heat
plla20cool(:,:,1)=load('plla0120cool.csv')    %load original pla @ 2.0C/m cool
plla20cool(:,:,2)=load('plla0220cool.csv')    %load cast pla @ 2.0C/m cool
plla20cool(:,:,3)=load('plla0320cool.csv')    %load cast plag @ 2.0C/m cool

almass=load('almass.csv')   %load al mass
```

```
plla04mass=load('plla04mass.csv')    %load pla mass @ 0.4C/m
plla20mass=load('plla20mass.csv')    %load pla mass @ 2.0C/m

for i=2:3
for j=1:3
amp_plla04heatmodify(:,i,j)=interp1(amp04heat(:,1,j), amp04heat(:,i,j),…
plla04heat(:,1,j))
amp_plla04coolmodify(:,i,j)=interp1(amp04cool(:,1,j), amp04cool(:,i,j),…
plla04cool(:,1,j))
amp_plla20heatmodify(:,i,j)=interp1(amp20heat(:,1,j), amp20heat(:,i,j), …
plla20heat(:,1,j))
amp_plla20coolmodify(:,i,j)=interp1(amp20cool(:,1,j), amp20cool(:,i,j), …
plla20cool(:,1,j))

al_plla04heatmodify(:,i,j)=interp1(al04heat(:,1,j), al04heat(:,i,j), …
plla04heat(:,1,j))-amp_plla04heatmodify(:,i,j)
al_plla04coolmodify(:,i,j)=interp1(al04cool(:,1,j), al04cool(:,i,j), …
plla04cool(:,1,j))-amp_plla04coolmodify(:,i,j)
al_plla20heatmodify(:,i,j)=interp1(al20heat(:,1,j), al20heat(:,i,j), …
plla20heat(:,1,j))-amp_plla20heatmodify(:,i,j)
al_plla20coolmodify(:,i,j)=interp1(al20cool(:,1,j), al20cool(:,i,j), …
plla20cool(:,1,j))-amp_plla20coolmodify(:,i,j)

end
end
```

```
amp_plla04heatmodify(:,1,:)=plla04heat(:,1,:)
amp_plla04coolmodify(:,1,:)=plla04cool(:,1,:)
amp_plla20heatmodify(:,1,:)=plla20heat(:,1,:)
amp_plla20coolmodify(:,1,:)=plla20cool(:,1,:)

al_plla04heatmodify(:,1,:)=plla04heat(:,1,:)
al_plla04coolmodify(:,1,:)=plla04cool(:,1,:)
al_plla20heatmodify(:,1,:)=plla20heat(:,1,:)
al_plla20coolmodify(:,1,:)=plla20cool(:,1,:)

for i=1:3
al_plla04heatmodify(:,2:3,i)=al_plla04heatmodify(:,2:3,i)/almass(i,1)*plla04mass(i,1)
al_plla04coolmodify(:,2:3,i)=al_plla04coolmodify(:,2:3,i)/almass(i,1)*plla04mass(i,1)
al_plla20heatmodify(:,2:3,i)=al_plla20heatmodify(:,2:3,i)/almass(i,1)*plla20mass(i,1)
al_plla20coolmodify(:,2:3,i)=al_plla20coolmodify(:,2:3,i)/almass(i,1)*plla20mass(i,1)

end

plla04heatmodify(:,1,:)=plla04heat(:,1,:)
plla04coolmodify(:,1,:)=plla04cool(:,1,:)
plla20heatmodify(:,1,:)=plla20heat(:,1,:)
plla20coolmodify(:,1,:)=plla20cool(:,1,:)

plla04heatmodify(:,2:3,:)=-(plla04heat(:,2:3,:)-amp_plla04heatmodify(:,2:3,:)-…
```

```
al_plla04heatmodify(:,2:3,:))
plla04coolmodify(:,2:3,:)=-(plla04cool(:,2:3,:)-amp_plla04coolmodify(:,2:3,:)-…
al_plla04coolmodify(:,2:3,:))
plla20heatmodify(:,2:3,:)=-(plla20heat(:,2:3,:)-amp_plla20heatmodify(:,2:3,:)-…
al_plla20heatmodify(:,2:3,:))
plla20coolmodify(:,2:3,:)=-(plla20cool(:,2:3,:)-amp_plla20coolmodify(:,2:3,:)-
al_plla20coolmodify(:,2:3,:))
```

Appendix C. Scanning rate and mass of materials in the DSC experiments and other results of DSC

Table C.1 Scanning rate and mass of materials in the DSC experiments.

No.	Scan rate °C/min	Material	Channel 1	Channel 2	Channel 3
1	0.4 and 2	Name	Baseline	Baseline	Baseline
		Mass g	0	0	0
2	0.4 and 2	Name	Al	Al	Al
		Mass g	0.15048	0.15065	0.15010
3	0.4	Name	Al	Al	Al
		Mass g	0.14879	0.14684	0.14699
		Name	Original PLA	Cast PLA	PLAG
		Mass g	0.10079	0.10320	0.09907
4	2	Name	Al	Al	Al
		Mass g	0.15026	0.15063	0.15107
		Name	Original PLA	Cast PLA	PLAG
		Mass g	0.10033	0.10384	0.10199

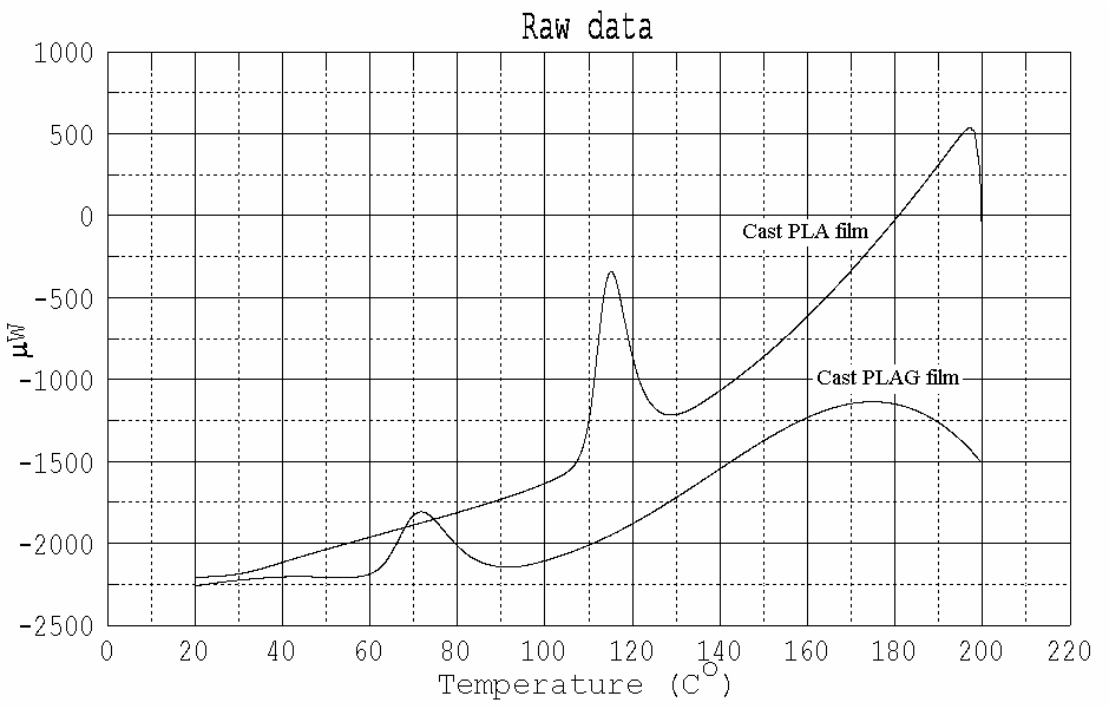

Figure C.1 DSC curves of cast PLA and PLAG film at 0.4 °C/min cooling rate.

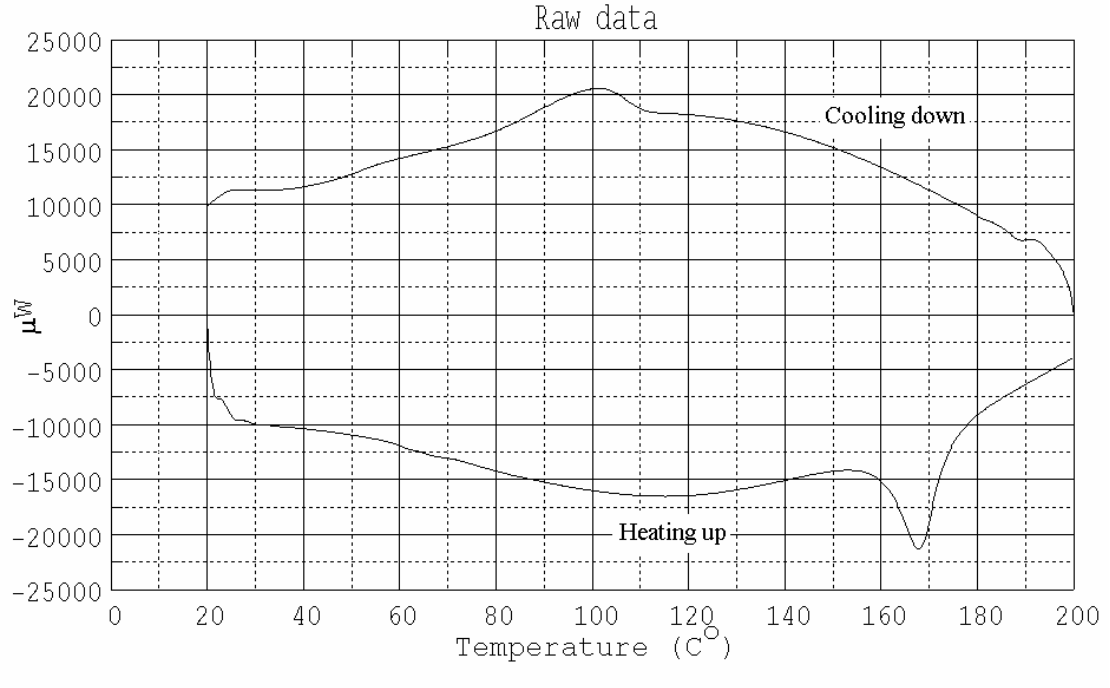

Figure C.2 Whole DSC results of original PLA film at 2.0 °C/min rate.

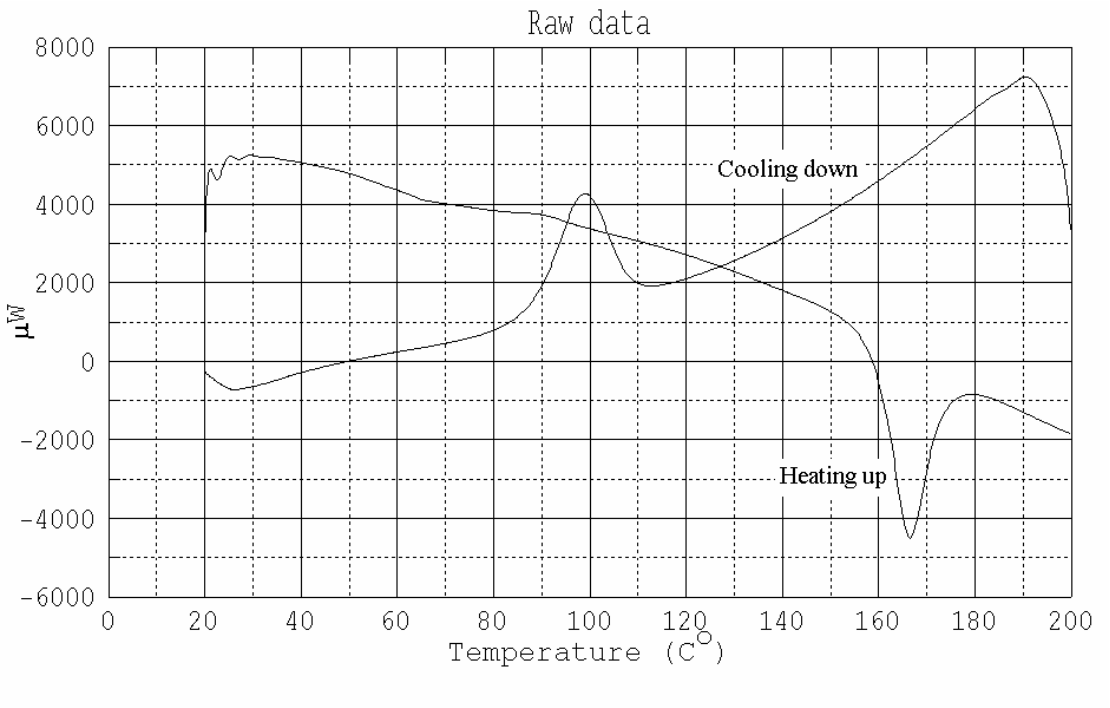

Figure C.3 Whole DSC results of cast PLA film at 2.0 °C/min rate.

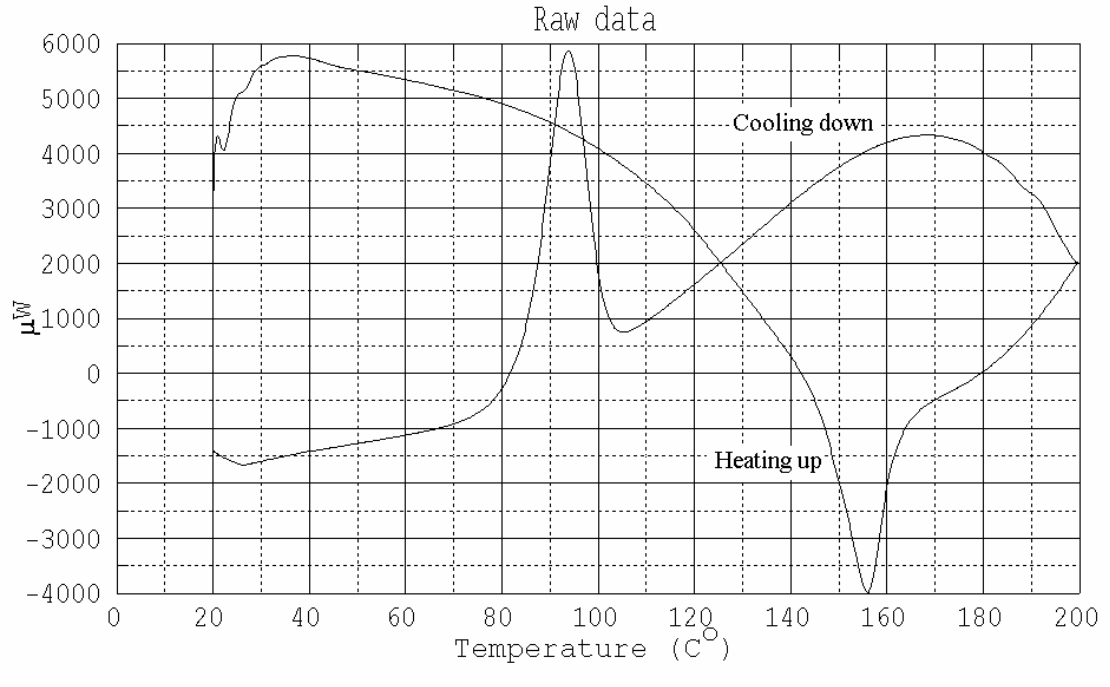

Figure C.4 Whole DSC results of cast PLAG film at 2.0 °C/min rate.